UCLouvain

epl

École polytechnique de Louvain

Formation and characterization of laccase - polyelectrolyte complexes and their integration in layer-by-layer assemblies.

for wastewater treatment

Author: **Brieuc Conet**
Supervisors: **Sophie Demoustier, Christine Dupont**
Readers: **Delphine Magnin, Cédric Vranckx**
Academic year 2022–2023
Master [120] in Biomedical Engineering

Abstract

Water is humanity's most vital resource. However, the growth of human activity has led to an alarming increase in untreated wastewater, contaminating soils, rivers, and other natural resources, posing a major threat to people and ecosystems.

Due to water scarcity and high demand, wastewater is now seen as a potential water source, rather than just waste. This transformation from waste to resource is done by wastewater treatment, which removes most pollutants from water. This study focuses on enzymatic bioremediation, an ecological and cost-effective method that offers some advantages, including the treatment of certain pollutants that conventional methods cannot treat. However, a main drawback comes with this process. To be cost-effective and implemented on a larger scale, enzymes must be immobilized to prevent their leaching from their carrying material.

In this work, we will study the immobilization of an enzyme from the oxidoreductase family, called laccase, by the Layer-by-Layer (LbL) technique. Previous work demonstrated that multilayers only composed of laccase and branched polyethylenimine (bPEI) lacked (structural) stability and were not suited for developing reusable materials. Therefore, this work aims at using Protein-Polyelectrolyte Complexes (PPC) as a new building block for LbL assembly. In theory, the use of PPC instead of free enzymes allows more efficient multilayer formation and results in more stable films. For that reason, this work focuses on the creation and characterization of Laccase-Polyelectrolyte complexes and their integration in LbL assemblies.

First, PPC were formed by mixing different amounts of laccase and poly(allylamine hydrochloride) (PAH). Complexes were detected and characterized by turbidity, zeta potential, and dynamic light scattering measurements. They exhibited different characteristics depending on the PAH/Laccase mass ratios. Not all the created complexes were suitable for LBL assembly but could be used in other applications or immobilization systems.

Then the selected PPC were immobilized by LbL using poly(sodium-4-styrene sulfonate) as counter-polyion. Obtained multilayers exhibited lower initial activity than those made of free laccase. However, LbL assemblies built with complexes show a slightly higher stability than assemblies with free laccase.

In conclusion, this work has led to the creation and characterization of different PPC of laccase. The results show that such complexes for multilayer formation only slightly improve stability while decreasing activity. In addition, this work highlighted a possible complexation method specific to laccase, that opens new approaches for laccase isolation.

Acknowledgements

Je tiens à exprimer ma profonde gratitude à toutes les personnes qui m'ont soutenu tout au long de ce mémoire.

Tout d'abord, un immense merci aux professeurs Sophie Demoustier et Christine Dupont, mes promotrices, pour leurs encadrements tout au long de ce mémoire semé d'embûches, mais des plus agréable grâce à leurs conseils. Vous m'avez permis détendre mes connaissances et de surpasser des obstacles complexes.

Je suis également reconnaissant envers Delphine Magnin et Cédric Vranckx qui ont accepté d'êtres les lecteurs de ce mémoire.

Je tiens à remercier Ian Coupez pour ses conseils et sa patience. Il a été une source d'inspiration et de correction. Un tout grand merci de m'avoir aidé au travers de cette année.

J'aimerais remercier mes bioingénieurs préférés, Juliette de Meuûs et Christophe Delcuve, pour leur ambiance dans notre bureau, mais aussi pour leurs conseils et leurs connaissances des plus riches.

Je remercie Alessio Malfanti (Louvain Drug Research Institute) pour m'avoir permis d'utiliser correctement le Zetasizer ainsi que son aide sur l'analyse de résultat.

Je tiens à remercier particulièrement mon frère Aymeric d'avoir accordé de son temps pour relire mon mémoire, de m'avoir apporté ses corrections et d'avoir supporté mes retours colériques. De manière plus générale, je souhaite remercier ma famille de leur soutien en ses temps compliqués.

Merci également, aux membres de l'IMCN (C2 et C3) de m'avoir accueilli ainsi qu'aux autres mémorant(e)s pour leur bonne ambiance et les pauses-café.

Finalement, j'aimerais remercier toutes les personnes qui aient pu m'aider aux travers de ces années.

À toutes personnes qui pourraient lire ce mémoire, j'aimerais vous dire ceci : Si vous devez écrire un mémoire ou un autre document, écrivez dès que possible les choses que vous avez faites avec leurs tenants et aboutissants, croyez-moi, c'est plus facile à dire qu'à faire, mais ça veut le coût. Et comme un vieil homme barbu l'a dit : "*Mais vous savez, on peut trouver le bonheur même dans les moments les plus sombres... Il suffit de se souvenir, d'allumer la lumière.*" Albus Dumbledore.

List of abbreviations

ΔD	Dissipation shift
Δf	Frequency shift
Δm	Mass shift
A_{350}	Optical density at 350 nm wavelength.
A_{420}	Optical density at 420 nm wavelength.
A_{562}	Optical density at 562 nm wavelength.
ABTS	2,2'-azino-bis(3-ethylbenzothiazoline-6-sulphonic acid)
BCA assay	BiCinchoninic acid assay
BL	bilayers
bPEI	branched, Polyethylenimine
[bPEI-LAC]	Multilayers of laccase and bPEI made by LbL
CLEA	Cross-linked enzyme aggregate
DLS	Dynamic light scattering
GLU	Glutaraldehyde
IEP	Isolelectric point
LAC	Laccase
LbL	Layer-by-Layer
LPC	Laccase - Polyelectrolyte Complex
LPC^{new}	LPC composed of laccase and PAH^{new}
LPC^{old}	LPC composed of laccase and PAH^{old}
LPC$_{0.04}$	PAH - LAC complexes with mass ratio equals to 0.04
PAH	Poly(allylamine hydrochloride)
PAH^{new}	PAH from a recent purchase
PAH^{old}	PAH already used in the lab
PDADMAC	Poly(diallyldimethylammonium chloride)
PDI	Polydispersity index
PE	Polyelectrolyte
PSS	Poly(styrene sulfonate)
[PSS-LPC]	Multilayers of LPC and PSS made by LbL
PPC	Polyelectrolyte-Protein Complex
QCM	Quartz crystal microbalance
QCM-D	Quartz crystal microbalance with dissipation monitoring
ToF-SIMS	Time-of-Flight secondary ion mass spectrometry
XPS	X-ray photoelectron spectroscopy

Assembly abbreviation: [Polyelectrolyte - Protein component]$_{\text{number of bilayers}}$

Contents

Chapter 1

Introduction

1.1 Context

Water is the most essential resource for humans, not only for drinking but also for various sectors of human activity such as agriculture, livestock, sanitation, electricity, mining activity, and industry [1, 2]. Human population growth and its increasing activity imply an even-growing water demand. In 2012, the Organization for Economic Co-operation and Development (OECD) projected an increase in water demand of 55% between 2000 and 2050 if no changes were brought to our water use [3].

Over the past decades, increased human activity has led to a rise in wastewater production. According to the United Nations (UN), about 80 percent of this wastewater is released without prior treatment. As a result, many pollutants and compounds that end up in wastewater will subsequently contaminate soils, rivers, or other natural resources [2, 4, 5]. Among them, pesticides, heavy metals, solvents, dyes, polycyclic aromatic hydrocarbons[1], estrogenic hormones or micropollutants from the pharmaceutical industry are found. Unfortunately, their presence not only decreases the water's quality but also poses a threat to public and ecosystem health [2, 5–11]. Figure 1 shows a schematic representation of different pollutants and their effects on human body.

[1]The well-known abbreviation PAHs is not used to avoid the confusion with the abbreviation of poly(allylamine hydrochloride), a polyelectrolyte used in this work. The only exception is on Figure 1.

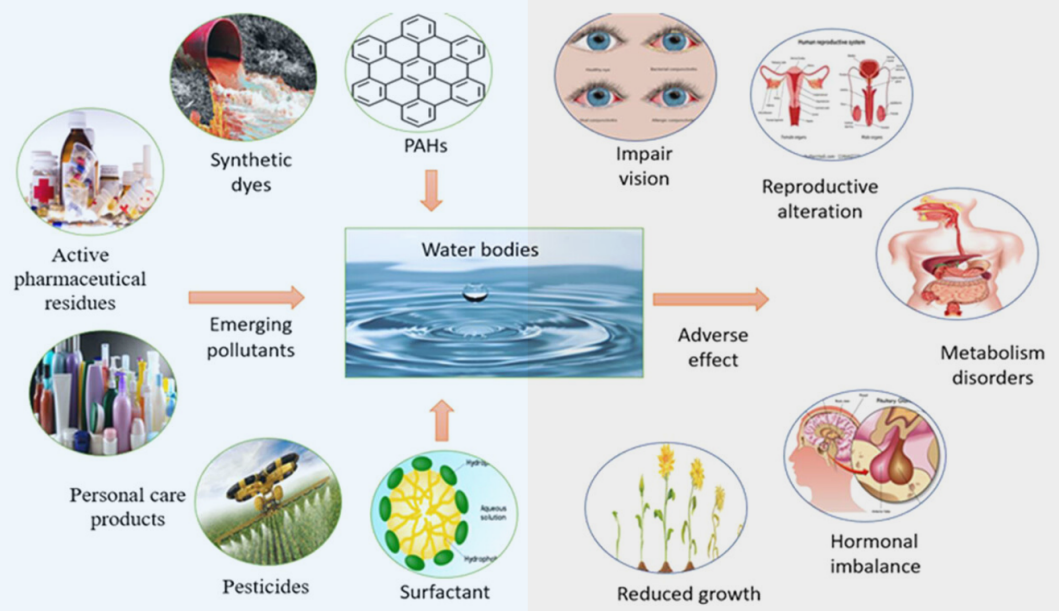

Figure 1: Some water pollutants and possible effects. Many pollutants present in wastewater come from industrial sectors. This includes synthetic dyes, pharmaceutical residues or pesticides. The presence of these compounds can disturb the physiological activity of humans and other organisms, as well as induce mutagenic changes. Figure reproduced from [5].

1.2 Wastewater treatment: a key solution

Due to water scarcity in some regions, worsened by climate change, wastewater is transformed from a waste product to an alternative water source [2, 4, 12]. In consequence, the treatment of wastewater is becoming fundamental to protect public health, the environment and to partly respond to even-growing water demand [4, 5].

1.2.1 Wastewater treatment

Wastewater treatment is not a new human activity, written traces of it dating back 4000 years can be found [13]. However, due to enhanced pollution and increased demand, the processes became increasingly complex and had to be scaled up. Nowadays, physical, chemical, and biological treatments are commonly used to treat wastewater, but there are also hybrid systems that use different approaches. This includes technologies such as adsorption, electro-dialysis, ion exchange, sedimentation, coagulation, flocculation, precipitation, filtration, oxidation, aerobic and anaerobic bioprocesses [14, 15].

Each of them has its disadvantages and advantages in terms of cost, efficiency, environmental impact, or nature of the treated compounds. The purification process shown in Figure 2 can employ various technologies simultaneously or independently in specific steps. In addition, the selection of technologies depends on the objectives of the wastewater treatment plant and the wastewater characteristics [14, 15].

The purification process, in general, can be decomposed in 5 consecutive steps. The two first ones, pretreatment, and primary treatment, will be carried out in the pre-treatment phase. They will remove the solid particles and suspended substances by using mechanical and/or physical methods. The third step called secondary treatment (or purification) uses biological, physical, or chemical techniques to remove chemical pollution. The penultimate step, the tertiary treatment, will remove the by-products that may have been generated in the previous step. The last step, as its name suggests, will treat the sludge created during the purification process.

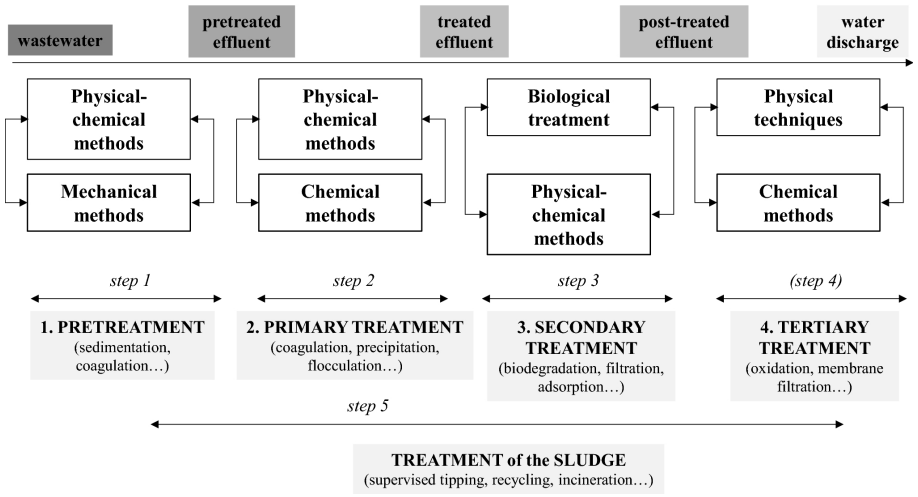

Figure 2: General scheme of the purification process. Figure reproduced from [14, 15].

Due to the different disadvantages of the existing wastewater treatment methods, research for better alternatives from an economic and efficiency point of view is always in progress. For example, physical treatments are in general way cheaper but are not effective at removing dissolved pollutants. In the case of chemical treatments, they are more effective but can produce a large amount of hazardous by-product (sludge) and are more expensive. Biological treatment aims to be safer and more environment-friendly than the two previous ones but for now, it requires specific conditions and it also generates by-products [5, 9, 11, 14, 15].

1.2.2 Enzymatic bioremediation

At the interface between chemical and biological treatments, a new technique based on the use of enzymes to degrade different toxic compounds is currently emerging. This technique, called enzymatic bioremediation, allows the treatment of some pollutants that are not treated by conventional methods. In consequence, enzymatic bioremediation emerges as a solution for achieving efficient, affordable, and environmental-friendly treatment. By utilizing enzymatic catalysis, this method operates under lower energy requirements, moderate conditions, and can produce non-toxic products. Therefore, it holds the key to a cost-effective and eco-friendly approach to wastewater treatment. [5, 9–11].

The common enzymes for enzymatic bioremediation are oxidoreductases (EC 1) such as laccase, peroxidase, cytochrome P450, dehydrogenase, dehalogenase. They can oxidize a wide range of substrates, including different wastewater pollutants in less harmful by-products, and are produced by diverse bacteria, fungi, and plants [5, 9, 16, 17].

1.2.2.1 Laccase

Among the different enzymes available for water bioremediation, laccase comes out. This enzyme (EC 1.10.3.2, p-diphenol : dioxygen oxidoreductase) is part of the family of multicopper oxidases and can be found in plants, fungi, and bacteria. In recent years, interest in laccase has increased because it presents several advantages. The first is versatility. Indeed, laccase is capable of oxidizing a wide variety of organic and inorganic substrates which are residues of industrial processes, such as aromatic compounds, phenols, non-phenolic compounds, or even amines. The second advantage is that laccase uses dioxygen and generates only water, which is eco-friendly. These properties make of laccase a remarkable green candidate for many different types of biocatalysis applications, including bioremediation [1, 5, 18–23].

Laccase structure

As shown in Figure 3, laccase has 4 copper atoms that form the active site. These copper atoms are separated into 3 types. The type 1 copper atom (Cu T1) is the site where the substrate is oxidized. The type 2 (Cu T2) and the two type 3 (Cu T3) copper atoms form a trinuclear copper cluster. At this place, the oxygen is reduced. The transfer of electrons between Cu (T1) and the trinuclear copper cluster occurs through the histidine-cysteine pathway [18, 21].

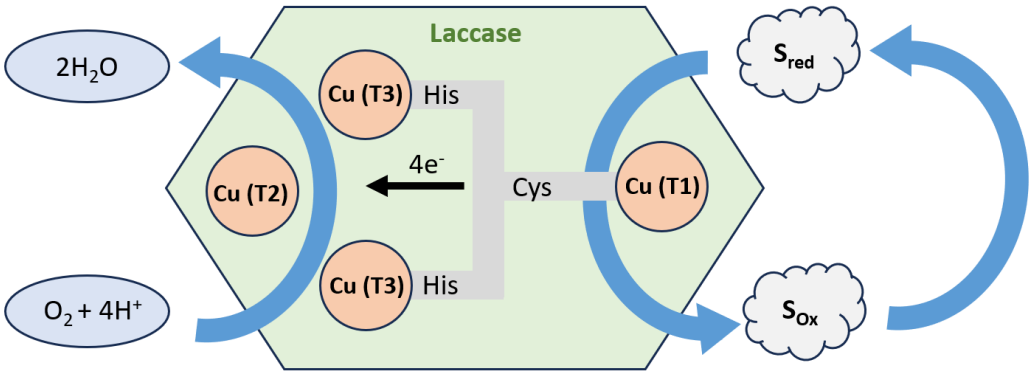

Figure 3: Simplified reaction mechanism of substrate oxidation by laccase. The laccase oxidizes 4 substrates (S_{red}) at the T1 copper site. The electrons transfer is realized by the histidine (His) - cysteine (Cys) pathway from the T1 copper site to the T2 and T3 copper sites. The trinuclear cluster reduces oxygen to form water. The Figured is a reproduction from [24].

Laccase properties

Based on its origin, laccase characteristics can vary greatly. For example, fungal laccase usually possesses a much higher redox potential (E°) compared to bacterial ones, making it capable of oxidizing a much broader range of substrate molecules and therefore making of it a more interesting candidate for bioremediation applications [18, 21]. In terms of weight, fungal laccase is usually found between 60 and 70 kDa, even though the molecular weight can sometimes be as high as 390 kDa. These enzymes are all globular, with dimensions around 70 Å× 55 Å×50 Å. Finally, the isoelectric point (IEP) of fungal laccase is usually around 4, although this characteristic varies greatly depending on their host organism, ranging from 2.6 to 6.9 [19, 19, 21, 25].

On Figure 4, the molecular structure as well as the surface charge of laccase from *Trametes versicolor* can be found.

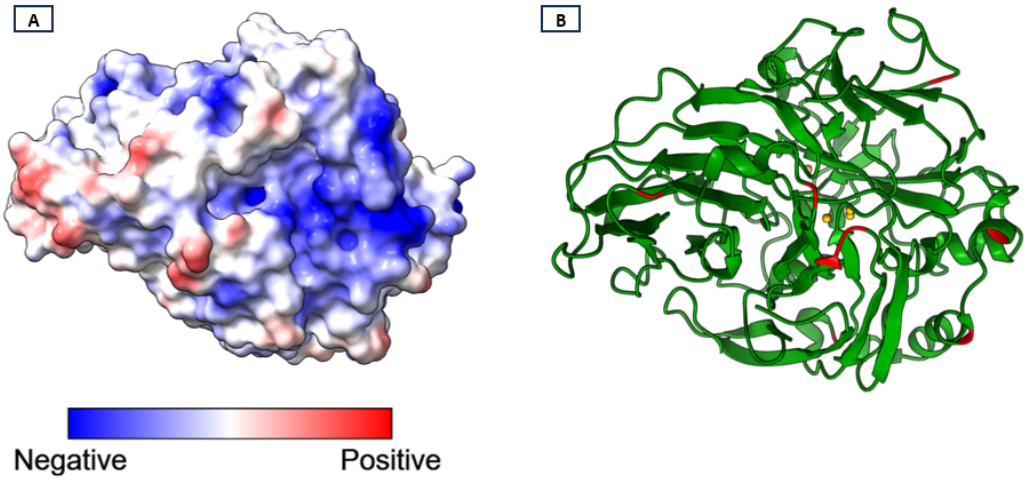

Figure 4: Laccase from *Trametes versicolor*: Tertiary structure representation and coulombic surface coloring. (A) Molecular structure of laccase with coulombic surface coloring. The electrostatic static surface potentials are colored in blue for negative and red for positive charges. (B) Simplified backbone ("Cartoon") representation of laccase. The 4 copper atoms are in orange. Lysine is in red. Figure produced on ChimeraX

1.3 Enzyme immobilization

Despite many advantages of enzyme-based bioremediation in terms of energy cost and pollutant degradation, many drawbacks still prevent its implementation at a larger scale. From an economic point of view, enzyme production and purification is still an extremely expensive process. Furthermore, free enzymes have a lack of stability and reusability, with a loss of activity over time. In fact, enzymes have a short lifespan due to hard and varying conditions, such as pH, temperature or species in solutions. In addition, the use of enzyme remediation in real applications (wastewater treatment plants) will aggravate the problem of denaturation of the enzyme and enzyme washout due to the continuous flow of effluent [26]. In this context, immobilization of enzymes on a solid and reusable substrate appears as a very seducing strategy to overcome these limitations [9]. On the one hand, immobilization helps to maintain the enzyme characteristics even under harsh and varying conditions. On the other hand, this allows retention of the enzyme in the process. Consequently, the cost of the process can be reduced by transitioning from free to immobilized enzymes [11, 16, 19, 27].

1.3.1 Enzyme immobilization techniques

Enzyme immobilization is accomplished using various techniques. They are divided into two classes depending on the type of interactions, physical or chemical, between the enzyme and the support as shown in Figure 5. Physical immobilization works thanks to weak interactions such as van der Waals forces, hydrogen bonds, hydrophobic or electrostatic interactions. This usually allows the preservation of the enzyme structure (structural stability) and so its activity to be better preserved, while it may not be sufficient to obtain high enzyme retention. On the other side, chemical interactions use covalent bonds and per consequence can favor better retention (system stability) while possibly modifying the enzyme activity [9, 26]. The best immobilization technique would therefore be one that provides good structural stability of the enzyme, and good system stability via good enzyme retention.

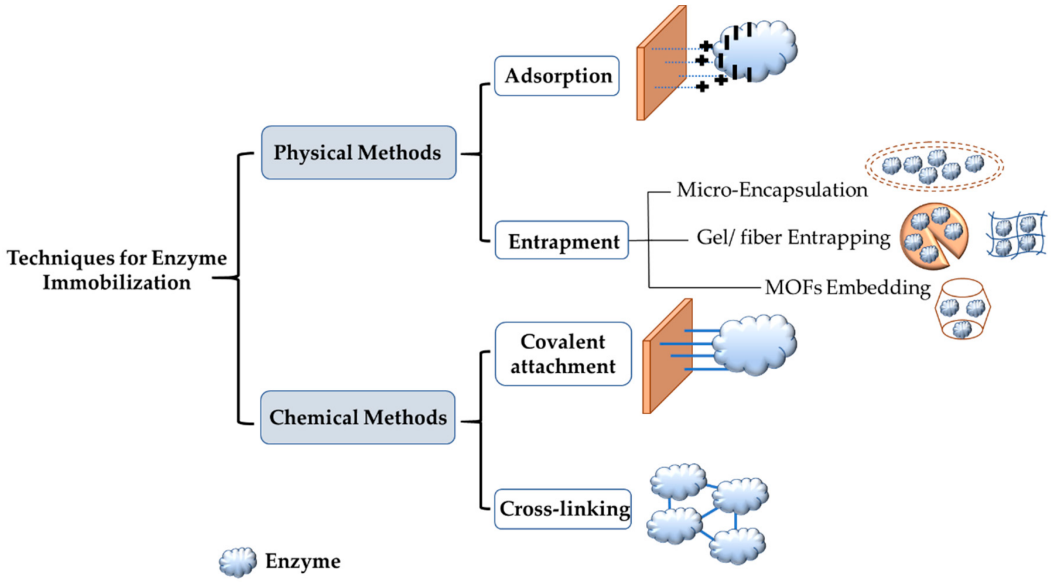

Figure 5: Enzyme immobilization techniques. Figure from [9].

Adsorption is a physical immobilization technique where enzymes are, as mentioned above, linked thanks to electrostatic interactions, van der Waals forces, hydrophobic interactions and hydrogen bonds. This reversible technique is simple and low-cost but enzyme leakage is important. Further, the technique is sensitive to pH, ionic strength and the choice of solid support.

Entrapment (or encapsulation), the second physical immobilization method, consists in confining the enzyme in a network of molecules or the pores of the support, making the technique irreversible. The network will act as a porous membrane retaining the enzyme while allowing the substrate to pass through. Different types of entrapment are possible as metal-organic frameworks (MOFs), microencapsulation or gel/fibre entrapment [9]. Furthermore, the choice of the network and its properties will impact the substrate and product exchanges [28].

The first chemical method, covalent attachment, uses functional groups of the enzyme to create a covalent bond to attach it to an inorganic or organic material, therefore the process is irreversible. While this method improves retention, it may result in conformation changes and block the active site, which would affect the enzyme activity.

Cross-linking, the second chemical method, is based on the formation of covalent bonds between the different species, no support is required. If the involved species are composed mainly of enzymes, the resulting structure is a cross-linked enzyme aggregate (CLEA). Cross-linking involves chemical species called cross-linking agents. One of the most famous is glutaraldehyde (GLU). The main drawbacks are enzyme denaturation, high operational costs and control issues of the reaction [1, 9, 11, 19, 26, 27, 29].

1.3.2 Layer-by-Layer assembly

Among the numerous surface functionalization techniques, the one called Layer-by-Layer (LbL) assembly appeared as a very seducing candidate to immobilize enzymes. This is a bottom-up method that was developped in the early 1960s with Iler, but the concept of layer-by-layer or LbL assembly came much later in the 1990s with the works of Decher et al [30]. The LbL method is a simple, versatile, and flexible technique that allows the creation of multilayer films or coatings with the possibility to control the thickness of the final assembly and also the hierarchical material composition. In consequence, LbL allows tuning the properties of the assembly [29, 31–34].

The assembly of the different layers can be achieved thanks to numerous interactions such as electrostatic interactions, hydrogen bonding, hydrophobic interaction. This variety of interactions allows the assembly of a broad range of materials on different substrates. As shown in Figure 6, the substrate can have different characteristics. It can be organic or inorganic and have different shapes, sizes and porosities. It is also true for the layer materials; it goes from DNA to proteins by passing through lipids and nanoparticles.

In this work, the assembly is mainly realized through electrostatic interactions between the molecular species. Therefore, the focus will be on creating a layer-by-layer assembly for this type of interaction, and a more detailed explanation will be provided. The most commonly used molecules when discussing LbL relying on electrostatic interactions are charged soluble polymers, specifically polyelectrolytes. By using the attraction between oppositely-charged molecules, the LbL method will create multilayer films by alternating the deposition of oppositely-charged components [29, 31–38].

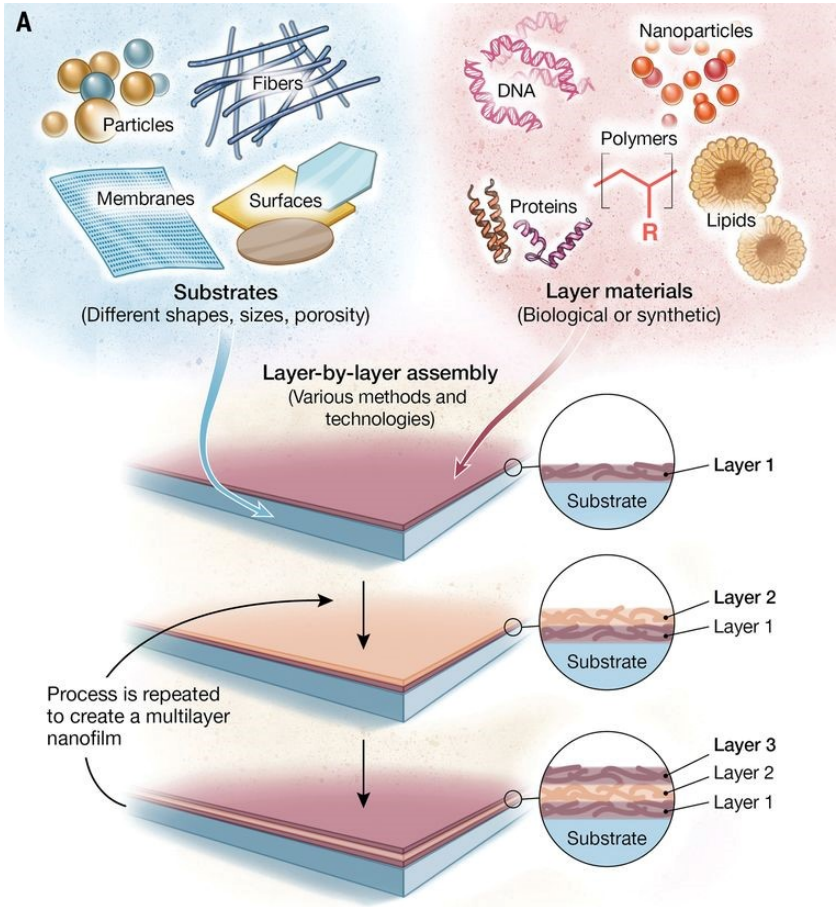

Figure 6: Schematic overview of LbL assembly. The LbL assembly can be achieved on diverse types of substrates such as fibers, particles, surfaces and membranes. The assembly can be done with various methods and technologies but will follow the principle of adding one layer after another. The layer can also be made of different materials, such as nanoparticles, proteins and polymers. Figure reproduced from [38].

1.3.2.1 Polyelectrolytes as building blocks for LbL

Polyelectrolytes (PE) are polymers having ionizable functional groups on their repeating units. These polymers can be dissociated in two parts, the charged polyion and the counterions. There are different families of PE depending on the charge of the repeating units. These include polyanions and polycations. The first one is PE with negatively-charged functional groups and the second one is PE that contains positively-charged repeating units.

PE are classified in two classes: Strong PE and weak PE. A strong PE is characterized by the conservation of its charge over the entire pH range. In the opposite, a weak PE will be dissociated in a limited range of pH, in consequence its global charge is tunable as a function of the pH. At the pK_a of the ionizable group, the polymer will have half of the repeating units protonated and the other half deprotonated. A polyanion will be charged in solution of pH above the pK_a value and uncharged below and vice versa for a polycation [39].

For example, poly(sodium 4-styrenesulfonate) (PSS) is a strong polyanion with a $pK_a \approx 1.0$, and always bears negative charges [40]. Poly(allylamine hydrochloride) (PAH) is a weak polycation with a $pK_a \approx 8.0 - 9.0$, so it is charged at pH below pK_a value [29]. The branched polyethyleneimine (bPEI) is also a weak polycation and due to its branched structure, has a pK_a in the range of 7.9 to 9.6 [41].

1.3.2.2 Layer-by-Layer assembly methods

There are different methods to realize the LbL assembly. Figure 7 contains schematic representations of the three main methods used to perform LbL assembly. First, let's explore the principle of LbL through the immersive technique, using for example the assembly of two oppositely-charged PEs. In this method, the substrate is put in contact with different PE solutions to allow the adsorption of the material at each step. Between each solution of PE, there is a step of washing to remove the excess PE (non-adsorbed or loosely attached molecules) and also to avoid cross-contamination between the different solutions, as visible in Figure 7A. This assembly of two different PEs is called a bilayer (BL). If a second loop of the sequence is done, two bilayers (2BL) are obtained, and this pattern continues with additional loops (3BL, 4BL, etc.). Additionally, it is possible to consider a trilayer consisting of three distinct elements [29, 31–38].

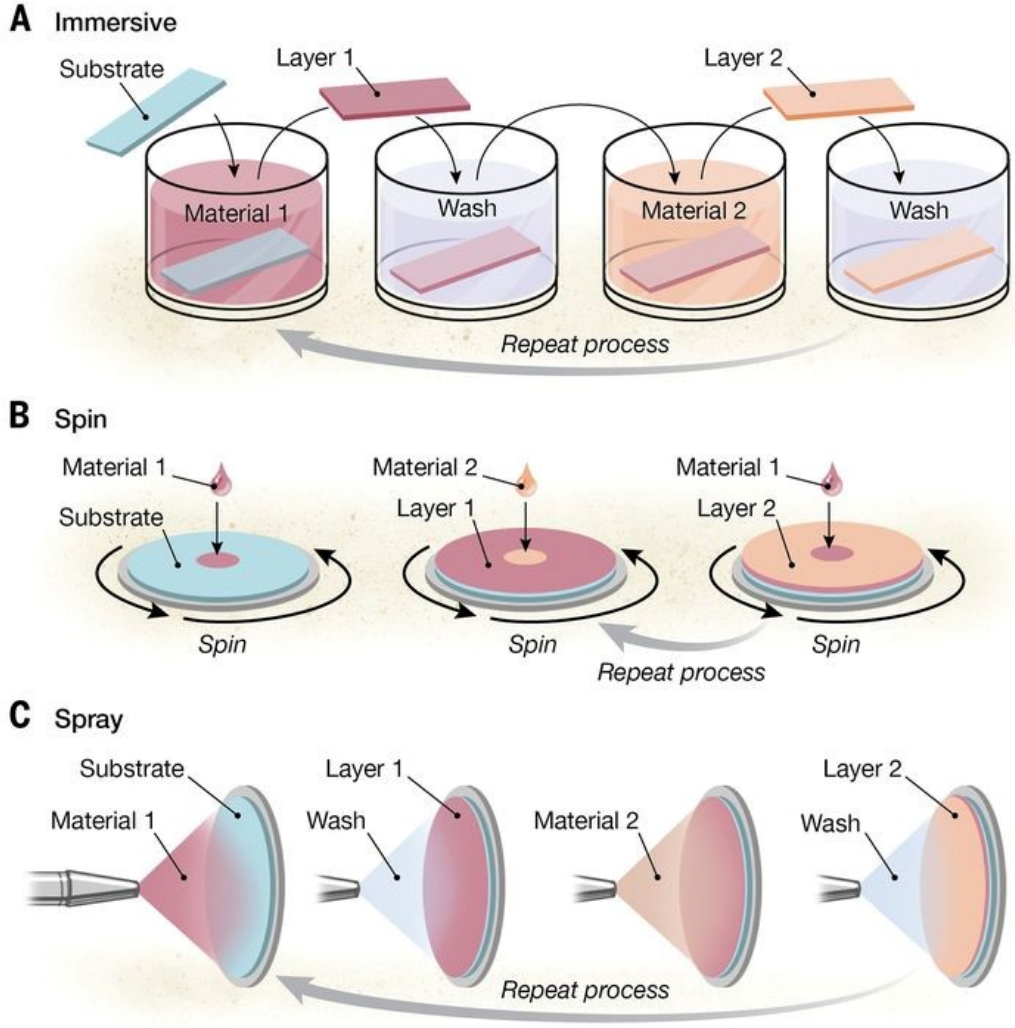

Figure 7: Schematic of LbL assembly techniques. Figure from [38].

Immersive assembly

The immersive assembly is the commonly used technique to build LbL assembly thanks to its simplicity of construction (Figure 7A) with a variety of materials and substrates. The films created by this method are characterized by thick, interpenetrated layers. To submerge substrates in solution, it requires the use of large quantities of solutions. This is the first disadvantage of the technique. The second main drawback of the method is that the process is time-consuming. Despite the availability of other methods, immersive assembly continues to be the preferred approach for coating complex 3D substrates and also allows the formation of the assembly in solution [38].

Spin assembly

The spin assembly uses rotating substrates to deposit layers and remove excess material (no washing step required) as shown on Figure 7B. The method allows the creation of thinner, more organized and stratified multilayers than immersive assembly. However, the technique is limited to flat surfaces. The technique is much faster and allows a better control of film thickness than with immersive technique [38].

Spray assembly

Spray assembly (Figure 7C) is realized by aerosolizing coating solutions and spraying them onto the substrate. The resulting films are well organized and stratified layers. This technique is highly relevant for industrial applications because of its fast and effortless approach to coating large and nonplanar substrates. [38] .

1.3.2.3 Use of LbL as enzyme immobilization technique

What about the use of LbL for enzyme immobilization? It is not easy to immobilize enzymes in relation to PE. Indeed, proteins, including enzymes, are more complex molecules composed of amino acids among which only some possess or can possess an electric charge. Proteins are therefore polyampholyte molecules. Polyelectrolytes, on the other hand, are composed of the repetition of sequences that are either positively or negatively charged. Both are charged molecules; however, unlike PE where the charge density is more homogeneous, proteins have a heterogeneous charge density with charged patches of different sizes. Moreover, proteins have a complex three-dimensional structure. Due to this heterogeneity, proteins are difficult to assemble in LbL. There is notably a lack of charge overcompensation. In other words, the use of proteins makes it difficult to obtain a sufficient charge at the surface in order to create a new layer. Enzymes, as well as proteins in general, are large polyampholyte molecules that can be assembled with suitable partner molecules using LbL assembly. In this case, the oppositely-charged PE corresponds to the PE having a charge opposite to the net charge of the protein. The use of such technique can allow the entrapment of great amounts of enzymes within a multilayer film, classifying this method as a physical immobilization. Additionally, the formed film can be reinforced through various chemical methods, such as crosslinking between enzymes and PE to reinforce the multilayers [29, 36].

1.3.2.4 Parameters affecting the characteristics of the LbL assembly

The LbL method has to be well-controlled. In fact, the characteristics of the final LbL assembly can vary greatly with small changes in extrinsic or intrinsic parameters. Physicochemical properties are extrinsic parameters. These include pH, ionic strength, temperature, adsorption time, sequence of assembly, and concentration of species. The intrinsic parameters are linked to the properties of the different building blocks of the multilayer, such as the nature and characteristics of PE or the protein [29, 31–38].

pH of the assembly solution

The pH of the assembly solution, especially when the assembly relies on electrostatic interactions between the different materials, is probably the most critical parameter to affect the assembly process. Indeed, in the case of using weak PE, their charge (density) will change with the pH according to their pKa. According to J. Borges & J.F. Mano [33], a very small change in pH can lead to major changes in the growth mechanism, thickness, level of interpenetration depths, and surface wettability of PE multilayers films.

Furthermore, the net charge of protein will change based on their IEP and the pH value. It will be positive in case of pH below IEP and negative in the contrary case. This modification will change the choice of PE for LbL as it requires an oppositely-charged PE. In addition, the gap between the pH and the IEP ($|pH - IEP|$) is correlated with the protein amount adsorbed on the multilayers [29, 33, 37].

Ionic strength

The ionic strength can impact LbL film build-up. When the ionic strength increases, Debye length decreases, which modifies the interactions between the charges in the system. Debye length represents the distance over which electrostatic interactions are significant. At short distances, ions associate with the charged elements of proteins and PE. At longer distances, electrostatic screening occurs, reducing the interactions between charged particles.

Furthermore, the conformation of PE is influenced by the salt concentration. With increasing salt concentration, electrostatic attraction diminishes, causing PE to adopt a more compact, coiled structure in the solution. Consequently, this favors the formation of polymer loops, facilitating the overcompensation of charges during the adsorption of new layers. However, achieving optimal film growth requires finding a compromise between pH and salinity [29, 31–38].

In this regard, Dubas and Schelnoff conducted a study on the growth of PE multilayers films using PDADMAC (poly(diallyldimethylammonium chloride)) and PAA (poly(acrylic acid)) or PSS. They observed that the thickness of the films depended on the salt concentration. Initially, there was a positive correlation between the salt concentration and the thickness of the film, but after reaching a concentration of 0.3 M, the film thickness rapidly decreased until complete dissociation of the multilayer when the salt concentration exceeded 0.6 M. In the case of a system containing PE and protein, the same observation is done. Until a certain value of salt concentration, the flexibility of the PE increases allowing a screening effect of lateral repulsion between proteins. This leads to an augmentation of protein adsorbed in the multilayer films. This behaviour after a threshold will give way to a decrease of electrostatic attraction, making the LbL growth unachievable [29,33,37].

In conclusion, ionic strength significantly affects the construction of LbL films by influencing the interactions between charges in the system, the conformation of the PE, and the film's stability.

Other parameters such as temperature, adsorption time, and species concentration in solution will not be discussed in this work.

1.3.2.5 Methods to characterize LbL assembly - focus on QCM-D

There are many methods for characterizing thin films, including atomic force microscopy (AFM), scanning electron microscopy (SEM), Fourier-transform infrared spectroscopy (FTIR), and X-ray photoelectron spectroscopy (XPS). Among these techniques, when it comes to LbL, quartz crystal microbalance with dissipation monitoring (QCM-D) is the one to choose before the others. QCM-D is a real-time and in situ surface-sensitive technique allowing the monitoring of thin film formation and layer properties [42]. Other techniques, such as ToF-SIMS and XPS, allow the characterization at the end of the assembly and of dried systems.

Quartz Crystal Microbalance (QCM) is a technique that detects the change of mass at the surface of a sensor with a nanoscale resolution. Indeed, mass resolution is of the order of ng/cm^2. Its extended version with dissipation monitoring, QCM-D, allows the recording of changes in energy loss to provide information about viscoelastic properties of thin films. It also gives information on the layer structure, at the sensor surface, such as swelling, collapse, crosslinking of the layer [29, 42, 43].

The QCM technique is based on the resonance of a thin quartz crystal disk placed between two electrodes and submitted to an applied voltage. The resonance frequency is a function of the mass and the thickness of the disk. A change of mass will modify the frequency of a value Δf. With QCM-D, a shift in dissipation ΔD is also measured. The dissipation can provide information regarding the viscoelastic properties of the assembled materials. The principle of QCM is illustrated on Figure 8 [29, 42, 43].

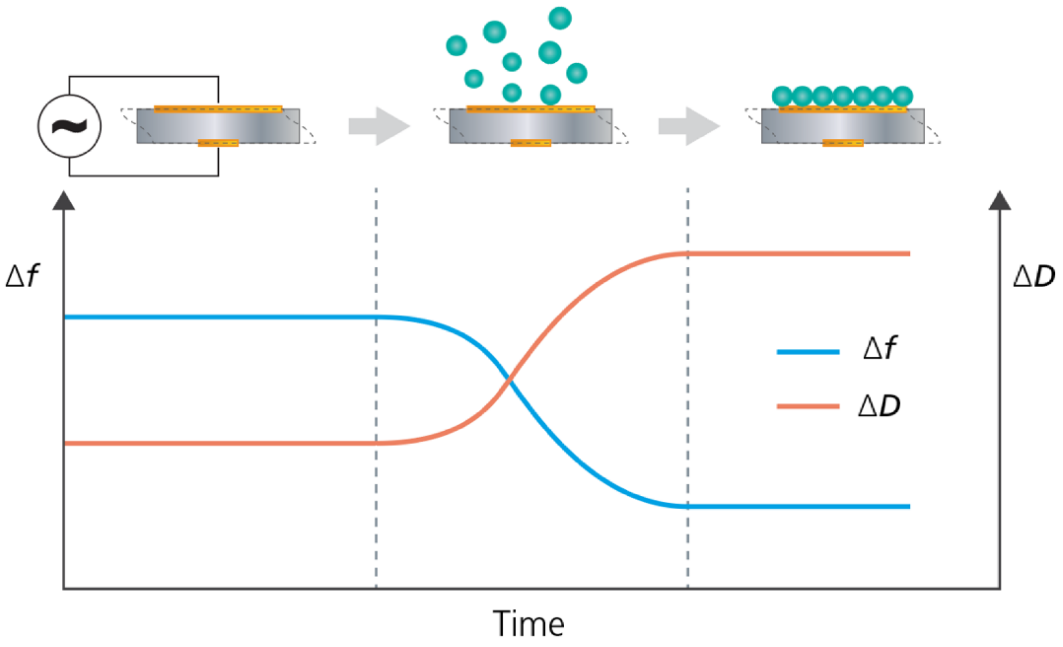

Figure 8: Illustration of QCM-D principle. Thin quartz crystal between two electrodes (depicted in orange) with an applied voltage. The molecular adsorption creates a shift in the frequency and the dissipation. Figure reproduced from [42].

To determine the mass, Δm $[ng \times cm^{-2}]$, adsorbed on the surface, calculations are performed based on the Sauerbrey equation 1.1 where C is the mass sensitivity constant depending on the quartz properties and n is the number of the used harmonic [29, 42, 43].

$$\Delta m = -C \times \frac{\Delta f}{n} \tag{1.1}$$

Some hypotheses have to be valid to apply Sauerbrey equation. A thin, rigid, and strongly adhering layer is assumed as well as a homogeneous film. Otherwise, the mass will be underestimated, other models exist in this case. As a rule of thumb, the Sauerbrey equation can be used if $\left|\Delta D_n / \frac{\Delta f}{n}\right| \ll 4 \times 10^{-4}$ Hz [43].

1.4 Protein - Polyelectrolyte Complexes

1.4.1 Principles

Protein-Polyelectrolyte complexes (PPC) are self-assembled materials resulting from the spontaneous interactions of complementary charges from protein and polyelectrolyte. The main driving forces are the electrostatic interactions between the surface charges of protein and charges present on polyelectrolyte chain. PPC formation is possible thanks to the liberation of counterions allowing a gain of entropy. The formation of PPC is often reversible due to the involvement of weak interactions. The PPC are generally defined by their polyelectrolyte-to-protein charge ratio due to the importance of electrostatic interactions [37, 44–50].

Polyelectrolyte - Enzyme complexes

Polyelectrolyte - Enzyme complexes [2] are a subclass of PPC where the protein is an enzyme. During the formation of PPC, either a loss or an enhancement of enzyme activity in PPC has been reported, depending on the enzyme as well as the type of PE used for complexation [50].

1.4.2 Protein - polyelectrolyte complex characteristics

The properties, the composition and the structure of PPC are highly determined by the ones of its components. The electrostatic interactions at the origin of PPC formation can be impacted by various factors, as illustrated in Figure 9, including the distribution, density, patchiness, and ionization state of ionizable groups present on protein surface and on PE chains [37, 44–50].

As a consequence, pH and ionic strength of the solution will influence the formation and the characteristics of PPC by modifying its fundamental components. To form PPC, the ionic strength has to be low enough for electrostatic interactions to occur at sufficiently long distance, and elements in solution must be charged, which depends on pH value [37, 44–50].

[2] In the literature, the abbreviation PEC is used at the same time for Polyelectrolyte - Enzyme complexes and for Polyelectrolyte (- Polyelectrolyte) complexes. Thus, abbreviation will not be used and here only the general notion of PPC will be conserved.

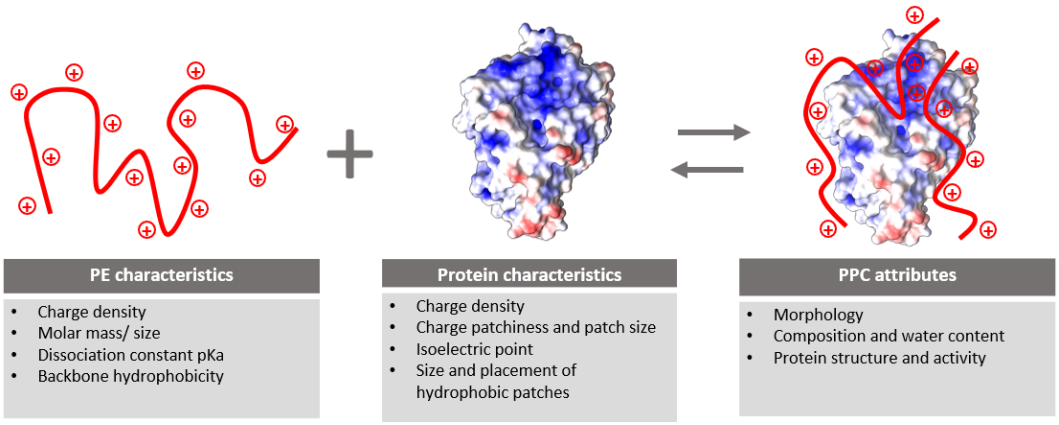

Figure 9: Illustration of PPC with key characteristics of its components that influence PPC attributes. Inspired from [44].

The size as well as the concentration of protein and PE will also modify the state of PPC. The PPC can be classified into 2 groups: soluble PPC and aggregative PPC. Soluble PPC are characterized by a size smaller than 100 nm and an excess charge resulting in a dispersion in aqueous medium. Aggregative PPC possess a size bigger than 100 nm, and tend to form non-soluble aggregates in solution [49]. As illustrated in Figure 10, with a low concentration of PE, the PPC tend to aggregate due to charge neutralization between PE and proteins. A higher concentration will cause a diminution of the attraction between PPC.

1.4.3 PPC as building block for LbL

In the context of LbL assembly, PPC could be used as a building block to improve the adsorption of enzyme. On the one hand, enzymes would benefit from a more uniform load thanks to the complexation with PE. On the other hand, according to literature, the use of PPC in LbL enables the formation of highly hydrated multilayers allowing an enhancement of the enzymatic activity of immobilized enzymes in standard LbL films [37, 50]. An illustration of LbL assembly with enzyme and PPC is shown in Figure 11.

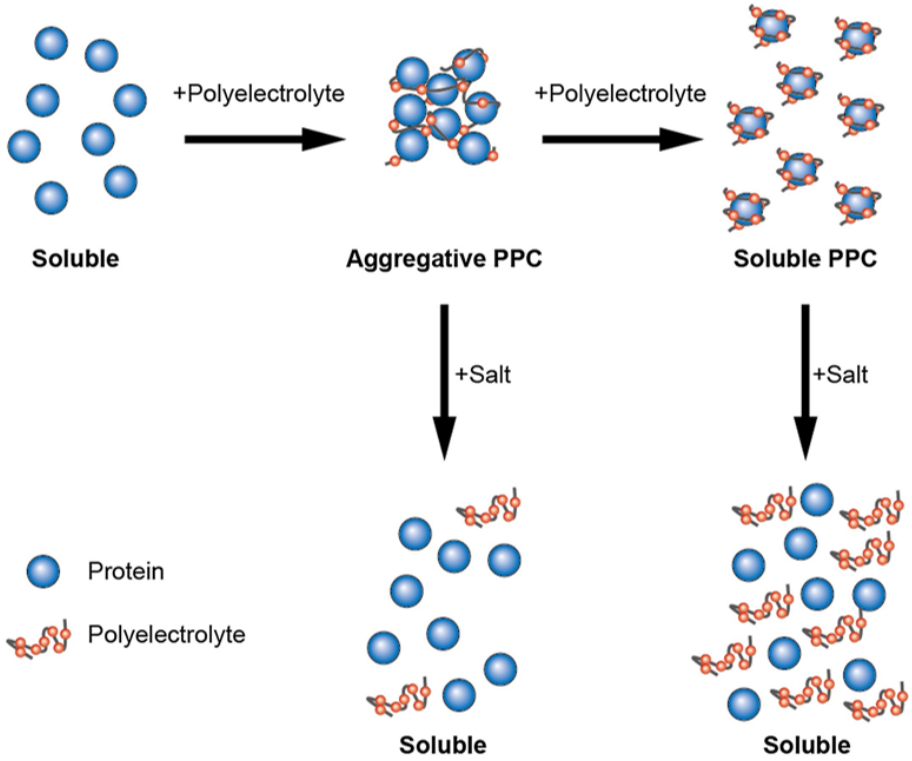

Figure 10: Illustration of Aggregative and Soluble PPC with the impact of polyelectrolyte and salt addition. A low concentration of PE allows the creation of aggregative PPC, but their excess induces the creation of soluble PPC. The addition of salt induces complex dissociation. Figure reproduced from [49].

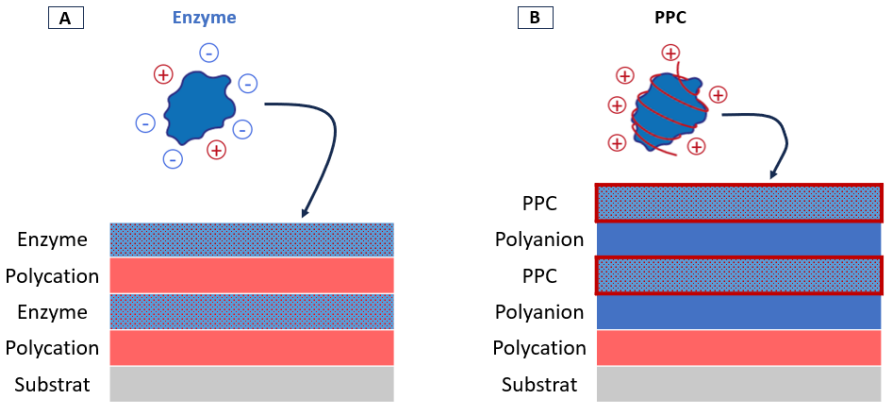

Figure 11: Schematic representation of LbL films with enzyme and PPC. (A) LbL assembly with enzyme (B) LbL assembly with PPC. A pattern is used to illustrate the non-uniform distribution of charge across the surface of the enzyme.

1.4.4 Methods to detect and characterize PPC

The detection and characterization of PPC can be accessed by numerous techniques as shown in Figure 12. The following section describes the principles behind some of them.

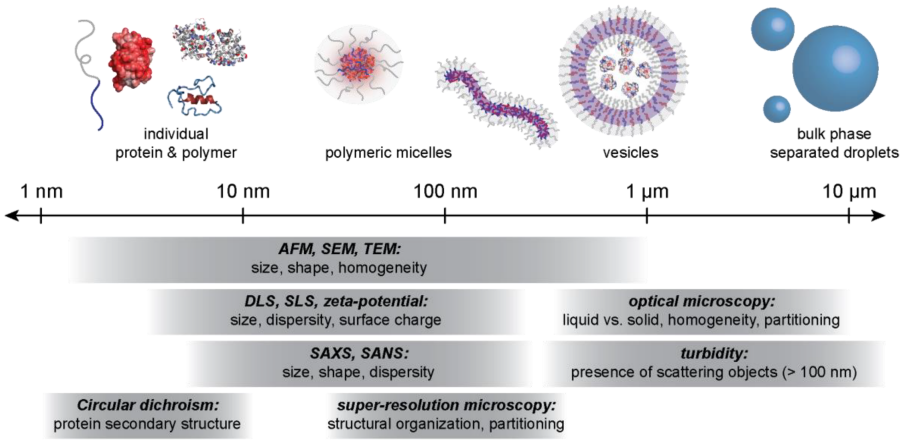

Figure 12: Common methods for PPC characterization and imaging. Figure from [47].

1.4.4.1 Turbidimetry

Turbidimetry is a method that measures the loss of intensity of a light beam transmitted through a sample. The decrease in intensity is due to light scattering by unsoluble species in suspension. The turbidity will increase with the particle size and therefore be used as an indicator to PPC formation. However, other factors such as shape, concentration, and polydispersity can influence the turbidimetry measurement [29, 44, 51–54].

1.4.4.2 Dynamic light scattering

Dynamic light scattering (DLS) is a measurement technique based on the Brownian motion of dispersed particles in liquid allowing the analysis of size distribution of these particles. As shown in Figure 13, a laser beam passes through the suspension of particles. The scattered light intensity is measured across time. In case of small particles, their rapid movements will induce rapid fluctuations of intensity. It is the opposite for larger particles. This provides a correlation function that will give, after mathematical analyses, the diffusion coefficient. By applying the Stokes-Einstein equation, the hydrodynamic radius can be found, defining the

diameter of a hard spherical particle that diffuses at the same rate as the detected element [29, 55–57].

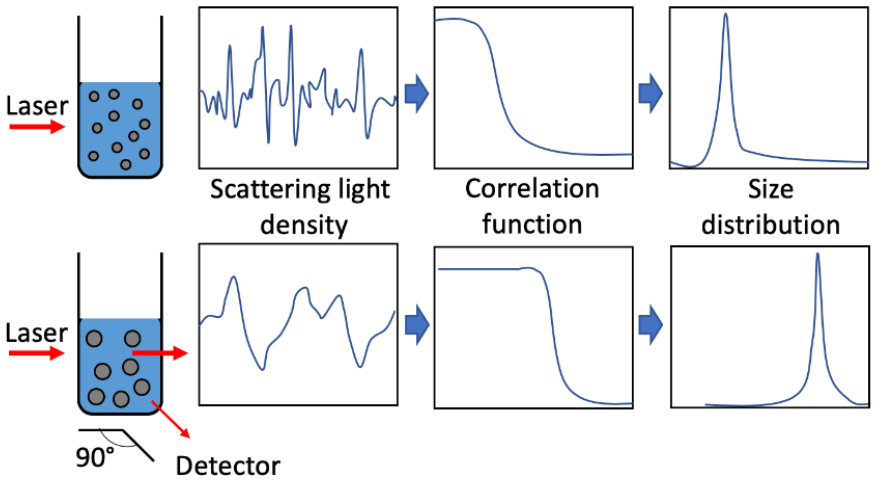

Figure 13: Schematic of the DLS principle for small and large particles in suspension. Figure from [29].

DLS will give the mean size of particles in suspension and the polydispersity index (PDI). PDI is a value between 0 and 1 based on the size, and is determined by evaluating the standard deviation of the distribution with respect to the mean size. PDI gives information on the heterogeneity of a sample. A lower value indicates a narrower size distribution and a monodisperse sample, whereas a higher value suggests a broader size distribution and a more polydisperse sample.

1.4.4.3 Zeta potential measurement

Zeta (ζ) potential, i.e. the eletrokinetic potential, is the electrical potential at the interface between mobile fluid (diffuse layer) and stationary fluid close to the surface (stationary layer).

Figure 14 illustrates a scenario where a negatively-charged particle is suspended in a solution. In such cases, the distribution of ions in the solution undergoes modifications. Specifically, certain positively-charged ions tend to accumulate around the charged particle, forming what is known as the Stern layer. Beyond this layer, there exists a diffuse layer, where ions are loosely bound and dispersed throughout the solution. As a result, the solution can be effectively characterized

by two distinct layers: the stationary layer and the diffuse layer. The ζ-potential is measured by analyzing the movement of particles due to the application of a voltage and is expressed in millivolts (mV) [29, 58, 59].

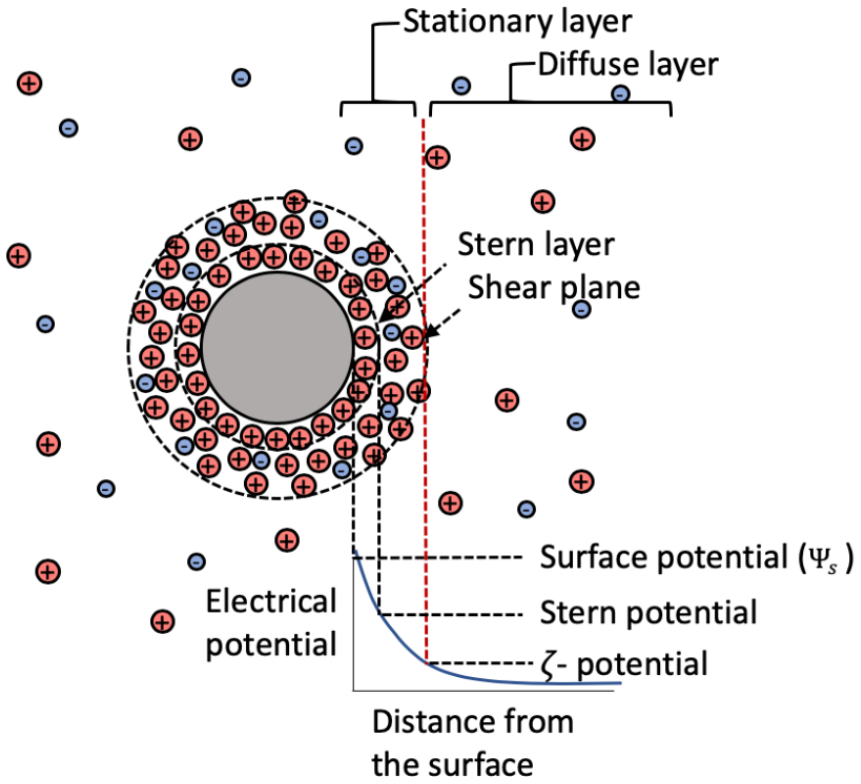

Figure 14: Scheme of the electrical double layer at the solid-liquid interface. Figure from [29]

The zeta potential measurement gives qualitative information on surface charge of PPC through the value of surface potential. By knowing the charge, the choice of an oppositely-charged PE for LbL can be done. Zeta potential measurement also allows a more complete characterization of these.

1.5 Objectives & Strategy

The final objective of the project is to develop thin films of immobilized laccase for wastewater treatment. In this study, the focus is made on the immobilization of laccase through the use of PPC. The objectives of this study can be divided into two mains separated parts, as shown in Figure 15.

The first one consists of obtaining and characterizing Laccase-PE complexes (LPC). To meet these objectives, different PE as well as laccase-PE concentration ratio were initially screened using turbidity measurements to detect the presence of LPC. After this screening step, the focus was placed on LPC composed of laccase and PAH, a polycation. The characterization of this LPC has been realized thanks to different methods, such as turbidimetry (A_{350}), dynamic light scattering (DLS) with the measurement of the size and the polydispersity index (PDI) and zeta potential measurement. A systematic control with laccase alone (without PE) has been done. Furthermore, after the formation of the desired complexes in different conditions, some of them were centrifugated, collected and resuspended. The amount of protein as well as the laccase activity found in the initial solution, pellets, and supernatants were evaluated using BCA and activity assay respectively, to be compared with non-complexed laccase.

The second objective consists into the integration of the previously formed LPC into Layer-by-Layer assembled films using another oppositely-charged PE, PSS in this case. The assembly of PSS and LPC was initially monitored using QCM-D to verify the successive formation of the layers. Then, the multilayers were assembled in polystyrene 96 well plates to evaluate their resulting activity and stability over time. The assembly in plate allows the comparison with an initial assembly made of laccase and bPEI.

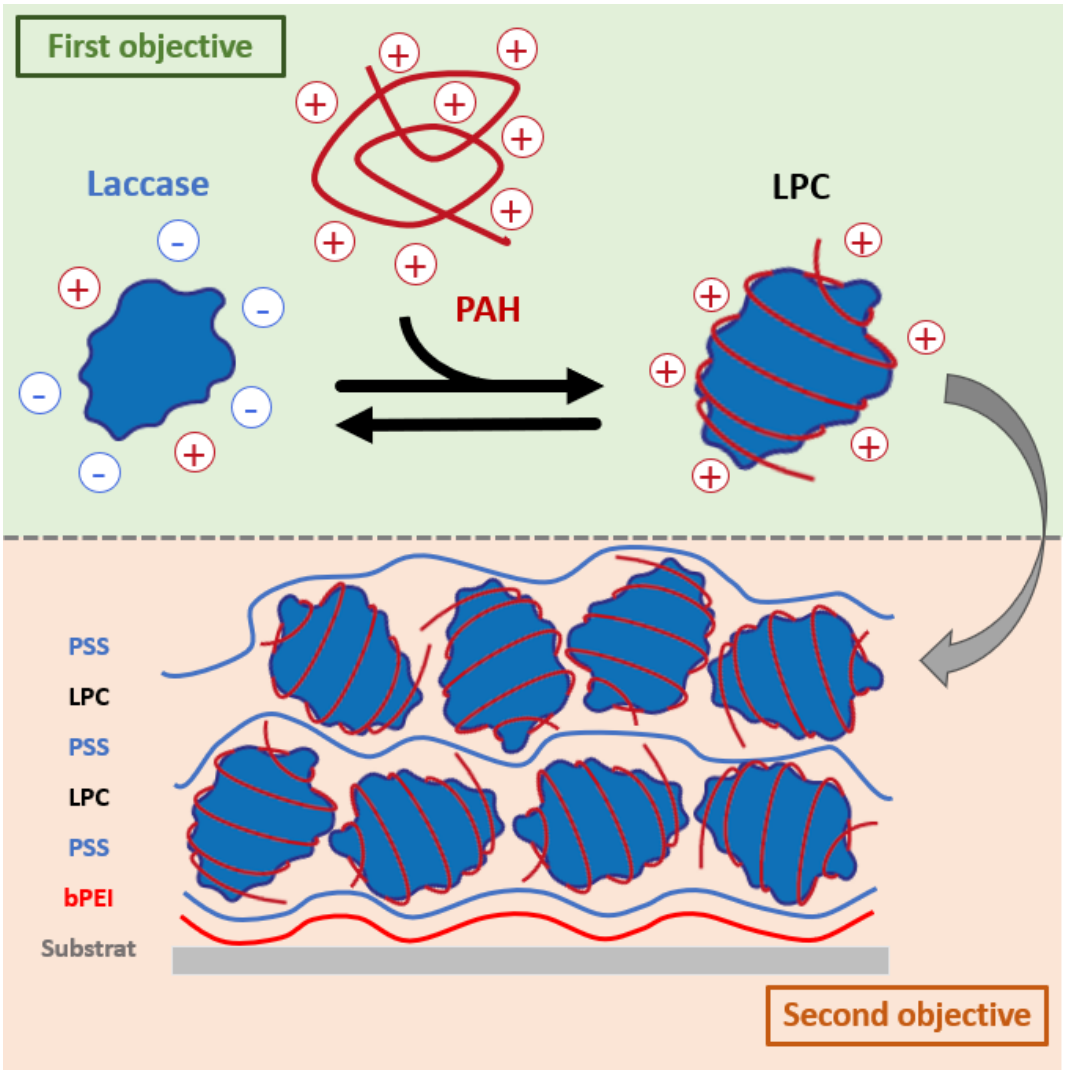

Figure 15: Schematic representation of objectives. First objective: LPC formation and characterization. Second objective: Complexes immobilization using LbL assembly.

Chapter 2

Methodology

2.1 Materials

The chemicals species and kit used in this work are presented in Table 1. The chemical structures of PE used are shown in Figure 16.

Table 1: Chemical species and kit used in the experiments.

	Abbreviation	Supplementary information	Supplier	Reference
ENZYME				
Laccase (from Trametes versicolor)	LAC	Powder Mw ~ 56 kDa	*Sigma-Aldrich*	38429-10G
POLYELECTROLYTEs				
Polyethylenimine, branched	bPEI	Powder Mw ~ 25,000 g/mol	*Sigma-Aldrich*	408727
Poly(allylamine hydrochloride)	PAH	Powder Mw ~ 17,500 g/mol	*Sigma-Aldrich*	283215 - 5G
Poly(diallyldimethylammonium chloride)	PDADMAC	20 wt% in H_2O Mw ~ 200,000 - 350,000 g/mol	*Sigma-Aldrich*	409022 - 1L
Poly(sodium-4-styrene sulfonate)	PSS	30 wt% in H_2O Mw ~ 70,000 g/mol	*Sigma-Aldrich*	527483-1L
ASSAY's				
2,2'-Azino-bis(3-ethylbenzothiazoline -6-sulfonic acid)	ABTS	Tablets of 10 mg	*Sigma-Aldrich*	10 102 946 001
Bicinchoninic acid	BCA	Kit	*Thermo scientific*	23225
BUFFER				
Sodium acetate		Powder	*VWR*	27653.292
Acetic acid		$\geq$ 99.7%	*Sigma-Aldrich*	695092
OTHERs				
Glutaraldehyde	GLU	25% in H_2O	*Sigma-Aldrich*	G6257 - 100 ML
Sulfuric acid	H_2SO_4	$\geq$ 95%	*Fisher Scientific*	S/9240/PB15
Hydrogen peroxide	H_2O_2	30%	*VWR*	23619.297

It is important to note that two PAH powders were used. The first powder, which came from an older stockpile, had a yellowish color and a crystalline appearance. On the other hand, the second powder, obtained more recently, was characterized by its white powdery texture. To differentiate them in further sections, old and new PAH will be referred to as PAH^{old} and PAH^{new} respectively.

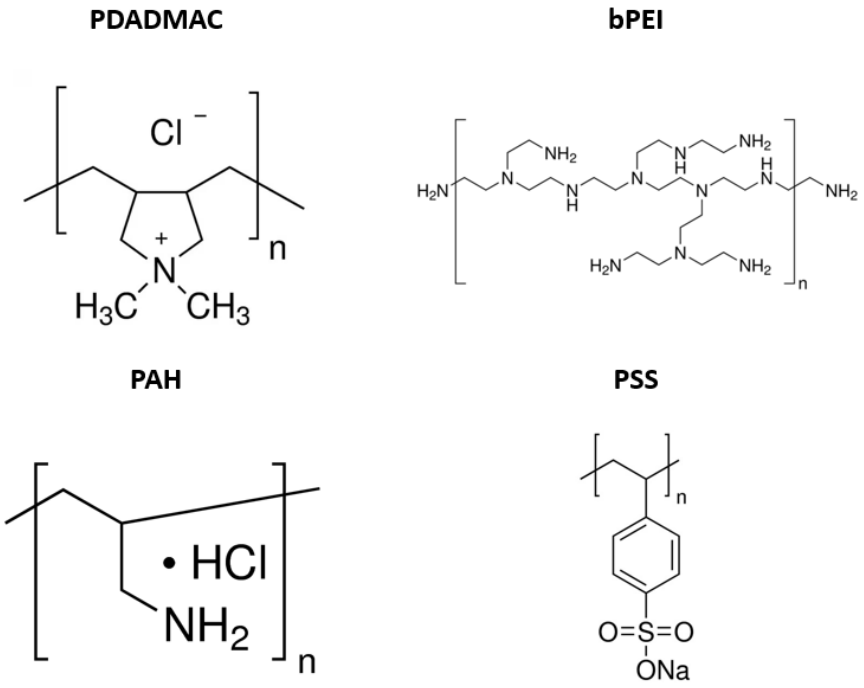

Figure 16: Chemical structures of PE.

Since protein and polyelectrolyte charge is a crucial characteristic in the context of complex formation, Table 2 provides relevant pieces of information concerning the charge of the different used materials, including the sign of their charge at a pH of 7, as most experiments were carried out in this condition.

Table 2: Key informations on polyelectrolytes and protein. [21, 29, 40, 41, 60]

Polyelectrolyte	Strength	pKa	Charge at pH 7
Polyethylenimine, branched	Weak	∼7.9-9.6	Positively charged
Poly(allylamine hydrochloride)	Weak	∼8.0-9.0	Positively charged
Poly(diallyldimethylammonium chloride)	Strong	High	Positively charged
Poly(sodium-4-styrene sulfonate)	Strong	∼1	Negatively charged
Protein	**Strength**	**IEP**	**Net charge at pH 7**
Typical fungal laccase	Weak	∼ 4	Negatively charged

2.2 Methods and Equipment

2.2.1 Laccase enzyme assay

2.2.1.1 Principle

Laccase activity can be determined thanks to using one of its substrates, 2,2'-azino-bis(3-ethylbenzothiazoline-6-sulfonic acid) (ABTS). The oxidation of ABTS by laccase, as shown in Figure 17, generates ABTS$^{\bullet}$, a radical species that strongly absorbs light at a wavelength of 420 nm. Solution becomes greener through oxidation of ABTS [20, 61–63].

2.2.1.2 ABTS$^{\bullet}$ calibration

A calibration was performed to convert A_{420} into µmol of oxidized ABTS. Solutions containing varying concentrations of ABTS ranging from 0 to 0.4 g/L were prepared. 20 µL of laccase were added to each solution to reach complete ABTS oxidation overnight. A_{420} of 200 µL of each solution was measured twice in 96-well plate using SpectraMax iD3 (Molecular Devices). Experiment was repeated 3 times. The calibration equation is given in Figure 18.

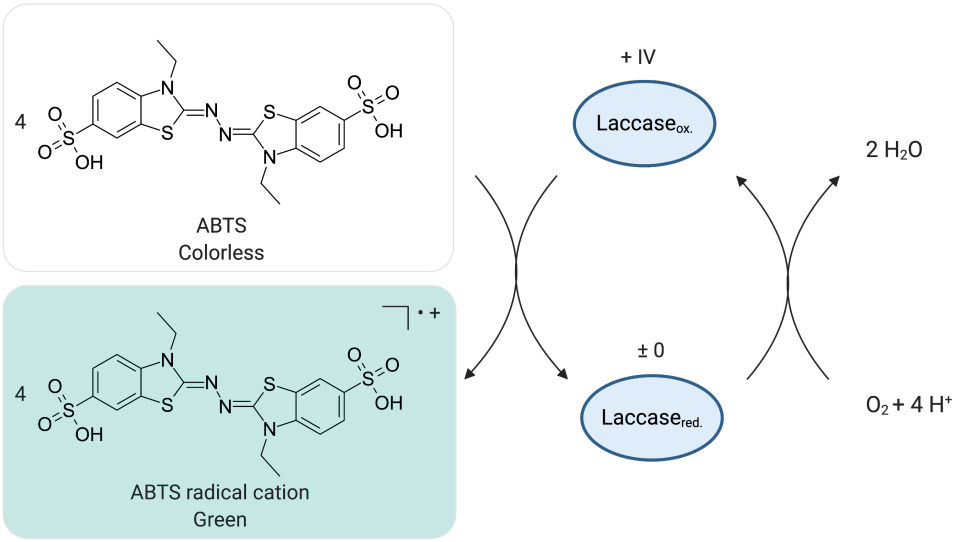

Figure 17: Oxidation of ABTS by laccase. The colorless solution turns green when the ABTS is oxidized. A UV/Vis−spectrocopy measurement at 420 nm can be performed, allowing the quantification of the activity of laccase. Figure from [63].

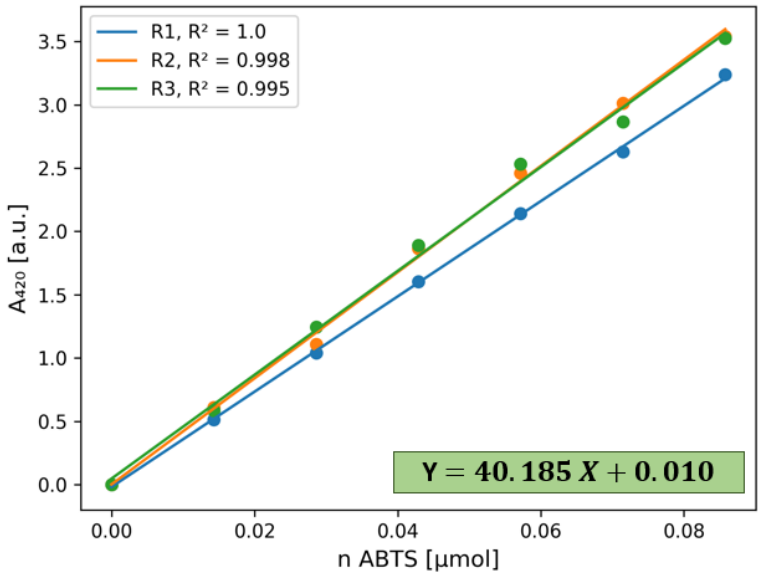

Figure 18: Calibration curve of ABTS. Final A_{420} of oxidized ABTS solutions for the 3 replicates with their coefficient of determination, R^2. The calibration curve equation is the mean of the 3 replicates (R1/R2/R3).

2.2.1.3 Activity measurement

Enzyme / complexes activity measurement

To compare different solutions containing free or complexed enzymes, based on their enzymatic activity, the measurements were carried out as follows. The measurement of enzymatic activity was done with 20 µL of solution to be analyzed and 180 µL of ABTS (0.2g/L) in acetate buffer (0.05M pH 5). A microplate reader, SpectraMax iD3 was used to measure A_{420}. Conversion from [A_{420}/min] into enzymatic unit U, [µmol$_{ABTS}$/min], was performed using the calibration curve in Figure 18.

Multilayers activity measurement

Activity measurement for multilayer assemblies is similar. The first step, Step 1, is removing the solution in the wells to remove loosely attached elements. Step 2 corresponds to the addition of 200 µL of ABTS in each well containing multilayers. After that, the reading of the plate at A_{420} can be realized (Step 3). At the end of the reading, the solution has become green as ABTS is oxidized. Before storing the plate, 2 washes were done to remove the whole solution (Step 4 & 5). A wash consists of adding 100 µL of water at pH 7 (medium used to create the assembly)

in wells and shaking the plate during 30 seconds. After the last washing step, the medium was replaced by water at pH 7. Finally, the plate was stored in the fridge until the next reading (Step 6). A schematic representation of the protocol is shown in Figure 19.

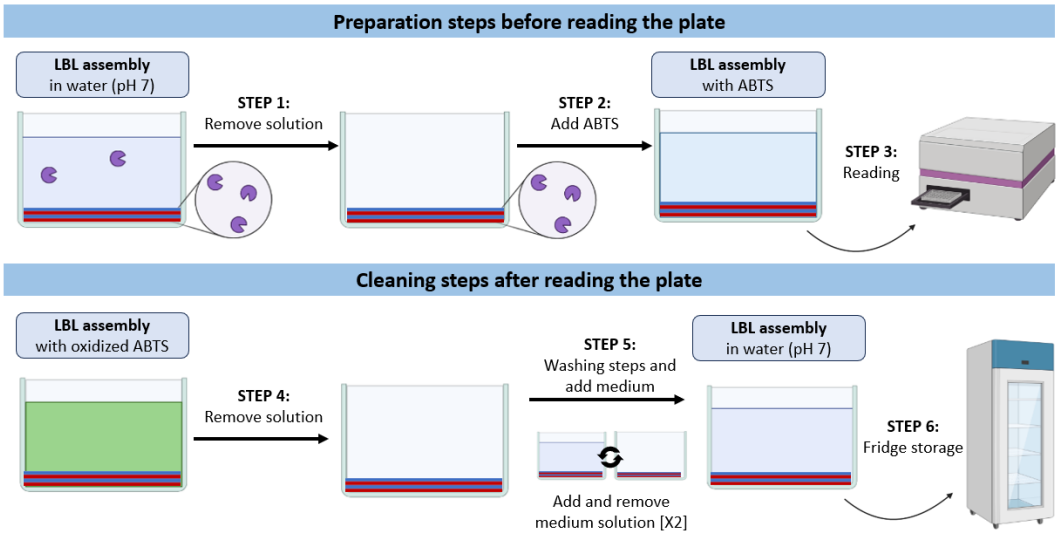

Figure 19: Illustration of activity measurement for laccase in LbL films (for one well). LbL films are represented by the red and blue lines. The first part of the figure contains the different steps to realize before measuring A_{420}. After the measure, the oxidized ABTS gives a green color to the solution. The second part includes the steps before restocking the plate in refrigerator.

2.2.2 BCA Protein Assay

2.2.2.1 Principle

Bicinchoninic acid (BCA) assay is a popular colorimetric method allowing the detection and quantification of protein in solution. The protein concentration in the solution should be between 20 $\mu g/mL$ and 2 mg/mL for good quantification. The BCA assay through two reactions produces a purple-colored complex that can be measured by spectrophotometry at 562 nm (A_{562}) (Figure 20). The first reaction is a reduction by amide bonds found in proteins (as Laccase) of Cu^{2+} ions, present in the BCA reagent to Cu^{+} ions. The BCA will then react with the Cu^{+} ions and produces the purple complex, it is the second reaction [29, 64–66].

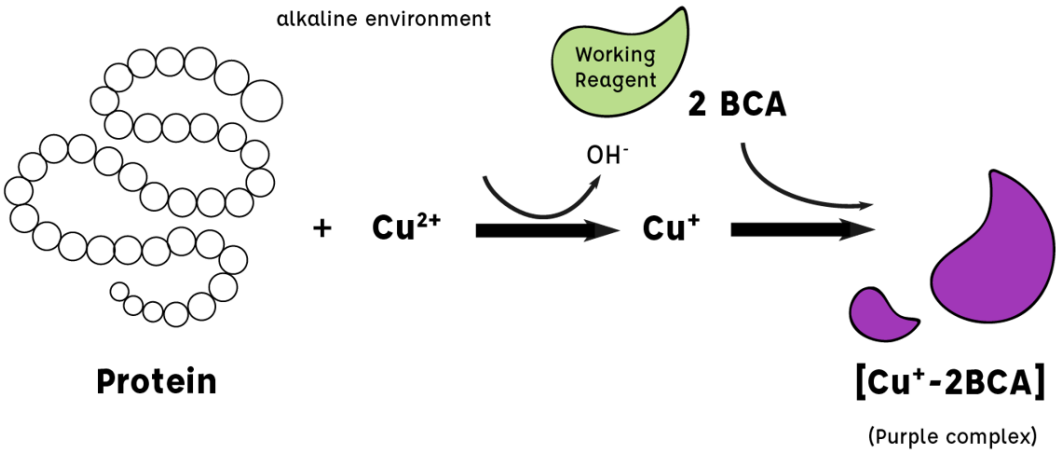

Figure 20: Schematic representation of the two chemical reactions of BCA assay. Protein in alkaline environment will reduce the Cu^{2+} available in the reagents. The Cu^{+} will form, with 2 molecules of BCA, a purple complex. Modified picture from [64].

2.2.2.2 Calibration curve and sample measurement

To obtain a quantitative value of protein concentration, a calibration curve is needed. For the following experiments, 20µL of solution to be analyzed was added to a mixture of BCA reagent of the $Pierce^{TM}$ BCA Protein Assay kit from Thermo Fisher Scientific. The mixture was composed of BCA reagent A and BCA reagent B in a volume ratio 50:1. In a 96-well plate, 200µL of mixture was added to 20 µL of studied solution. The plate is incubated for 30 minutes at 60°C and then cooled to room temperature. 180 µL of each well was transferred in a new plate before reading the absorbance at 562 nm (A_{562}). The calibration curve was done with the albumin standard from the kit with concentrations ranging from 0 to 0.2 g/L. Each experiment has its own calibration curve, an example is shown in Figure 21. The laccase, due to its lack of purity, has not been used to establish the curve.

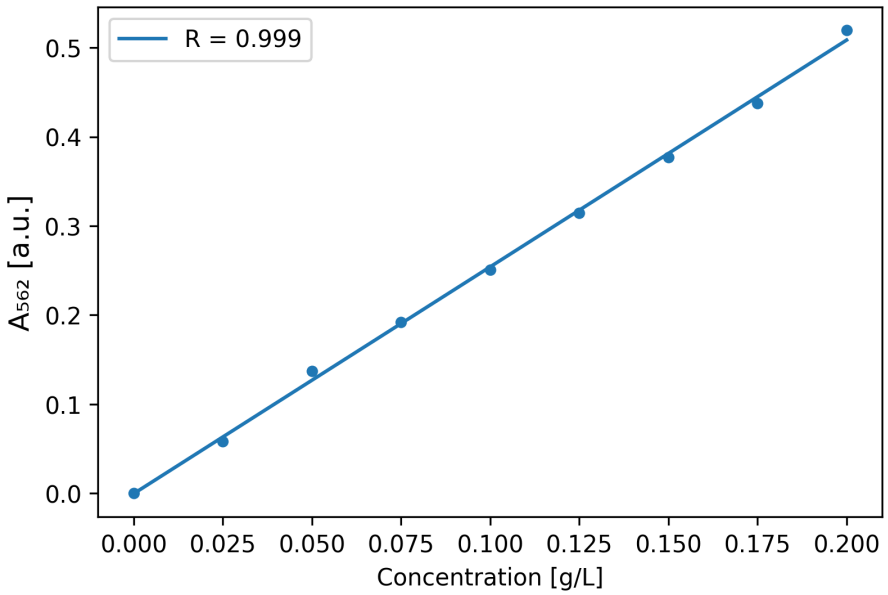

Figure 21: Example of calibration curve for BCA. A_{562} of BCA assay on albumin with the coefficient of determination, R^2. Each symbol is the mean of 2 or 3 values depending on the experiments.

2.2.3 Complex formation and characterization

The laccase - polyelectrolyte complexes (LPC) created in the following experiments were made of laccase and PAH. They are defined by their mass ratio of PAH over laccase. The complexes were always formed at a constant laccase concentration of 0.5 g/L (g of powder). Therefore PAH concentration in the sample was adapted to reach the desired ratio. LPC are referred to by their mass ratio in indexes. For example, LPC with a mass ratio 0.04 is noted $LPC_{0.04}$. The theoretical charge ratio, which is conventionally used for complexes, was not retained in this study due to poor laccase purity in the used powder.

The following section will give the main information on techniques used to detect and characterize the formed LPC. Each experiment has also been realized on laccase alone to obtain a reference value or behaviour.

2.2.3.1 Turbidimetry

In the different experiments, 200 µL of solutions containing various types of PE as well as various PE/protein ratios were placed in 96 well plates. A_{350} was measured by plate reader SpectraMax iD3 to detect LPC formation.

Some experiments have been performed with 900 µL in 24 well plates. For them the A_{350} was measured across time to observe the evolution of LPC behaviour.

2.2.3.2 Dynamic light scattering

Size and PDI were measured using a Zetasiser NanoZS (Malvern Instruments Ltd., UK) in ZEN0040 cuvette. The measurements were performed 3 times. The experimental parameters are available in Table 3.

2.2.3.3 Zeta potential

Zeta potential was measured by using a Zetasiser NanoZS (Malvern Instruments Ltd., UK) in DTS1070 cuvette. The measurements were performed 5 times. The experimental parameters are available in Table 3.

Table 3: Zetasizer parameters for DLS and Zeta potential measurements.

Size distribution and PDI	
Machine parameters	
Cell	ZEN0040
Material	Protein
Dispersant	Water
Measurement parameters	
Temperature	25°C
Equilibrum time	10 s
Number of runs	40
Run duration	1.68 s
Number of duplicate	3

Zeta potential	
Machine parameters	
Cell	DTS1070
Material	Protein
Dispersant	Water
Measurement parameters	
Temperature	25°C
Equilibrum time	10 s
Minimum number of runs	10
Maximum number of runs	100
Number of duplicate	5

2.2.3.4 LPC isolation using centrifugation

To determine the formation of complexes with laccase, centrifugation has been used. Centrifugation of a solution allows the separation of particles according to their size, density and shape. Therefore, centrifugation was used to separate a fraction of the created LPC, in particular aggregative LPC characterized by greater size and mass. Analysis with BCA assay and enzymatic assay have been done to characterize isolated elements. These tests will determine whether at least a fraction of the complexes created are indeed composed of laccase and not the other elements making up the laccase powder.

A large range of accelerations has been tested between 100g and 15,000g during different periods of time such as 5 minutes, 10 minutes and 1 hour (Heraeus multifuge X1, Thermofisher Scientific). The analyzes have been performed on 3 samples collected at different times during the experiment. The first one is the initial solution, collected before centrifugation. The second one consists in the pellet which was resuspended in an equivalent volume as the initial solution. The third one is the supernatant solution. The protocol is detailed on Figure 22.

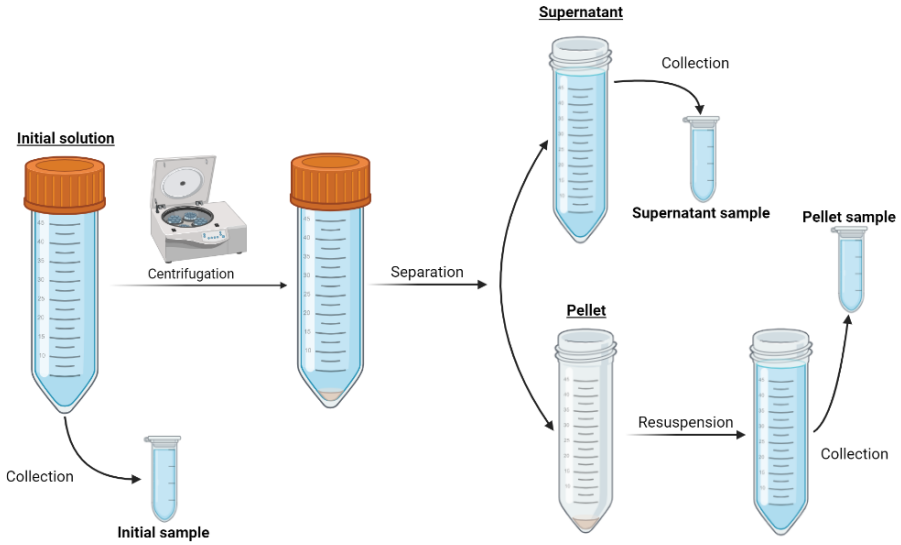

Figure 22: Representation of the centrifugation protocole.

2.2.4 Layer-by-Layer assembly

Second objective of the project was to use LPC as building blocks in layer-by-layer assembly, using PSS as counter-anion. The new system, referred to as [PSS - LPC] was compared with the initial LbL system composed of bPEI and laccase named [bPEI - LAC]. A schematic representation of the two assemblies is shown in Figure 23. The assembly was initially monitored using QCM-D to evaluate the success of the assembly of the different materials. Then the multilayers were assembled in 96 well plate to evaluate their enzymatic activity as well as their stability. The common used solutions were bPEI (0.5g/L), PSS (0.5g/L), LAC (0.5g/L) and $LPC_{0.04}$. The various solutions were prepared with pure water adjusted to pH 7 with NaOH and an ionic strength close to 0 mM as solvent.

2.2.4.1 Quartz Crystal Microbalance with Dissipation Monitoring

For the QCM experiments, the Q-Sense E4 system from Q-Sense (Stockholm, Sweden) was used. It contains 4 channels allowing the measurement of 4 conditions at the same time. The sensor used was quartz crystal sensor coated with gold (QSX 301) placed in flow module. The different elements are visible on Figure 24. The flow rate of the solutions was constant with a value of 20 µL/min, the mass sensitivity constant C equals 17.94 $[ng \times cm^{-2} \times Hz^{-1}]$ and the 7^{th} harmonic was used. Theoretical film thickness was estimated by approximating the volumic mass at 1 g/cm^3 as multilayers contain a high fraction of water and the volumic mass of their constituents is not much higher than the one of water.

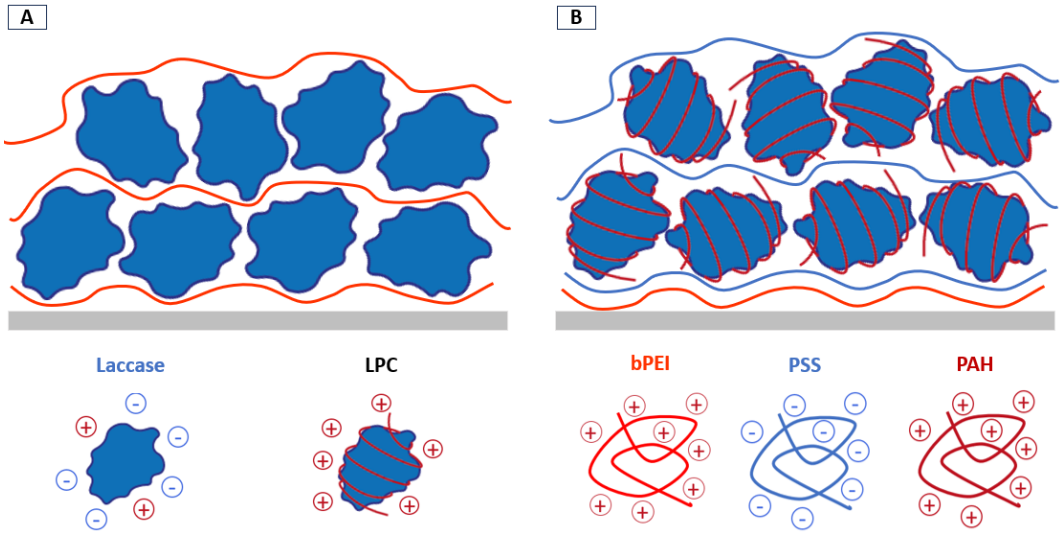

Figure 23: Schematic illustration of [bPEI - LAC] and [PSS - LPC]. (A) On a substrate, depicted in gray, is present a bPEI anchoring layer followed by $[\text{bPEI-LAC}]_2$ and finally a bPEI is placed on top. (B) After the anchoring layer, PSS layer is placed before the $[\text{PSS - LPC}]_2$. A final layer of PSS is placed on the top.

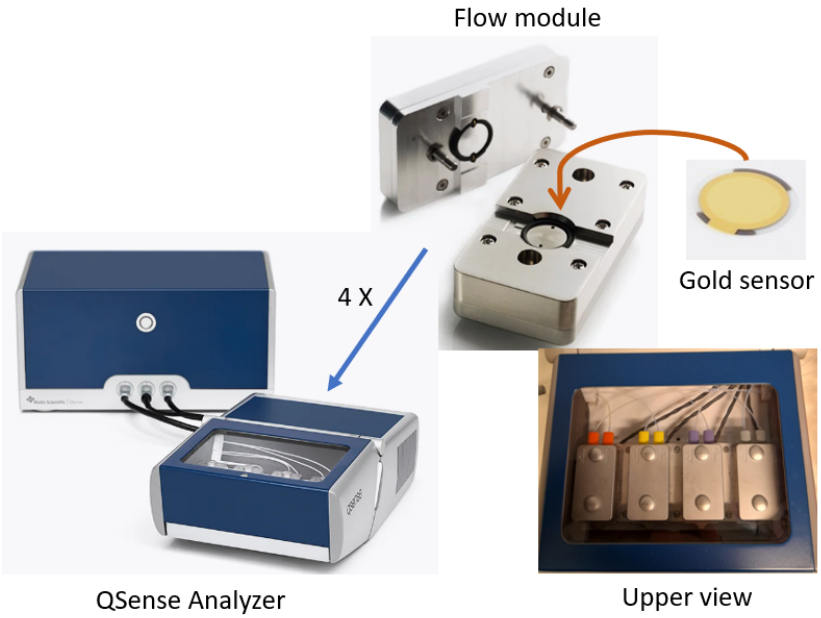

Figure 24: Elements of the QCM instrument. Schematic based on images from Biolin Scientific [42]

2.2.4.2 Assembly in 96-well plate

After the confirmation of successful LPC assembly by QCM, the following step consisted in the formation of LPC-PSS multilayers in 96 well plates, to evaluate their surface activity, as described in section 2.2.1.3.
Each well was initially functionalized with a bPEI anchoring layer. To do so, 100 µL of bPEI were added for 5 minutes. Between each adsorption step, 2 washings were performed during 30 seconds with 100 µL of water solution at pH 7.
The creation of bilayers can now begin, the following steps describe the protocol to be carried out for one bilayer.
At the beginning, 100 µL of polyelectrolyte (bPEI / PSS) is added and left for 5 minutes. After the washes, laccase or LPC are added and left for 20 minutes. A new bilayer can be built after washes by repeating the steps.
The different assembled systems are referred to using a standard notation: [Polyelectrolyte - Protein component]$_{\text{number of bilayers}}$. The most commonly used here are [bPEI - LAC]$_3$, [bPEI - LAC]$_6$, [PSS - LPC]$_3$ and [PSS - LPC]$_6$.
The activities of the different assemblies have been evaluated on the day of the assembly referred to as Day 0, one day after (DAY 1), DAY 3, DAY 6, and DAY 10. Each assembly has been done 5 times and the experiment has been reproduced 3 times.

Chapter 3

Results & Discussion

Chapter **Results & Discussion** is separated into 3 different parts.

PART 0, investigative experiments, retraces different preliminary experiments before the real construction of LPC. Given the many different factors influencing complexes formation (section 1.4.2) such as pH and ionic strength of the assembly medium, these preliminary experiments allowed us to identify the optimal medium conditions to be used for the rest of our experiments. Furthermore, this section also includes an investigation on laccase surface charge and its IEP.

PART I is focused on the first objective. It presents the formation of LPC with PAH^{old} and PAH^{new} and their characterization. Turbidimetry, DLS and ζ-potential measurements are used in this context and also isolation by centrifugation. This part consists into the 1^{st} objective of the project, namely the formation and characterization of Laccase-Polyelectrolytes Complexes. In accordance with results included in PART 0, PAH was selected arbitrarily as the candidate for the formation of these complexes. Turbidimetry was used to screen and detect the formed LPC, while DLS and zeta potential measurements allowed to characterize their size and charge, respectively. Finally, a fraction of the formed complexes was isolated using centrifugation to evaluate their activity and their protein content. This isolation allows to identify if LPC are composed of laccase and not of impurities present in laccase powder.

PART II gathers the experiments to meet the second objective on the LbL assembly. The first section checks whether assemblies with LPC are correctly assembled, with a comparison with assembly composed of free laccase. The second section contains experiments on the stability of the different assemblies based on the evolution of their enzymatic activity. Enzymatic activity measurement and QCM-D are the main techniques used in this part.

3.1 PART 0: Investigative experiments

3.1.1 Polyelectrolytes screening by turbidimetry

The first challenge was to select a polyelectrolyte that could effectively complex laccase and form LPC. This first experiment therefore consisted in a turbidimetry screening of different polyelectrolytes mixed with laccase at varying mass ratios ranging from 0.1 to 1.0. Absorbance measurements were performed at a wavelength of 350 nm on 200 µL of each PE/lac mix in 96 well plate. Each solution was in an acetate buffer (pH 5) and laccase concentration in each sample was at a fixed value of 0.5 g/L. The experiments were realized with the following PE: PDADMAC, bPEI, PAH and PSS.

Theoretically, with an IEP close to 4 and a solution at pH 5, laccase should have a net negative surface charge and therefore form complexes with polycations as bPEI, PAH and PDADMAC and should not be complexed by polyanion such as PSS. Unfortunately, no increased value of A350 could be detected with any of the tested PE/laccase mixes, as shown in Table 4.

Table 4: A_{350} of different concentrations of PE in laccase solution in the context of screening experiments. The mean and standard deviation of laccase absorbance are given. The mean A_{350} at different mass ratios of PE over laccase are separated according to PE used.

	Mass ratio									
PE	0.1	0.2	0.3	0.4	0.5	0.6	0.7	0.8	0.9	1.0
PDADMAC	0.126	0.123	0.122	0.121	0.121	0.122	0.124	0.121	0.122	0.127
bPEI	0.131	0.127	0.126	0.126	0.123	0.125	0.128	0.126	0.131	0.133
PAH	0.130	0.133	0.127	0.126	0.127	0.127	0.131	0.133	0.136	0.142
PSS	0.134	0.129	0.129	0.127	0.129	0.131	0.130	0.133	0.136	0.145

Laccase	mean	0.129	std	0.004

The resulting values of A_{350} were very close. The mean of all conditions are equal to the mean of laccase with 0.129, with a standard deviation of 0.007. Only some values differ from the average, but no trend appears in the results. At this stage, various hypotheses might be considered.

Firstly, the range of mass ratios and concentrations is not suitable for complex formation. Secondly, the ionic strength is too high with the acetate buffer. Lastly, as solutions with polycations and the polyanion show no significant difference in behavior, a question has arisen regarding the surface charge of laccase.

3.1.1.1 Focus on bPEI-LAC LPC

Following this first screening, a new experiment was designed to form LPC. Acetate buffer was replaced by deionized water at a pH of 4 in order to reduce ionic strength. An additional concentration of laccase of 2.5 g/L was tested along with 0.5 g/L. Only bPEI, with 4 different concentrations, has been tested as PE.

A_{350} of the different solutions are shown on Figure 25. It can be observed that the solution containing laccase alone at a concentration of 2.5 g/L exhibits a higher A_{350} than the one containing 0.5 g/L, highlighting initial absorbance due to proteins in solutions. Another difference is the non-monotone line of solution containing 2.5 g/L of laccase. Furthermore, when the concentration of bPEI is 0.05 g/L and that of laccase is 2.5 g/L, resulting in a PE/lac mass ratio of 0.02, a clear increase in A_{350} is observed, suggesting the formation of unsoluble complexes.

These results clearly highlight the importance of introducing the suitable mass ratio of PE and protein to form the desirable complexes. This experiment indicates that the range of mass ratio to build LPC is probably smaller than those tested previously. However, the observed behavior does not rule out the influence of solution pH and ionic strength on the system.

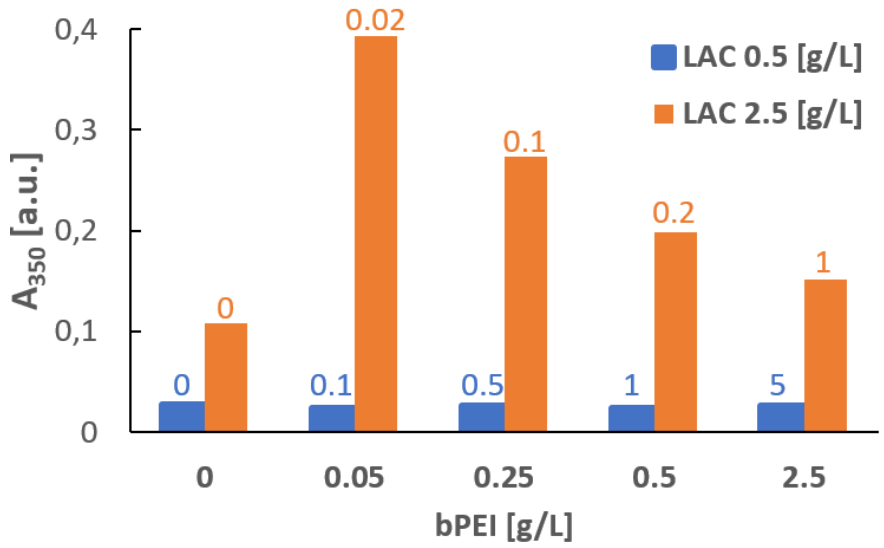

Figure 25: A_{350} of solutions containing laccase 0.5 g/L or 2.5 g/L with different concentrations of bPEI and their resulting mass ratios. Mass ratios are indicated at the top of the bars. The curve of laccase 0.5g/L is monotone, while the curve of solution with 2.5 g/L shows a maxima when the concentration of bPEI is 0.05 g/L given a mass ratio of 0.02.

3.1.2 Investigation on laccase charge

Isoelectric point (IEP) of laccase is further investigated in response to concerns about the charge of laccase. Starting from the principle that laccase used is a fungal laccase, its IEP is around 4. According to that, the surface net charge of laccase is positive under IEP and negative below. However, as previously stated in section 1.2.2.1, IEP can be in a wide range between 2.6 and 6.9. Therefore, different ways of finding out more about IEP have been explored.

Theoretical laccase surface charge

To have a better idea of IEP of laccase, PDB2PQR has been used [67]. This software computed the number of charges per laccase molecule as a function of pH. PDB2PQR is based on the amino acid sequence and structure of the laccase given by the PDB file 1GYC. The resulting graphical representation is shown in Figure 26.

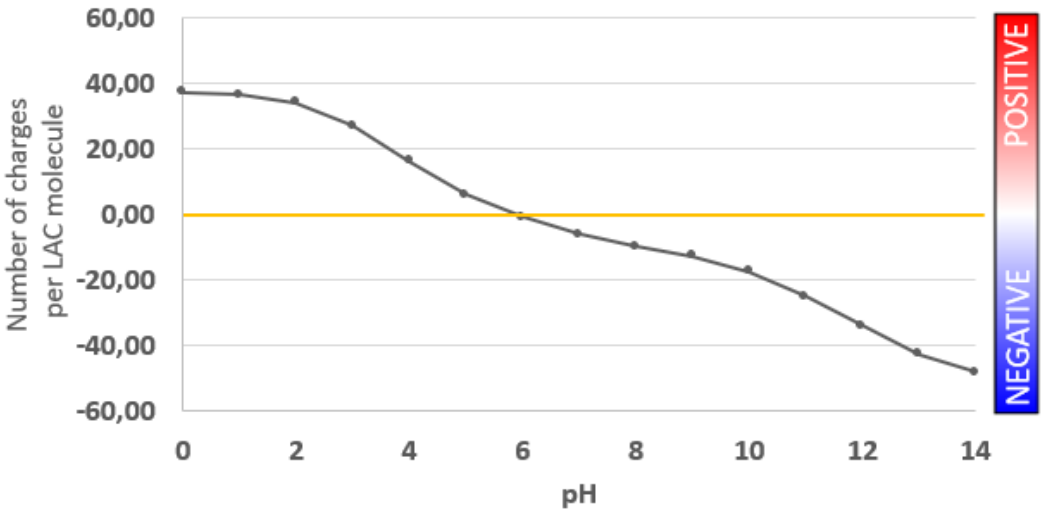

Figure 26: Graphical representation of the number of charges per laccase molecule according to PDB2PQR. The intersection with the neutral load axes according to PDB2PQR is 5.86.

The software gives, for laccase, a theoretical IEP value of 5.86. However, it does not take into account protein folding and potential interactions between amino acids. Therefore, experimental measurements are needed to determine the actual laccase IEP and its net surface charge.

ζ-potential

To determine experimentally laccase charge and obtain a more real IEP for laccase powder used, ζ-potential of laccase was measured at different pH. Different solutions of pure water set at pH between 3 and 8 have been made with a concentration of laccase of 1 g/L. The results are shown in Figure 27.

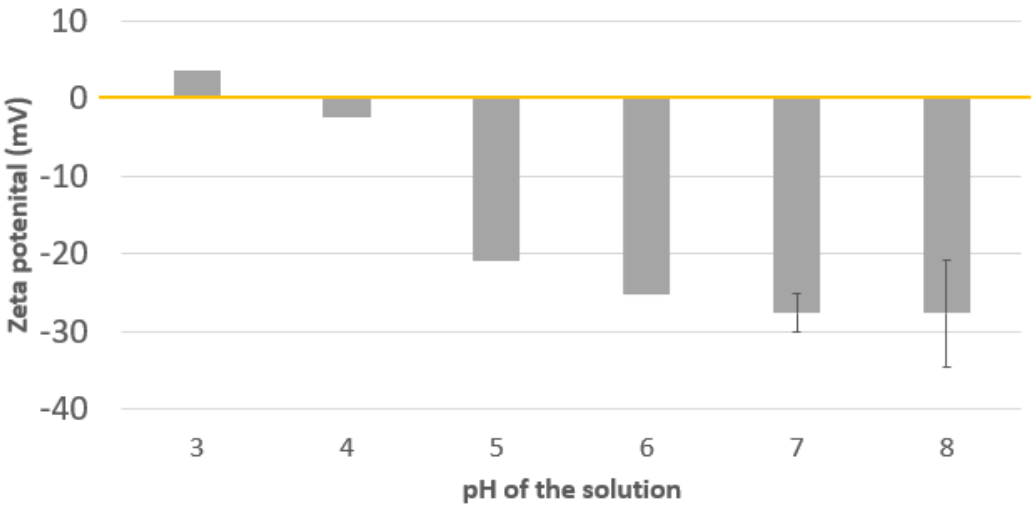

Figure 27: Zeta potential of laccase 1 g/L made in different pH solutions ranging from 3 to 8. Only the solution at pH 7 and 8 have been tested 2 times, the resulting standard deviation is added to the graph for these two values.

As visible in Figure 27, the IEP of laccase seems to be located between 3 and 4, where it has a neutral charge. Therefore, the experimental IEP is much lower than the theoretical one. This result explains why complex formation is possible at pH 4.

In summary, LPC can be formed in solution with a polycation if the pH is higher than the laccase IEP, with a value close to 4. Taking into consideration that a net negative load is required to form complexes with polycations, the following LPC will be formed in pure water set to pH 7, which corresponds to pH of raw wastewater [68].

Furthermore, a second Master's thesis carried out simultaneously showed that laccase powder used was not pure [69]. This information could explain the difference between the theoretical value of laccase IEP and the experimental one. The presence of impurities in the laccase powder might impact the formation of LPC.

3.2 PART I: LPC formation & characterization

Based on the previous observation that complexes were more easily formed under low ionic strength, we decided to keep working in a solution containing no buffer. The pH of each solution was set at 7 in order to favor laccase negative charge as indicated by zeta potential measurements. Finally, PAH has been arbitrarily selected as polycation, for the rest of the experiments, to form LPC.

The different experiments presented in this section allow to fulfill the objective linked to the formation and characterization of LPC.

3.2.1 Turbidimetry

Experimental design

To determine the mass ratio at which LPC form, a series of progressively narrower mass ratios have been investigated by turbidimetry with PAH^{old}. Figure 28 and Figure 29 show the results obtained for PAH/LAC mass ratio ranging from 10^{-4} to 1 and 10^{-2} to 10^{-1}, respectively.

After this, PAH^{old} has been replaced by PAH^{new}, the experiment has been reproduced and redesigned. At first, turbidity measurements, in endpoint (single measure), have been done in 3 replicates on mass ratios between 0.01 and 0.1. This measurement allows to obtain the new optimal mass ratio with PAH^{new} for the formation of LPC. After that, a second turbidimetry has been done in a bigger volume with mass ratios between 0 and 0.05, also in 3 replicates. This turbidimetry was a continuous measurement for one hour to obtain information on the uniformity of the solution's turbidity. The corresponding results are presented in Figure 30 and 31, respectively.

This last result, where evolution of LPC have been observed across time, is presented as a box plot for each condition on Figure 31. The box represents the interquartile range (IQR) of the data from 3 replicates, with the median shown as a line inside the box; the whiskers extend to the minimum and maximum values within the "non-outlier" range. Any data points beyond the whiskers are plotted individually as potential outliers.

Results analysis

The first result, Figure 28, shows a large peak on the mass ratio 0.05. In consequence, the zone of investigation has been reduced from 0.01 to 0.10.

The narrower range between 0.01 and 0.10 (Figure 29) exhibits a bell-shaped curve, with a maximal value at 0.06. For the same range, the maximal value with PAH^{new} is shifted to the left with a mass ratio of 0.03 and the bell-shaped curve is less present (Figure 30). Therefore, the LPC formation is more focused on a shorter area between 0.01 and 0.05.

The difference between the 2 PAH could be linked to the bad storage conditions of PAH^{old}. In the case of a hydrated powder, the quantity of PAH would be overvalued given a higher apparent mass ratio, as here with 0.06 instead of 0.03. In addition, the two figures (Figures 29 & 30) show different patterns, and therefore possibly different kinds of LPC. The differences can be linked to the storage issue with the presence of impurities or contamination with other elements, thus modifying the chemical environment.

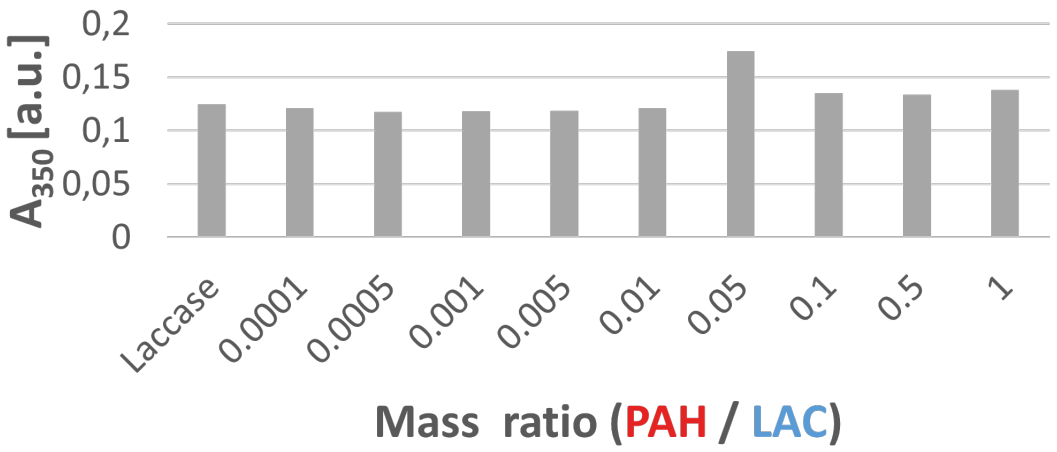

Figure 28: A_{350} of solution containing different mass ratios of PAH to LAC between 0.0001 to 1. The concentration of laccase was constant with a value of 0.5 g/L. The PAH used is PAH^{old}. A clear peak is visible on the mass ratio 0.05.

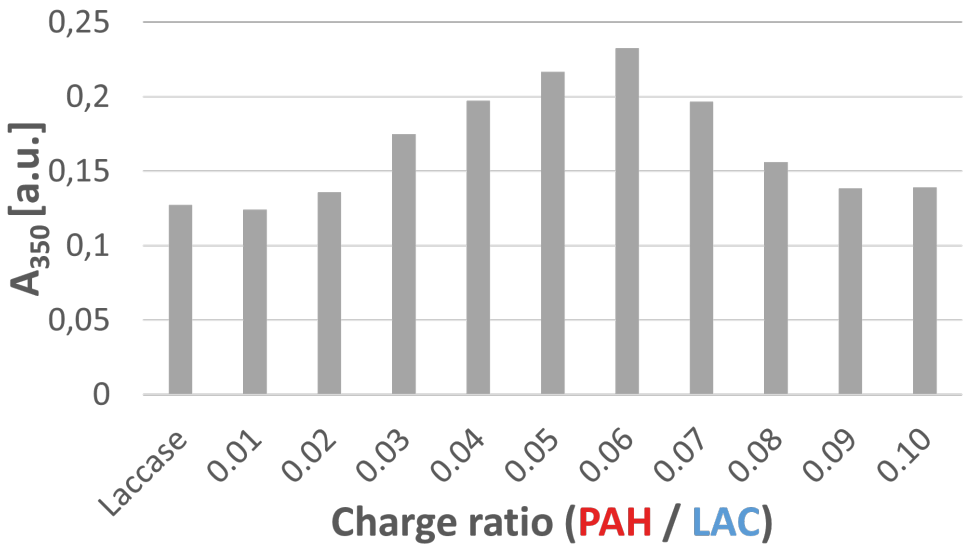

Figure 29: A_{350} of solution containing different mass ratios of PAH to LAC between 0.01 to 0.10. The concentration of laccase was constant with a value of 0.5 g/L. The PAH used is PAH^{old}. A bell-shaped curve is observed with a maximum value at mass ratio 0.06.

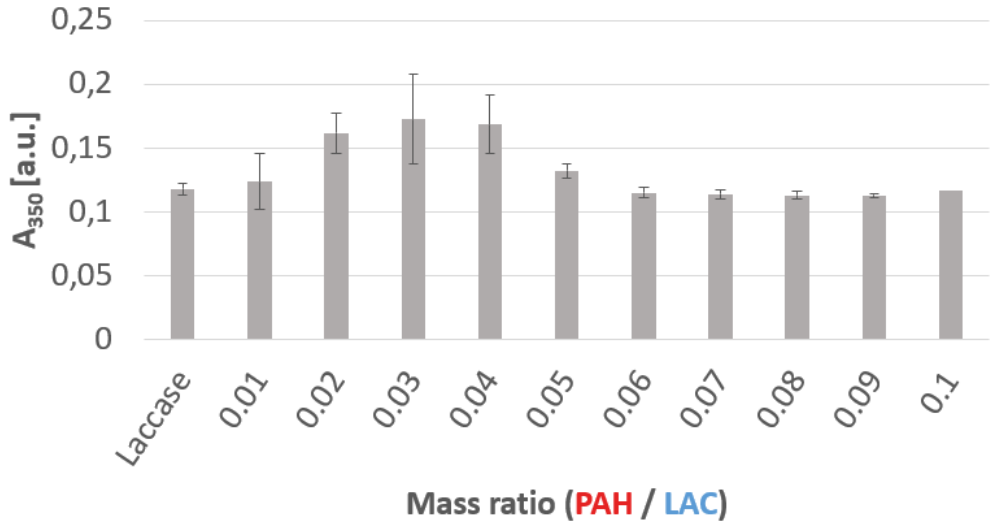

Figure 30: A_{350} of solution containing different mass ratios of PAH to LAC between 0 and 0.1. A_{350} shown is the mean of 3 replicates, standard deviations are presented as error bars. The concentration of laccase was constant with a value of 0.5 g/L. The PAH used is PAH^{new}. The curve peaks at mass ratio 0.03.

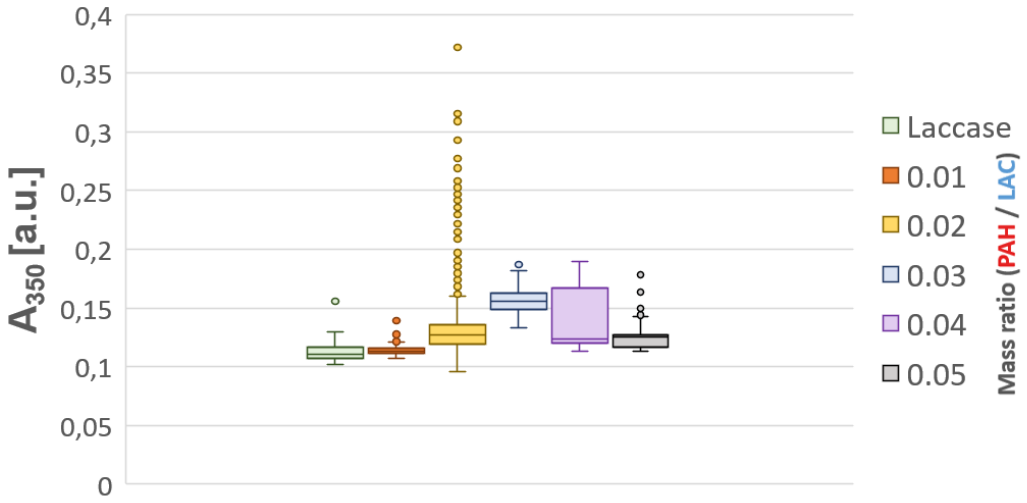

Figure 31: Box plot of A_{350} during 1 hour of solution containing different mass ratios of PAH to LAC between 0 and 0.05. Each box plot is formed using the A_{350} measurement taken over a one-hour period. Additionally, each box consists of three replicates. The concentration of laccase was constant with a value of 0.5 g/L. The PAH used is PAH^{new}. The curve peaks at mass ratio 0.03.

The kinetic measurements of A_{350} presented in Figure 31 reveals distinct behaviors exhibited by the various formed LPC composed of PAH^{new}.
On one hand, the solution of laccase and $LPC_{0.01}$ have stable turbidity over time with similar values, indicating that no complexes are formed.
On the other hand, $LPC_{0.02}$ exhibits the most disparate behavior, with a lot of outliers. It can be explained by the formation of filaments and non-homogeneity of the solution, as visible on Figure 32.
In contrast, $LPC_{0.03}$ have the highest median and their behavior seems stable in time. On Figure 32, LPC form a homogeneous structure similar to frog eggs.
Conversely, the least reproductive behavior belongs to the $LPC_{0.04}$. Indeed, through the 3 replicates, 2 are extremely similar with low A_{350} and the last one shows higher absorbance. In consequence, the median is far below in the box plot. This non-reproducibility could be explained by a slight alteration in the value of the mass ratio. Indeed, as visible in Figure 30, the turbidity decreases sharply between mass ratios 0.04 and 0.05. Visually, $LPC_{0.04}$ with the higher turbidity are a cloudy solution (Figure 32).
Lastly, $LPC_{0.05}$ exhibits similarities to $LPC_{0.01}$, but with higher turbidity values.

In consequence, distinct complex behaviors can be observed in this narrow range of mass ratios, showing that the ratio of PAH to protein is extremely sensitive and a determining factor in the formation of these complexes.

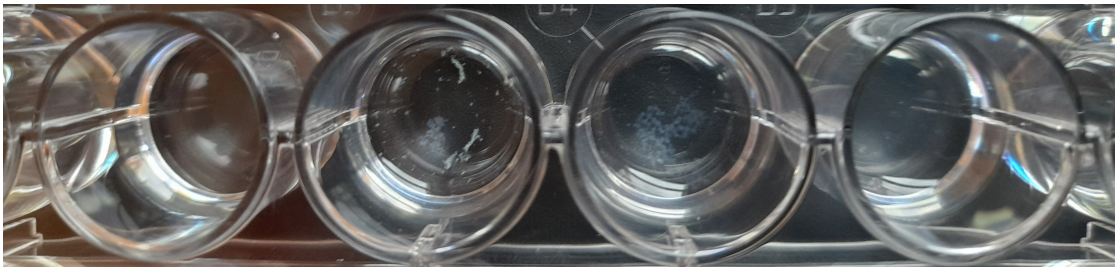

Figure 32: Picture realized after the last kinetic turbidimetry experiment. In the image, the leftmost LPC is $LPC_{0.01}$, followed by $LPC_{0.02}$, $LPC_{0.03}$, and the rightmost $LPC_{0.04}$. The PAH used is PAH^{new}

3.2.2 Zeta potential

Experimental design

To obtain information on the net surface of LPC as well as understand better the formation of aggregate and soluble LPC, ζ-potential measurements have been realized on the same range of turbidimetry, 0.0001 to 1 and 0.01 to 0.05. The graphical representation of the first one realized on PAH^{old} is in Figure 33. The second one made on the transition zone with PAH^{new} is represented in Figure 34.

A solution with a zeta-potential between -5 mV and 5 mV will be considered as having particles in suspension with neutral net charge. Below this range, particles will be considered to have a negative net charge and above, a positive net charge.

Results analysis

The first range, Figure 33, clearly shows the change of charge with the addition of PAH. At the beginning, a negative zeta potential value close to -30 mV can be explained by the high proportion of laccase in solution. The addition of PAH will gradually induce a change in sign until a positive value close to 25 mV. The switch of charge occurs between mass ratios of 0.01 and 0.05.

The same pattern can be observed for LPC with PAH^{new}. The charge inversion seems to occur at a mass ratio of 0.03. Furthermore, the neutral net charge of $LPC_{0.03}$ indicates that load compensation is complete and therefore a charge ratio 1:1 between PAH and LAC. In addition, $LPC_{0.03}$ created show large deposition in its container as visible in Figure 35, the other LPC did not show the formation of such deposition.

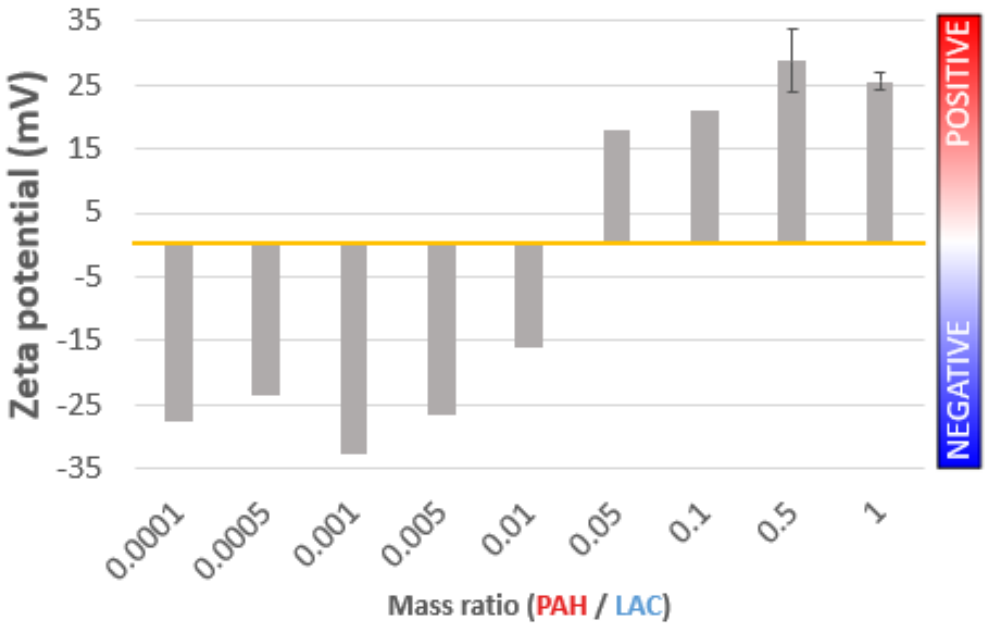

Figure 33: Zeta-potential of solution containing different mass ratios of PAH to LAC between 0.0001 to 1. The concentration of laccase was constant with a value of 0.5 g/L. The PAH used is PAH^{old}. The inversion of charge is between the mass ratio 0.01 and 0.05.

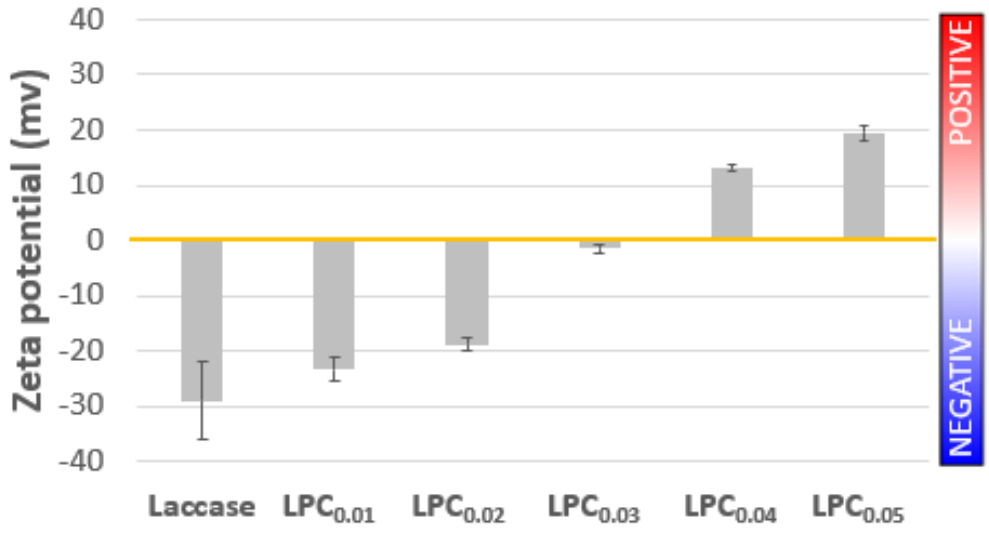

Figure 34: Zeta-potential of solution containing different mass ratios of PAH to LAC between 0 and 0.05. The concentration of laccase was constant with a value of 0.5 g/L. The PAH used is PAH^{new}.

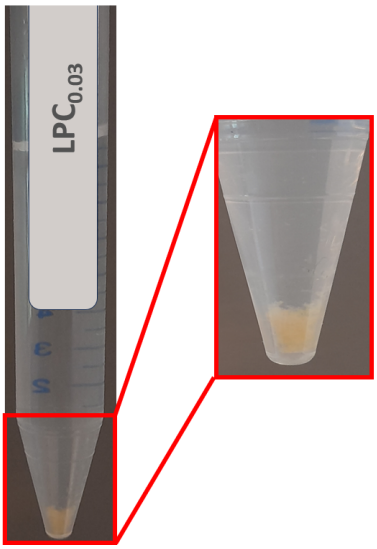

Figure 35: Solution $LPC_{0.03}$ produces for zeta-potential measurement. The PAH used is PAH^{new}.

3.2.3 DLS: LPC size & PDI

Experimental design

The measurements of size and PDI have been done only on LPC with mass ratios ranging from 0.01 to 0.05, as well as on a solution containing only laccase. The numerical results are available in Table 5 of Annex B.

Results analysis

Solution containing laccase powder only, as visible in Figure 36, contains elements of different size. As seen previously in the introduction, laccase should be contained in a rectangular parallelepiped of dimension 70 Å× 55 Å×50 Å. Therefore, only particles with a size less than 10 nm are likely to be laccase, while the other peaks are probably other components found in the original powder. The laccase powder is predominantly composed of elements with a size below 10 nm, such as laccase, accounting for approximately 99.9% of the composition (cyan curve on Figure 36). Indeed, the cumulative relative percentage of count in the interval between 1 and 10 nm is equal to 99.9%. However, the impurities, elements with size above 10 nm, represent most of the scattered light intensity (orange curve on Figure 36) with 93.5% which impacts the average size. Indeed, the average size is calculated from intensity weighted distribution. Therefore, the weighted average size by number (WAS) is probably the most reliable under these conditions.

For example, the size of laccase can be more accurately characterized by the weighted average size of 3 nm, which provides a better representation of its actual size, in contrast to the average size of 116 nm. The two sizes are shown in Figure 37, and values are available in Annex B.

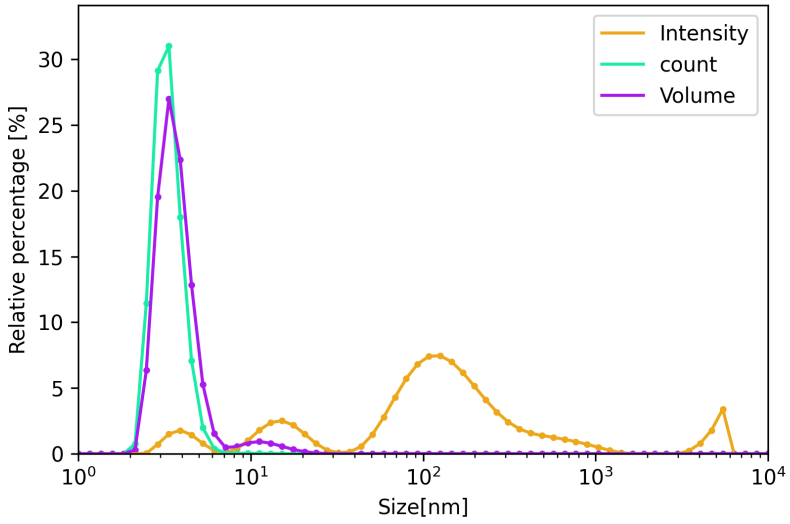

Figure 36: Size distribution of laccase by intensity, number and volume. Graph of the relative percentage of particles in different size classes plotted as a function of scattered light intensity (orange), number (cyan) and volume (violet).

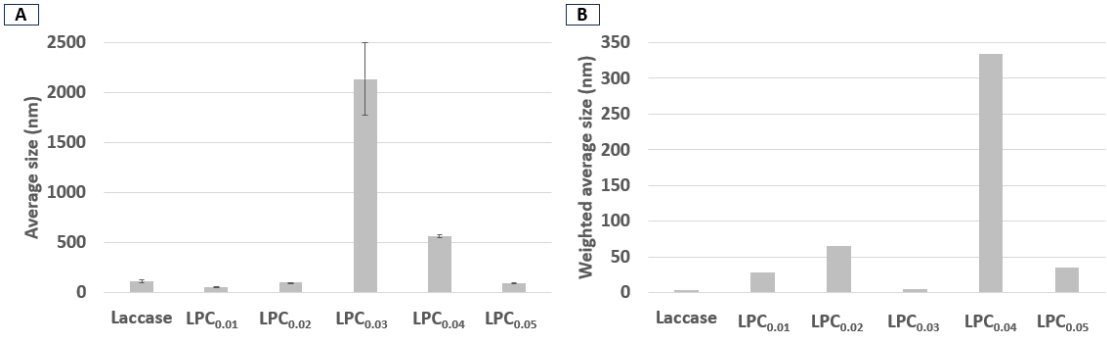

Figure 37: Average size and weighted average size of suspended element in solution containing different mass ratios of PAH to LAC. (A) Average size shown is the mean of 3 replicates, standard deviations are presented as error bars. (B) Weighted average size by number. The concentration of laccase is fixed at 0.5 g/L in every sample. The PAH used is PAH^{new}.

The size distribution of $LPC_{0.01}$, $LPC_{0.02}$, $LPC_{0.04}$ and $LPC_{0.05}$ present less peaks (Annex C: Figure 49). Therefore, a specific analysis of their distribution is not required compared with laccase solution. Indeed, as the intensity is similar to number, the average size and WAS have the same order of magnitude. On the contrary, a focus on the distribution of $LPC_{0.03}$ is done as it is a particular case, due to charge neutralization.

$LPC_{0.04}$ have the highest average size and WAS, with 567 nm and 335 nm, respectively. Such high values in size could indicate the formation of aggregative LPC at this mass ratio. Indeed, by looking at the four mass ratios, an increase in size followed by a decrease is observed. It is in line with the transition from soluble elements to aggregative LPC and then to soluble LPC, with the addition of PE. Only $LPC_{0.03}$ are not in line with this theory. Their distinct behaviors could be different due to the charge neutralization at mass ratio 0.03.

The WAS of $LPC_{0.03}$ is of 5 nm, but by looking at Figure 38, two peaks of intensity are observed. The first peak centered at 3 nm could correspond to unmodified elements that do not interact with PAH. The second peak centered in 8 nm could be caused by the presence of complexed elements that does interact with PAH and therefore sees their size increase. Given that the two peaks represent respectively around 66.5% and 33.5% of the number of elements present in the powder, the complexes are formed with one-third of laccase powder.

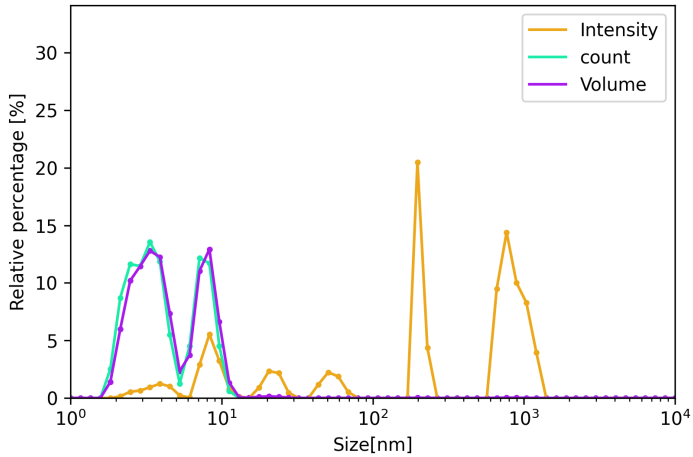

Figure 38: Size distribution of $LPC_{0.03}$ by intensity, number and volume. Graph of the relative percentage of particles in different size classes plotted as a function of scattered light intensity (orange), number (cyan) and volume (violet).

In consequence, there are three possible scenarios. The ideal scenario is one where the entire laccase, and exclusively the laccase, forms complexes. This will lead to a purity of laccase powder of 33.5%. The second scenario corresponds to the complexation of all the laccase, but also the complexation of impurities. The final scenario corresponds to the complexation of part of the laccase, as well as the impurities.

PDI value indicates the heterogeneity of the sample. As the laccase powder is not pure, values of PDI (Figure 39) are also impacted. Furthermore, the calculation of PDI is also done on the base of the intensity, giving possibly overvalued values in particular for laccase and $LPC_{0.03}$.

However, certain observations can be made. At first, the addition of PAH leads to a decrease of PDI and a uniformization of the particle size in solution. But at a mass ratio of 0.03, PDI increases sharply, indicating the possible presence of large aggregates. This is in agreement with turbidity measurements which have their maximum value at this ratio. Then, the further addition of PAH leads to an homogenization of the solution towards smaller particles, which is again consistent with the decrease in turbidity at these same ratios.

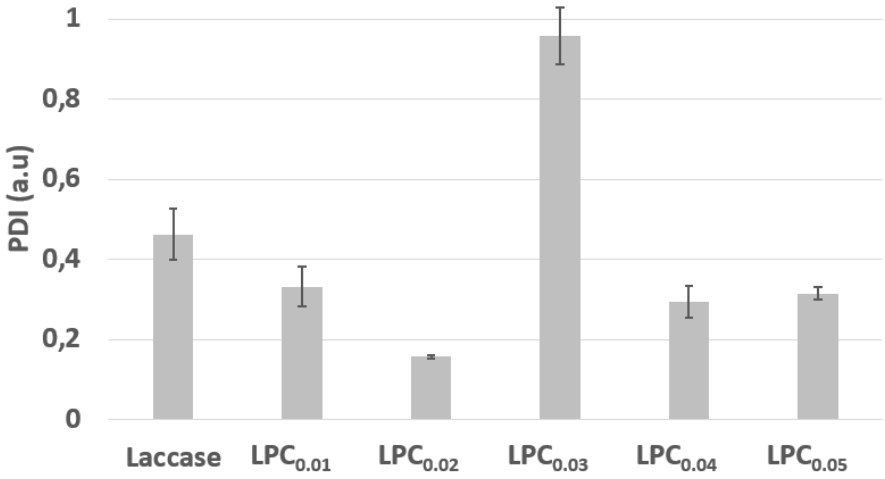

Figure 39: PDI of suspended element presents in solution containing different mass ratios of PAH to LAC between 0 and 0.05. PDI shown is the mean of 3 replicates, standard deviations are presented as error bars. The concentration of laccase is fixed at 0.5 g/L in every sample. The PAH used is PAH^{new}.

3.2.4 LPC isolation by centrifugation

Experimental design

To find out which of the 3 scenarios described above is the most realistic, experiments to isolate complex formed have been done. BCA assay and enzymatic activity assay have been performed on (i) the initial solution before centrifugation and (ii) the resulting pellets and supernatant after centrifugation, to determine the protein and the laccase content of the formed particles.

Various LPC isolation experiments were conducted, but many encountered protocol errors or led to the formation of unanalyzable pellets. Some solutions formed compacted pellets that could not be dissolved again, which is essential for analysis, possibly due to material compression. Different speeds have been tested. It turned out that a speed of 500g allows the gathering of suspended particles in $LPC_{0.02}$. For $LPC_{0.01}$ and $LPC_{0.03}$, a speed of 8,000 g was required to obtain a visible pellet. No visible pellets have been seen for laccase, $LPC_{0.04}$ and $LPC_{0.05}$ despite speeds of up to 15,000 g.

Results analysis

Figure 40 shows the different enzymatic activity of the six investigated conditions, with at first the initial activity of samples before centrifugation and secondly the activity of the supernatant and pellet after centrifugation. The last activity called I-S is the initial activity without the activity of the supernatant. This activity should therefore theoretically correspond to the activity found in the pellet and is used to assess eventual loss of activity due to factors such as material compaction or enzyme inactivation during the process. The different values are available in Annex D.

When comparing the initial activity of LPC with laccase, it appears that all LPC exhibit a lower enzymatic activity than laccase alone, with the lowest value for $LPC_{0.02}$. The enzymatic activities of LPC range from 75% to 90% of the laccase activity. The formation of LPC could limit access to the laccase active site.

After centrifugation, a loss of activity is observed. The supernatants of $LPC_{0.01}$, $LPC_{0.04}$, and $LPC_{0.05}$ retained over 80% of their initial activity, whereas $LPC_{0.02}$ and $LPC_{0.03}$ retained only 18% and 37% of their initial activity, respectively. The loss of activity of laccase can be due to protein denaturation or to the isolation of laccase in the pellet. According to the activity of pellet and I-S, the two explanations are possible.

Concerning $LPC_{0.01}$, its pellet contains the activity that is not in the supertatant. In the case of $LPC_{0.04}$ and $LPC_{0.05}$, despite their pellet activity, they are still about 10% missing. The protein denaturation could be one of the causes of this gap.

For $LPC_{0.02}$, the majority of its enzymatic activity is found in the pellet. However, 17% of its initial activity is still missing. In the case of $LPC_{0.03}$, this loss of activity represents 49% of the initial activity. This loss is likely caused by the formation of a compact material comprising agglomerated elements, resulting in a reduction in the number of accessible enzymes.

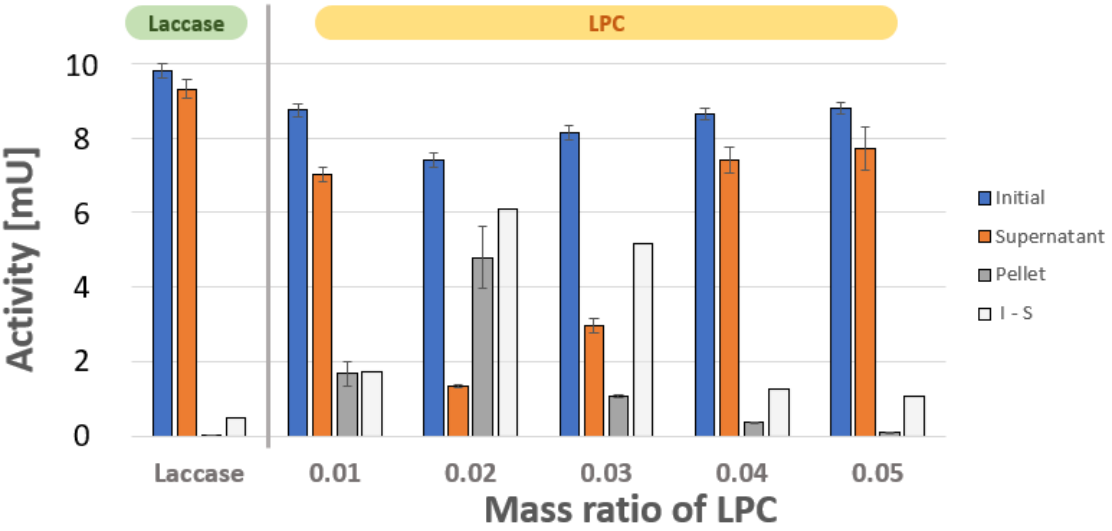

Figure 40: Enzymatic activity of 3 samples collected at different times during the isolation experiment. The activity of the initial, supernatant and pellet solution are represented with their mean and standard deviation on 5 replicates. The last activity referred to as "I-S" is the theoretical activity that the pellet could have, if we consider it to be the difference in mean activity of the initial solution and its supernatant. The concentration of laccase is fixed at 0.5 g/L in every sample. The PAH used is PAH^{new}.

The quantification of protein has also been done on the different solutions. For solutions with the 5 mass ratios and laccase, BCA assay has been realized on initial solution, supernatant and resuspended pellet. As solutions contain 0.5g/L of laccase powder, the concentration of protein should be at most 0.5g/L. However, as observed on Figure 41, the concentration of protein is approximately of 1g/L. No calculation or protocol errors have been identified so far, and if any exist, they are consistent across all conditions. Consequently, BCA assay results can only be analyzed relatively to each other, and not in absolute values.

Given that laccase solution does not sediment after centrifugation, unlike LPC solutions, it suggests that the sedimentation primarily involves the complexed elements. Additionally, the protein concentration analysis reveals similar values for the initial and supernatant samples, while the pellet contains a low amount of protein in all studied conditions. Therefore, it is reasonable to conclude that isolated complexes are composed of only a small quantity of proteins. These proteins, according to enzymatic tests, exhibit laccase enzymatic activity.

Based on this result, it seems that LPC present in pellets are made up mainly of laccase and not other proteins. Furthermore, the complexation process with mass ratios of 0.02 and 0.03 appears to exhibit higher specificity towards laccase compared to other proteins. As a result, these complexes facilitate the isolation of laccase from the other proteins in the initial powder.

As activity observed in the supernatant solution could be attributed to either free laccase or complexed laccase that does not undergo sedimentation, the 3 scenarios on the composition of complexes are still possible. However, these experiments show the presence of laccase-containing complexes.

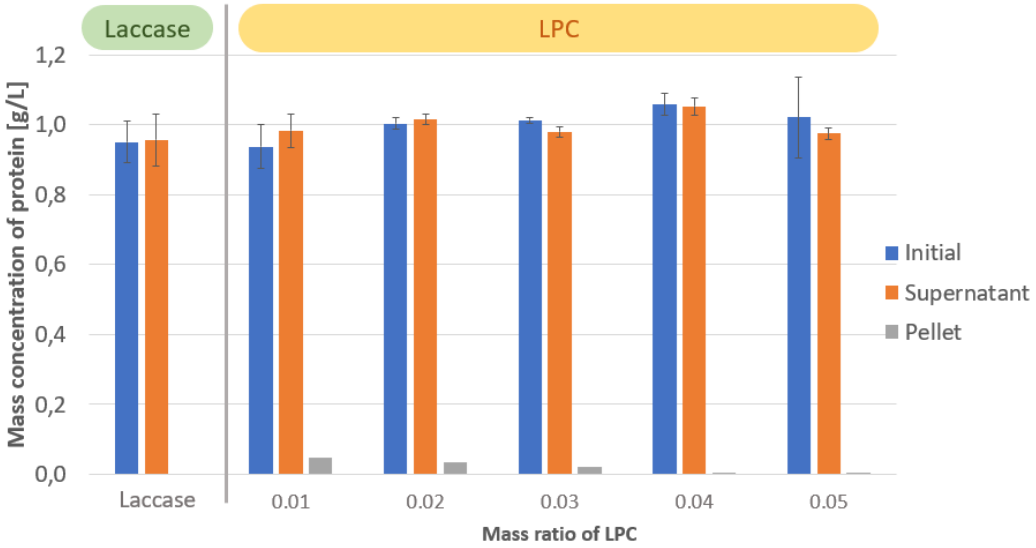

Figure 41: BCA assay of 3 samples collected at different times during the isolation experiment. The concentration of laccase is fixed at 0.5 g/L in every sample. The PAH used is PAH^{new}.

3.2.5 Part I summary

In summary, according to turbidimetry, LPC formed with PAH^{old} and PAH^{new} produce different complexes. The optimal mass ratio for LbL assembly should be 0.06 and 0.04, respectively to obtain LPC with the higher turbidity without formation of non-soluble elements. The two LPC will be called $LPC^{old}_{0.06}$ and $LPC^{new}_{0.04}$, respectively. In PART II, only one LPC will be used. LbL assembly will be made from $LPC^{new}_{0.04}$. However, some QCM experiments have been done with $LPC^{old}_{0.06}$ and are available in Annex E.

The different patterns present in turbidimetry are representative of the behavior illustrated in the introduction section (Figure 10). The progressive addition of PAH initially results in the formation of large insoluble aggregates, reaching their maximum size at a mass ratio of 0.03. However, further addition of PAH appears to promote formation of more soluble complexes. The range of mass ratio between 0.01 and 0.05 clearly shows this transition between aggregative to soluble LPC.

Furthermore, thanks to zeta potential measurement, the net surface charge of LPC can be determined. The transition zone at which the most unsoluble complexes are formed corresponds to the region where charge compensation is achieved and the global charge of particles switches from negative to positive. Indeed, LPC with the higher turbidity have zeta potential value really close to 0 mV and in consequence have a surface net charge close to neutrality. $LPC^{new}_{0.04}$, which will be used in PART II, are positively-charged LPC due to their zeta potential value of 13 mV.

DLS measurements highlight the lack of purity of laccase powder. The presence of unidentified impurities complicates the interpretation of the results. Working with a purer laccase would be beneficial in this regard and could simplify the creation and characterization of complexes. However, DLS results are in agreement with the presence of large non-soluble aggregates around mass ratio 0.03. In addition, the size behavior of other LPC corresponds to the expected theoretical behavior. With the addition of PE, laccase initially forms increasingly larger aggregative LPC species, such as $LPC_{0.01}$, $LPC_{0.02}$, and $LPC_{0.04}$. Subsequently, it undergoes a size reduction, resulting in formation of soluble LPC as $LPC_{0.05}$.

Finally, despite the presence of impurity in the powder, the isolation experience highlighted the presence of laccase-containing LPC. In particular, the isolation of non-soluble complexes formed at ratios 0.02 and 0.03 highlights the specificity of the complexation phenomenon towards laccase compared to other proteins. These two complexes are maybe not the best candidates for LbL assembly but could be used to isolate laccase from other powder constituents.

3.3 PART II: LPC as building blocks for LbL assembly

Based on the results about the formation and characterization of LPC, we decided to use the $LPC_{0.04}^{new}$ as building blocks in various LbL assemblies.

3.3.1 QCM

Experimental design

Before evaluating the enzymatic activity and stability of LbL assembled films with LPC, it is necessary to verify that the assembly is correctly formed. For that, the following assemblies were monitored using QCM-D. Initially, non-complexed laccase was assembled either using bPEI or PSS as counter PE. Then, a similar experiment was performed but replacing laccase with $LPC_{0.04}^{new}$. The assemblies are referred to as [bPEI - LAC], [PSS - LAC], [bPEI - LPC] and [PSS - LPC]. These assemblies have been chosen to provide continuity with the previous work on laccase. In addition, the use of both PSS and bPEI allows to have control assemblies that theoretically do not allow optimal adsorption via electrostatic interactions. Schematic representation of assemblies are shown in Figure 42.

As QCM has a limited number of modules and that each condition (assembly) requires at least two modules to have replicates, QCM experiments were divided into three subparts. The first one was the construction of multilayers with LAC and PSS. The second one contains assemblies with LAC and bPEI. The last QCM was assemblies with $LPC_{0.04}^{new}$ and with the two PE. The subparts are depicted in figures that include a QCM graph of one of the two replicates and a graph illustrating the evolution of the assembly thickness at each layer. The complete result of each QCM, with second replicates, and graphical verification of the Sauerbrey equation are available in Annex E. Overtone 7 frequency shift is directly used to see the good adsorption of layers. Dissipation shift is used as an additional verification of adsorption.

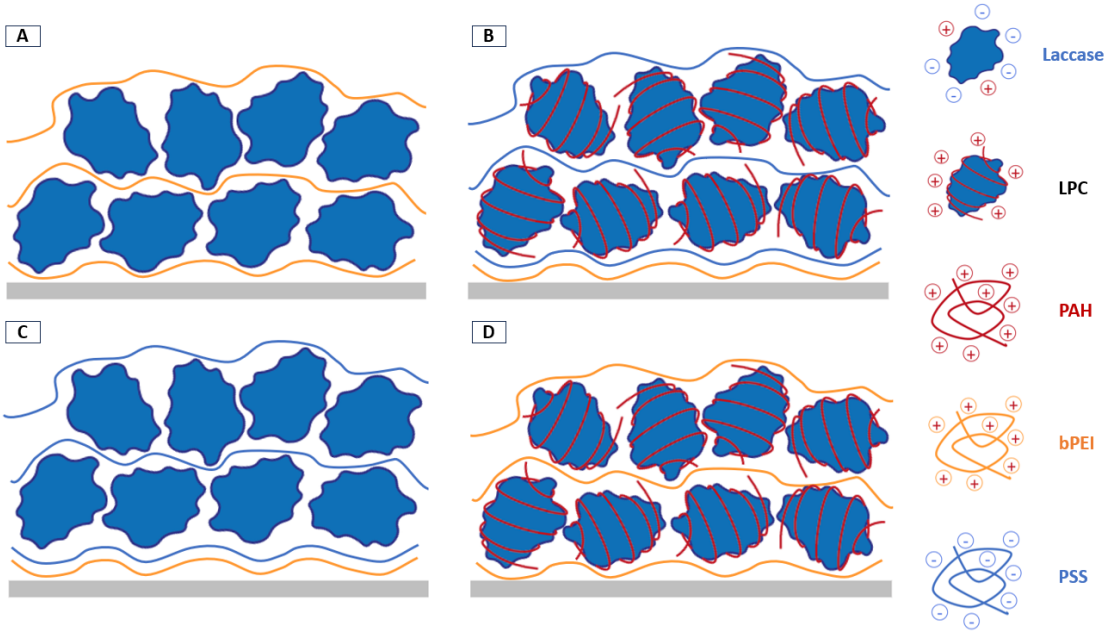

Figure 42: Schematic representation of the laccase and LPC immobilization using LbL assembly. (A) Initial LbL assembly of laccase, named [bPEI - LAC]. (B) New LbL assembly with LPC, referred to as [PSS - LPC]. (C) & (D) Control of the two assemblies with oppositely-charged PE.

Results analysis

As shown on Figure 43, the assembly [PSS - LAC], as expected, does not work. Indeed, only a first adsorption of PSS on bPEI is visible on the graph and a small adsorption of laccase is observed after that. This adsorption can be explained by the interaction between bPEI and LAC. By comparing with the [bPEI - LAC], Figure 44, a difference in behavior is clearly evident. The staircase pattern indicates good adsorption at each step. The two thicknesses after 2 BL, or in other words after the second adsorption of laccace, are 5.5 nm and 18.5 nm, respectively, noting that the first one contains an additional PE layer. This observation confirms the previous statement that laccase harbors a negative net charge at pH 7.

Assemblies with $LPC^{new}_{0.04}$ show clearly a different behavior. As shown in Figure 45, the staircase pattern is still present but appears in the two assemblies [bPEI - LPC] and [PSS - LPC]. However, although the thickness of [PSS - LPC] is 8.2 nm after 2 BL, which is greater than its control (5.8 nm), this value remains well below the 18.5 nm of [bPEI - LAC].

According to these results, a multilayer assembly composed of PSS and LPC can be realized but contains possibly less laccase than an assembly made of bPEI and PSS.

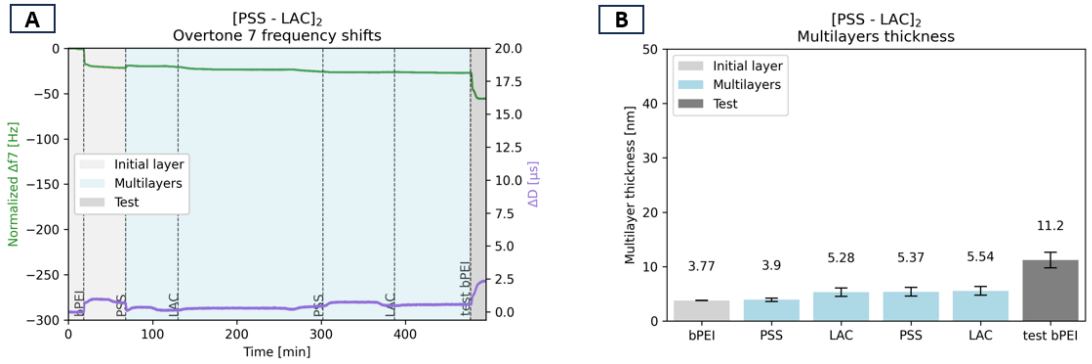

Figure 43: QCM-D analysis of [PSS-LAC]$_2$. (A) QCM results of [PSS-LAC]$_2$: Overtone 7 frequency shift (green) with dissipation shift (purple). The background color indicates the assembly phase. The dotted lines mark solution changes. (B) Multilayers thickness at the different layers. The thicknesses are the mean of 2 replicates, the standard deviations are given as error-bars. The bar color indicates the assembly phase. The results are taken from experiments where [PSS-LPC]$_2$ with LPC$^{old}_{0.06}$ has also been tested.

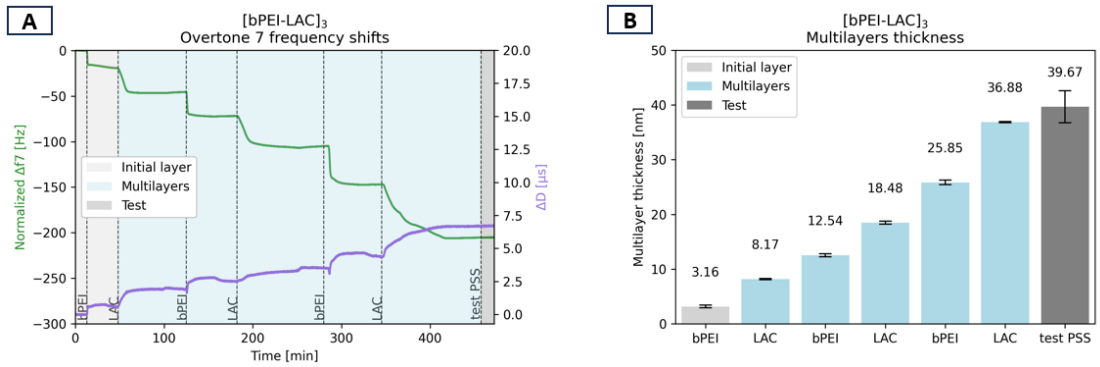

Figure 44: QCM-D analysis of [bPEI - LAC]$_3$. (A) QCM results of [bPEI-LAC]$_2$ (2) QCM results of [bPEI-LPC]$_2$ (A) Overtone 7 frequency shift (green) with dissipation shift (purple). The background color indicates the assembly phase. The dotted lines mark solution changes. (B) Multilayers thickness at the different layers. The thicknesses are the mean of 2 replicates, the standard deviations are given as error-bars. The bar color indicates the assembly phase. The results are taken from experiments where [bPEI - LPC]$_3$ with LPC$^{old}_{0.06}$ has also been tested.

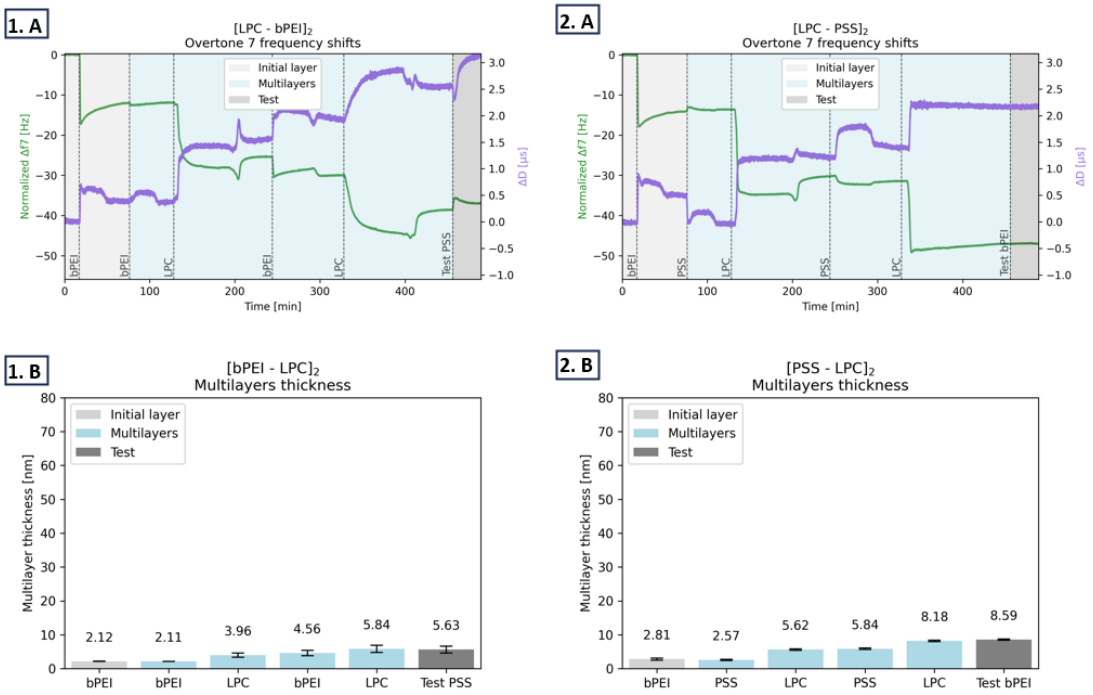

Figure 45: QCM-D analysis of [bPEI - LPC]$_2$ & [PSS - LPC]$_2$. LPC used is LPC$^{new}_{0.04}$. (1) QCM results of [PSS - LPC]$_2$ (2) QCM results of [bPEI - LPC]$_2$ (A) Overtone 7 frequency shift (green) with dissipation shift (purple). The background color indicates the assembly phase. The dotted lines mark solution changes. (B) Multilayers thickness at the different layers. The thicknesses are the mean of 2 replicates, the standard deviations are given as error-bars. The bar color indicates the assembly phase.

3.3.2 Multilayers activity and stability

Different multilayer films, build in 96 well plates, have been compared on the base of their activity and their stability over time. These results were obtained before LPC were fully characterized, and in consequence, some parameters may need to be changed for a new study.

Experimental design

Stability experiments have been done on LPC$^{new}_{0.04}$. As observed in QCM, the assembly is possible even if it does not show results equivalent to [bPEI - LAC] in terms of adsorption at each layer. The two assemblies, [bPEI - LAC] and [PSS - LPC] have been studied. The full results, with their control assemblies [PSS - LAC] and [bPEI - LPC] are available in Annex F.

Results analysis

Before comparing stability, it is interesting to look at the initial activity of multilayers at DAY 0 in Figure 46. As expected, more layers mean greater activity and also additional variability in final assembly. Film assembled using LPC instead of free laccase resulted in lower initial activity. This result is in accordance with what was observed in QCM, where multilayer thickness was lower for LPC than laccase.

Quantitatively, the assembly with LAC has an activity more than 3 times larger than the activity of assembly with LPC. The factor is of 3.6 and 3.1, respectively, for 3BL and 6BL. It should be noted that this is only an order of magnitude, as the thickness determined by QCM does not provide any information concerning the type of material adsorbed.

In consequence, according to film thickness, it seems that more laccase can be immobilized when using free laccase than LPC, for a same number of bilayers. Furthermore, the control conditions show also that laccase are better immobilized with a polycation and that LPC are better immobilized with polyanion. This is consistent with the results of their zeta potential value.

With regard to their stability, looking through the days, a loss of activity is visible on each assembly, but it seems to be gradually stabilizing. This loss of activity can be explained by enzyme leakage, but is can also be linked to the handling of the wells at each stage.

At DAY 10, the activity of $[PSS - LPC]_6$ is greater than the activity of $[bPEI - LAC]_3$, with 0.6 mU and 0.4 mU, respectively.

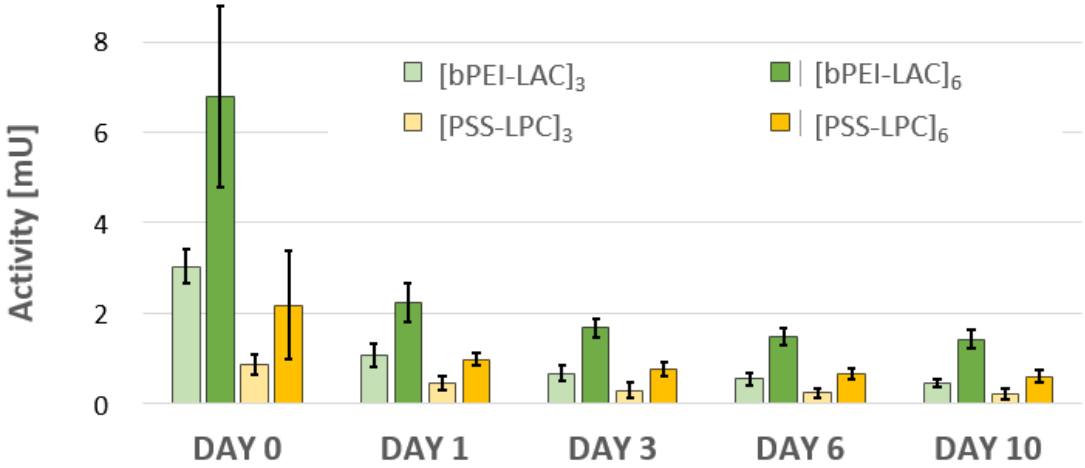

Figure 46: Activity and stability over 10 days of 3 and 6 BL of [bPEI - LAC] and [PSS - LPC]. The activities are the mean of 3 replicates, the standard deviations are present as error-bars.

Figure 47 shows the various activities, but as a percentage of the initial activity on day 0, this conversion allows observing the stability of activity over time for the different LbL assemblies. A decrease of activity over time is clearly observed, but it is becoming weaker and weaker, as previously seen with Figure 46.

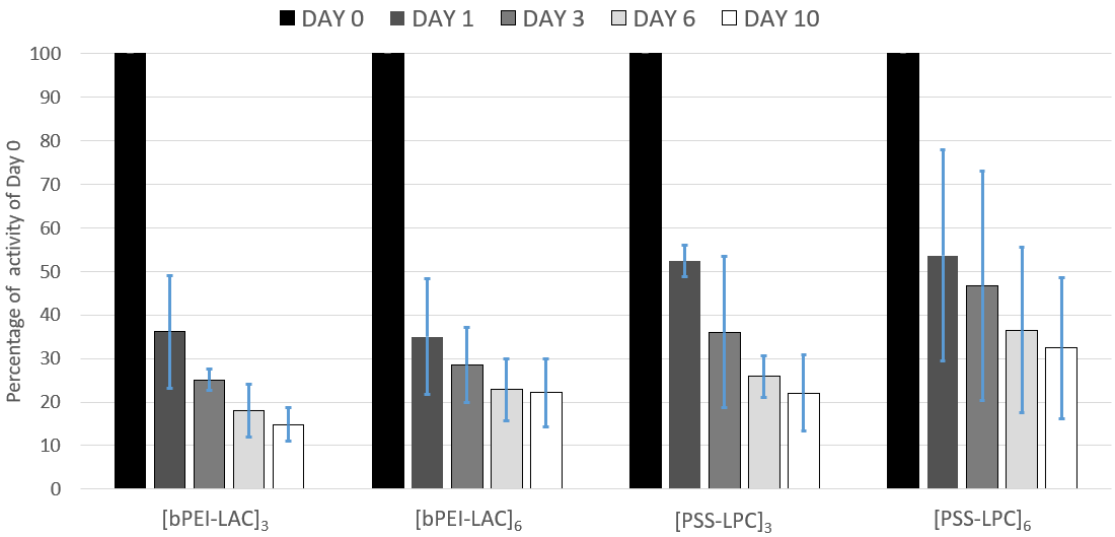

Figure 47: Activity and stability over 10 days of 3 and 6 BL of [bPEI - LAC] and [PSS - LPC] in percentage of initial activity (DAY 0). The percentage activities are the mean of 3 replicates, the standard deviations are present as error-bars.

Furthermore, assembly with 6 BL have slightly more stable activity compared to assembly with 3 BL. However, this behavior would undoubtedly be different in the case of dynamic activity measurement.

The percentages at DAY 10 are 15, 22, 22 and 32% for [bPEI - LAC]$_3$, [bPEI - LAC]$_6$, [PSS - LPC]$_3$ and [PSS - LPC]$_6$, respectively. These results show that the enzymatic activity remains more stable when increasing the number of layers and when using enzyme complexes instead of free enzymes for the LbL assembly. However, assemblies with LPC show wide variation between the 3 replicates, due in particular to the wide variation in initial activity.
These results are obviously preliminary and do not allow to definitively conclude on the usefulness of this type of LPC to build up enzymatically active LbL assemblies. However, there does not seem to be a huge advantage in using them for this type of application, especially considering a significant reduction of enzymatic activity for LPC.

Chapter 4
Conclusion

In conclusion, the development of new enzyme immobilization strategies constitutes a real challenge to obtain highly active and reusable biocatalytic materials. More precisely, laccase has been shown to be a promising candidate for bioremediation applications. In this context, the aims of this work were on a first hand to form and characterize Laccase-Polyelectrolytes complexes (LPC). On a second hand, these complexes were to be immobilized using the Layer-by-Layer assembly technique.

Firstly, LPC were created by mixing different amounts of laccase and poly(allylamine hydrochloride) in pure water set at pH 7. As shown by zeta potential measurement, it seems that charge compensation between PAH and laccase occurs between mass ratios of 0.02 and 0.04. LPC formed in this mass ratio range exhibit different sizes. Additionally, it seems that the complexation mechanism is rather specific to laccase, as indicated by high fractions of protein and laccase found respectively in supernatant and pellet during centrifugation experiments.

These results are preliminary and require further investigation. Some adjustments should be made as working in buffer solution to provide more stable pH conditions, and therefore, obtain more consistent results. Furthermore, using a purer laccase would facilitate interpretations.

Secondly, some experiments using $LPC_{0.04}$ have been done to form multilayers with PSS. Despite slightly greater relative stability compared to multilayers formed with non-complexed enzymes, the usefulness of LPC remains a subject of debate as the obtained multilayers have very low activity. Additionally, exploring multilayers formed with the other LPC could be beneficial for further improvements.

In the end, the obtained results so far indicate that LPC are not particularly interesting for laccase immobilization by LbL. However, despite their limited application in LbL, the created LPC could serve as new standalone materials or be directly used to form membranes, usable in wastewater treatment. Moreover, some LPC could be reevaluated for their potential in isolating laccase from complex protein mixes.

Annexes

A Experiments containing glutaraldehyde

Some experiments have been done with a percentage of GLU in the LPC to observe the modification of behaviors and characteristics. However, the different results will not be give due to GLU effect. Indeed, GLU being a reducing agent, its presence modifies the enzymatic test, by reducing the oxidized ABTS, as well as the BCA assay, by reducing the Cu^{2+}. As the results cannot be analyzed correctly, they will not be presented. As an example, the following graph shows the effect of GLU on the enzymatic test. For a same concentration of laccase, the computed activity would be smaller. The enzymatic activity would therefore be underestimated and in the case of BCA assay, the number of proteins would be overestimated.

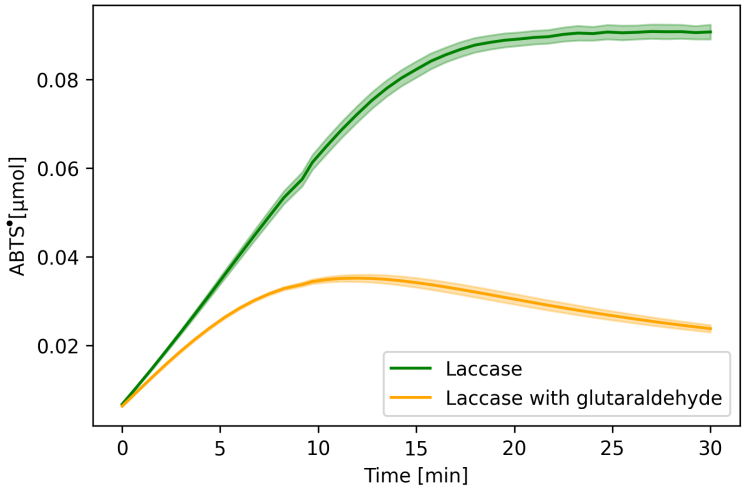

Figure 48: Evolution of oxidized ABTS over time in presence of laccase without and with glutaraldehyde. The solutions tested contain laccase 0.45 g/L. 1% of GLU is present in the second solution. The curves are the mean of 5 replicas, and the resulting standard deviations are shown as a cloud.

B Numerical results linked to zeta potential and DLS measurements.

Table 5: Results from Zetasizer experiments on laccase and LPC with mass ratio between 0.01 and 0.05

	Laccase	$LPC_{0.01}$	$LPC_{0.02}$	$LPC_{0.03}$	$LPC_{0.04}$	$LPC_{0.05}$
Zeta-potential [mv]	-29,12	-23,35	-18,82	-1,49	13,11	19,44
std of zeta-potential [mv]	7,01	2,16	1,12	0,69	0,58	1,27
Average size [nm]	116,1	57,48	99,65	2133	566,6	94,96
std of average size [nm]	16,91	0,55	0,25	362,80	15,79	0,52
Weighted average size [nm]	3,35	28,98	65,98	4,71	334,77	34,73
PDI [\]	0,4621	0,3321	0,1563	0,9587	0,2934	0,3151
std of PDI [\]	0,06338	0,04844	0,00296	0,07150	0,03941	0,01454

C Size distribution

$LPC_{0.01}$

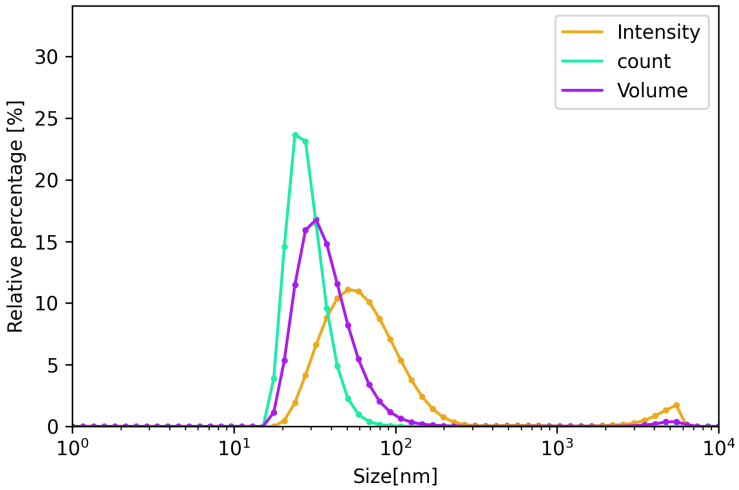

$LPC_{0.02}$

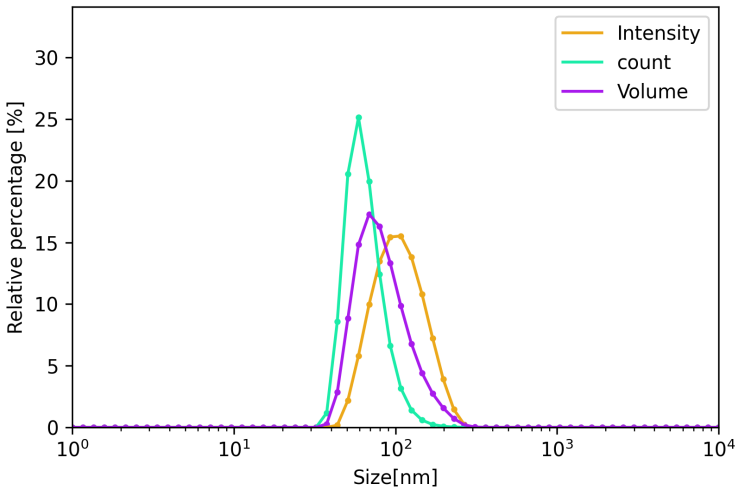

$LPC_{0.04}$

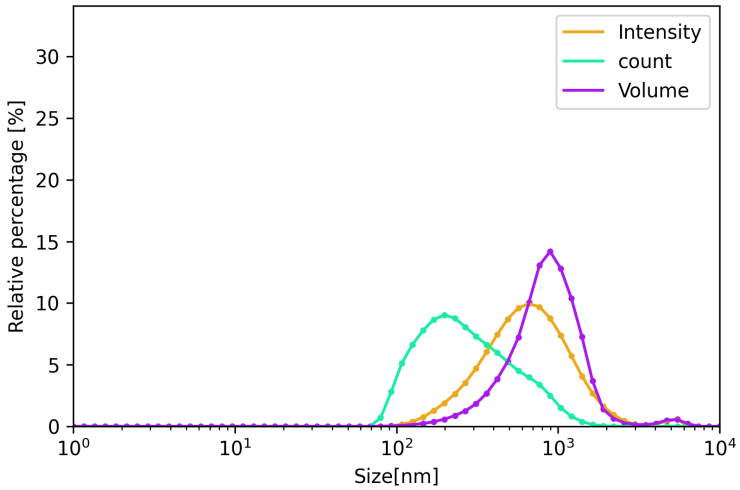

$LPC_{0.05}$

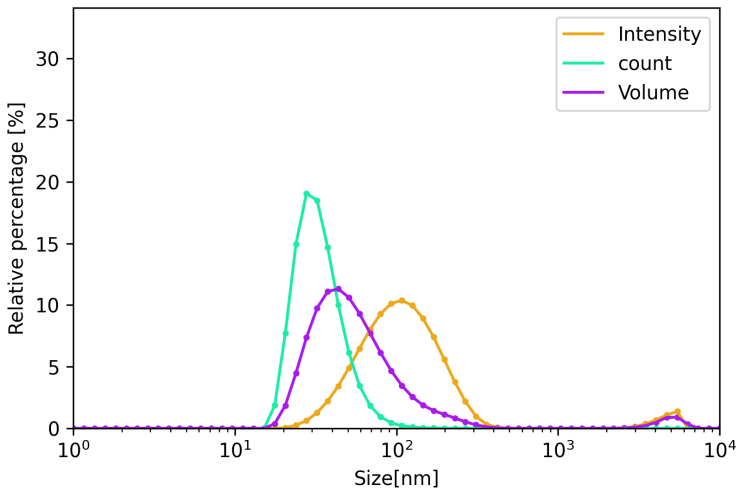

Figure 49: Size distribution of $LPC_{0.01}$, $LPC_{0.02}$, $LPC_{0.04}$ and $LPC_{0.05}$ by intensity, number and volume. Graph of the relative percentage of particles in different size classes plotted as a function of scattered light intensity (orange), number (cyan) and volume (violet).

D LPC isolation by centrifugation

Table 6: Results from isolation experiments on laccase and LPC with mass ratio between 0.01 and 0.05. Mean and standard deviation of enzymatic activities of initial solution, supernatant, and pellet. Percentage of initial activity are given alongside values of supernatant and pellet. I-S contains the enzymatic activities of inital solutions minus that of the supernatant. The percentage given in I-S corresponds to the difference of activities between the initial solution and the sum of the activities of the supernatant and the pellet.

MEAN [mU] (%)	Initial	Supernatant	Pellet	I - S [mU] (Δ%)
Laccase	9,8	9,3 (95%)	0,0 (0%)	0,5 (5%)
$LPC_{0.01}$	8,7	7,0 (80%)	1,7 (20%)	1,7 (0%)
$LPC_{0.02}$	7,4	1,3 (18%)	4,8 (65%)	6,1 (17%)
$LPC_{0.03}$	8,1	3,0 (37%)	1,1 (14%)	5,2 (49%)
$LPC_{0.04}$	8,7	7,4 (85%)	0,4 (5%)	1,3 (10%)
$LPC_{0.05}$	8,8	7,7 (88%)	0,1 (0%)	1,1 (12%)

std [mU]	Initial	Supernatant	Pellet
Laccase	0,2	0,3	0,2
$LPC_{0.01}$	0,2	0,2	0,3
$LPC_{0.02}$	0,2	0,0	0,8
$LPC_{0.03}$	0,2	0,2	0,0
$LPC_{0.04}$	0,2	0,3	0,0
$LPC_{0.05}$	0,2	0,6	0,0

E QCM

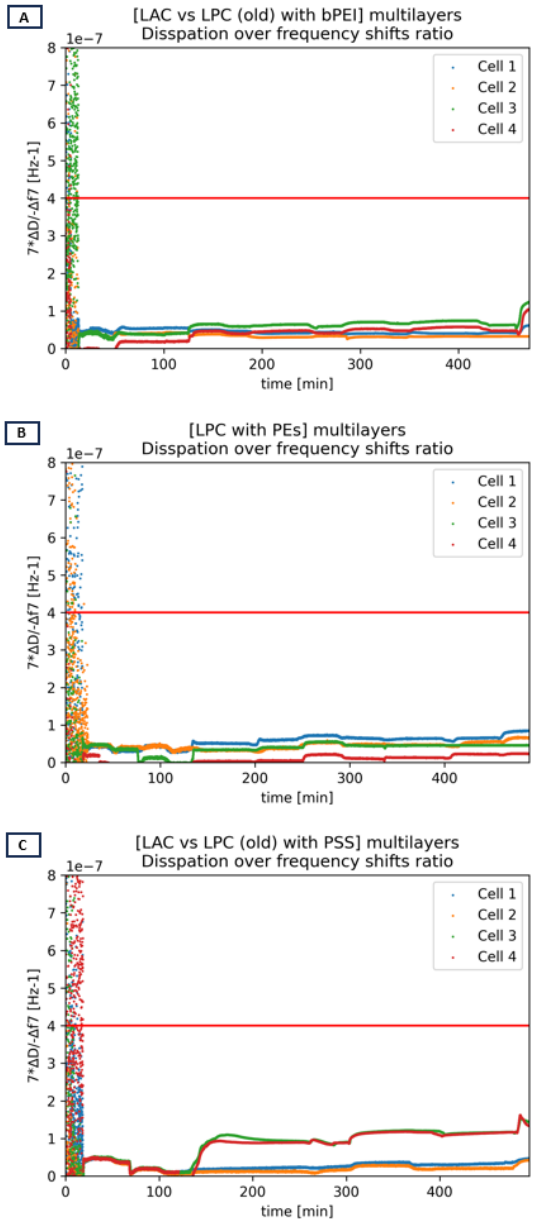

Figure 50: QCM-D analysis: Dissipation over frequency shifts ratio over time The red line indicates the limit at which Sauerbrey equation is no longer valid. The 3 QCM experiments are separated. (A) LAC and $LPC_{old}^{0.06}$ with bPEI. (B) $LPC_{new}^{0.04}$ with PEs. (C) LAC and $LPC_{old}^{0.06}$ with PSS.

Table 7: QCM results: mean and standard deviation of multilayers thickness after each layers. As some experiments did not follow the same protocol the values are shifted in order to be placed in the columns of the corresponding bilayers. The values shown in red correspond to the end of the second bilayers for the 6 assemblies.

MEAN (nm)	**Assembly**	**Cushion (bPEI)**	**PE**	**LAC / LPC**	**PE**	**LAC / LPC**	**PE**	**LAC / LPC**	**TEST**
Laccase	**[PSS - LAC]**	3.8	3.9	5.3	5.4	5.5			11.2
	[bPEI - LAC]	3.2		8.2	12.5	18.5	25.8	36.9	39.7
LPC_{old}	**[PSS - LPC]**	3.8	3.9	36.3	41.0	67.1			61.3
	[bPEI - LPC]	2.4		5.1	6.6	8.2	8.2	9.4	9.9
LPC_{new}	**[PSS - LPC]**	2.8	2.6	5.6	5.8	8.2			8.6
	[bPEI - LPC]	2.1	2.1	4.0	4.6	5.8			5.6

std (nm)	**Assembly**	**bPEI cushion**	**PE**	**LAC / LPC**	**PE**	**LAC / LPC**	**PE**	**LAC / LPC**	**TEST**
Laccase	**[PSS - LAC]**	0.0	0.3	0.8	0.8	0.8			1.4
	[bPEI - LAC]	0.3		0.1	0.3	0.3	0.4	0.1	2.9
LPC_{old}	**[PSS - LPC]**	0.1	0.2	1.0	0.9	2.2			3.6
	[bPEI - LPC]	0.0		0.2	0.1	0.2	0.1	0.1	0.1
LPC_{new}	**[PSS - LPC]**	0.3	0.1	0.2	0.2	0.2			0.2
	[bPEI - LPC]	0.0	0.0	0.6	0.8	1.1			1.0

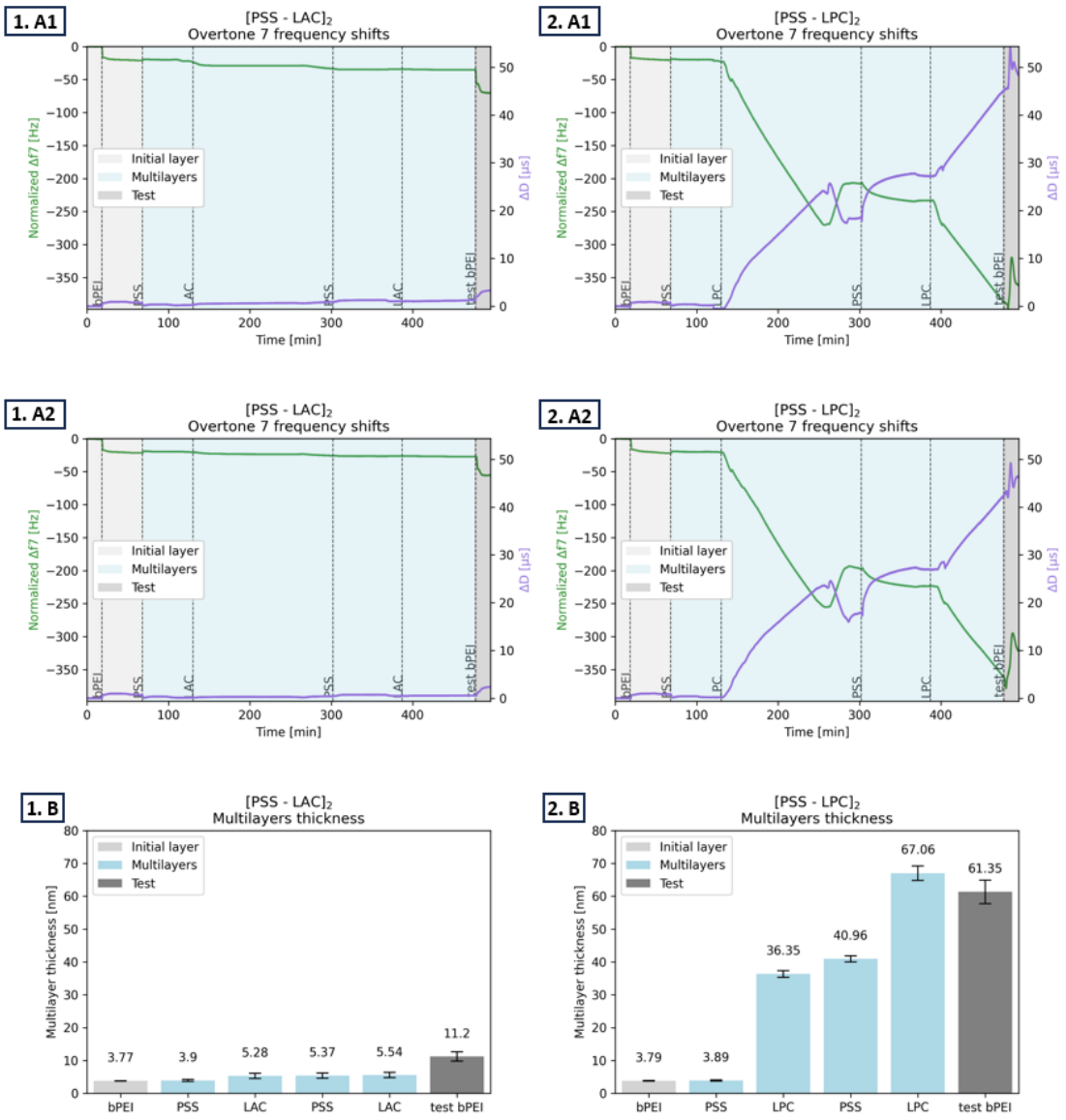

Figure 51: Complete results of QCM linked at Figure 43.

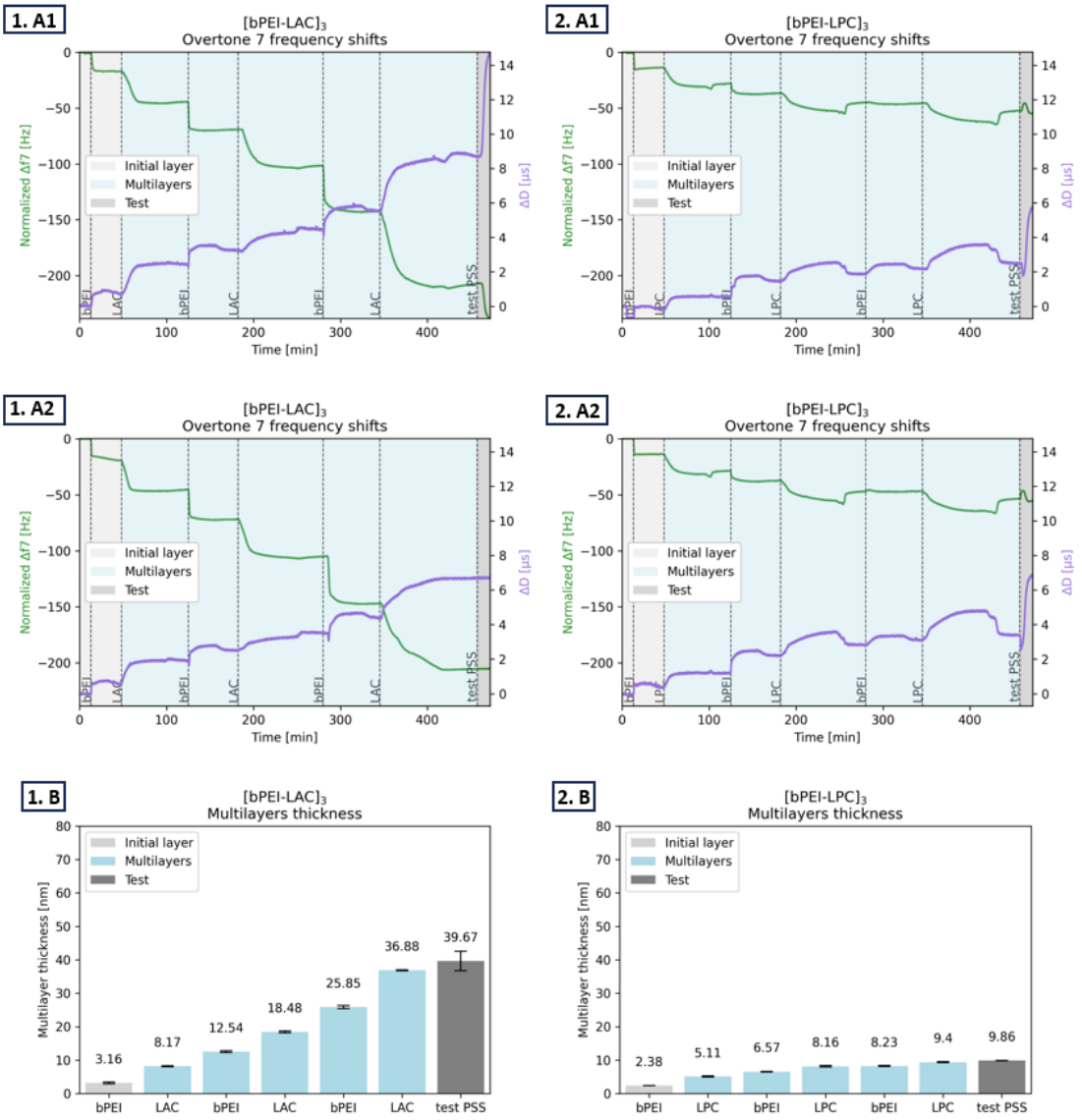

Figure 52: Complete results of QCM linked at Figure 44.

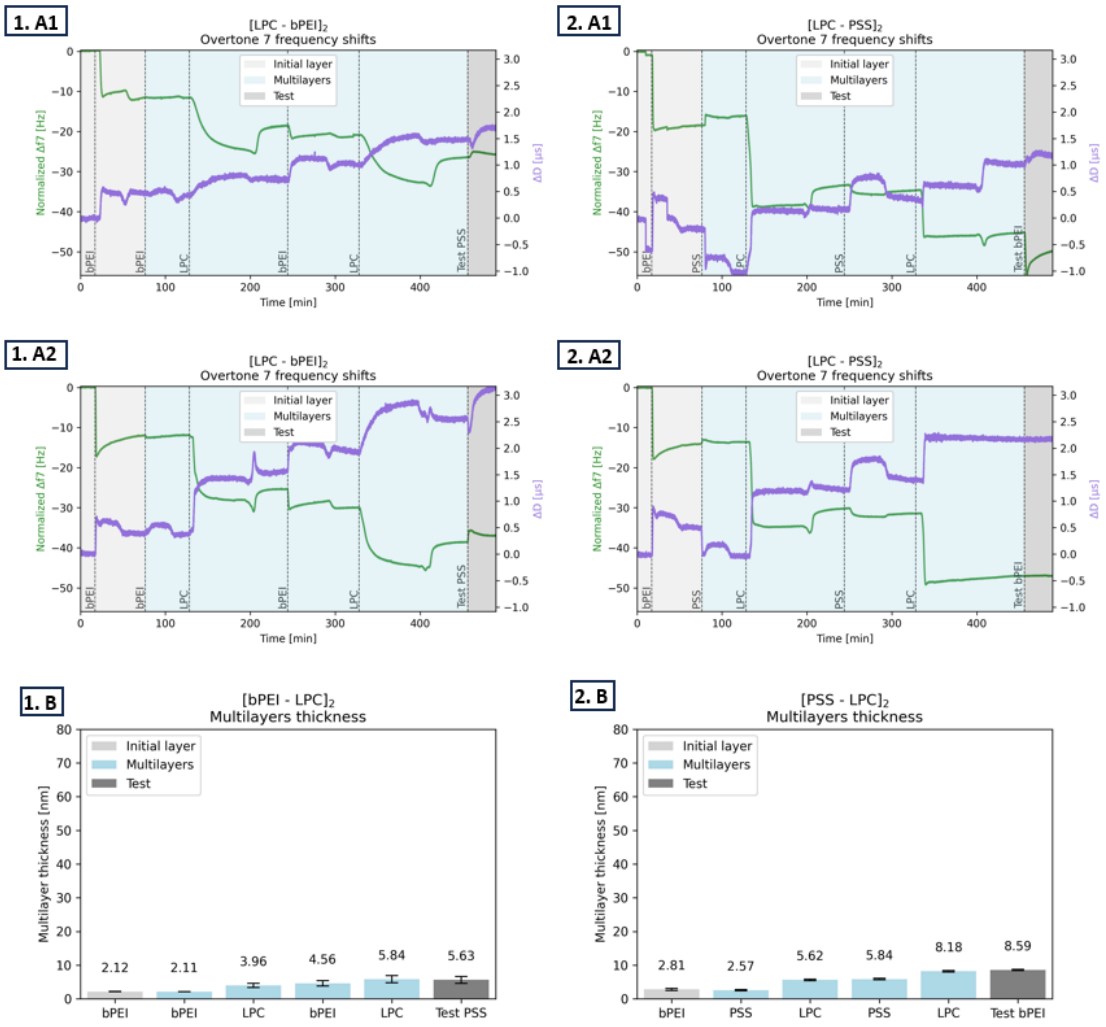

Figure 53: Complete results of QCM linked at Figure 45.

F Stability study with controls

Table 8: Data linked to stability experiments: mean and std activities through the days.

MEAN [mU]	BL	DAY 0	DAY 1	DAY 3	DAY 6	DAY 10
[bPEI - LAC]	3	3,03	1,11	0,77	0,53	0,44
	6	6,88	2,23	1,77	1,55	1,41
[PSS - LAC]	3	0,11	0,06	0,05	0,05	0,05
	6	0,11	0,11	0,11	0,11	0,11
[bPEI - LPC]	3	0,51	0,21	0,13	0,11	0,10
	6	0,84	0,33	0,22	0,22	0,22
[PSS - LPC]	3	0,99	0,45	0,33	0,23	0,20
	6	2,22	0,97	0,88	0,76	0,66

STD [mU]	BL	DAY 0	DAY 1	DAY 3	DAY 6	DAY 10
[bPEI - LAC]	3	0,39	0,27	0,16	0,14	0,07
	6	2,02	0,42	0,21	0,19	0,21
[PSS - LAC]	3	0,06	0,00	0,01	0,02	0,01
	6	0,03	0,02	0,02	0,02	0,02
[bPEI - LPC]	3	0,11	0,04	0,04	0,03	0,05
	6	0,27	0,07	0,01	0,00	0,03
[PSS - LPC]	3	0,23	0,15	0,16	0,10	0,13
	6	1,21	0,13	0,14	0,11	0,14

Table 9: Data linked to stability experiments: mean and std percentage of day 0

MEAN (% DAY 0)	BL	DAY 0	DAY 1	DAY 3	DAY 6	DAY 10
[bPEI - LAC]	3	100	36	25	18	**15**
	6	100	35	28	23	**22**
[PSS - LAC]	3	100	70	58	62	61
	6	100	81	80	78	74
[bPEI - LPC]	3	100	41	29	22	19
	6	100	35	28	21	20
[PSS - LPC]	3	100	52	36	26	**22**
	6	100	54	47	36	**32**

STD (% DAY 0)	BL	DAY 0	DAY 1	DAY 3	DAY 6	DAY 10
[bPEI - LAC]	3	0	13	2	6	4
	6	0	13	9	7	8
[PSS - LAC]	3	0	34	28	29	26
	6	0	6	24	36	9
[bPEI - LPC]	3	0	1	10	1	8
	6	0	10	15	7	9
[PSS - LPC]	3	0	4	17	5	9
	6	0	24	26	19	16

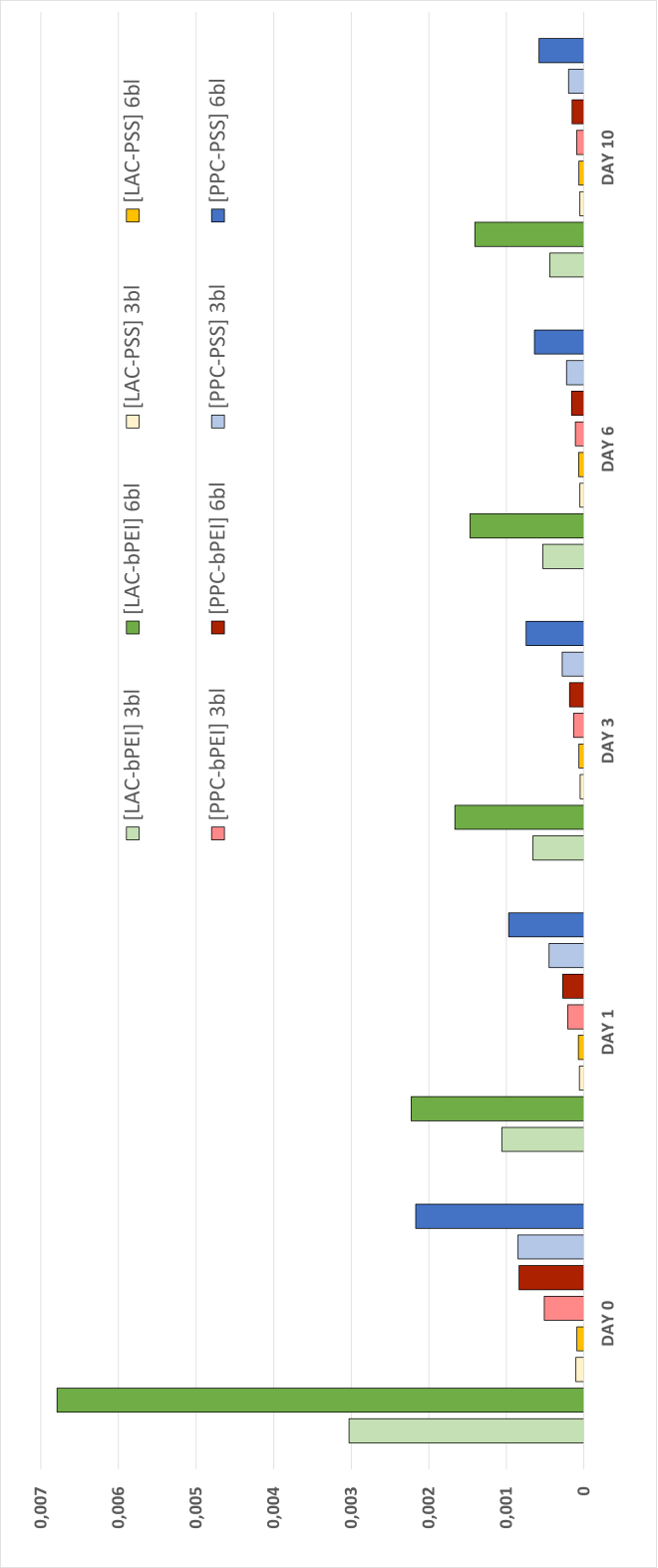

Figure 54: Complete version of Figure 46 (without std) in [U].

Bibliography

[1] J. Zdarta, L. N. Nguyen, K. Jankowska, T. Jesionowski, and L. D. Nghiem, "**A contemporary review of enzymatic applications in the remediation of emerging estrogenic compounds**," *Critical Reviews in Environmental Science and Technology*, vol. 52, pp. 2661–2690, Aug. 2022. Publisher: Taylor & Francis https://doi.org/10.1080/10643389.2021.1889283.

[2] S. Bijekar, H. D. Padariya, V. K. Yadav, A. Gacem, M. A. Hasan, N. S. Awwad, K. K. Yadav, S. Islam, S. Park, and B.-H. Jeon, "**The State of the Art and Emerging Trends in the Wastewater Treatment in Developing Nations**," *Water*, vol. 14, p. 2537, Jan. 2022. Number: 16 Publisher: Multidisciplinary Digital Publishing Institute https://doi.org/10.3390/w14162537.

[3] OECD, "**OECD environmental outlook to 2050: the consequences of inaction**," *International Journal of Sustainability in Higher Education*, vol. 13, July 2012. https://doi.org/10.1108/ijshe.2012.24913caa.010.

[4] Programme mondial de l'UNESCO pour l'évaluation des ressources en eau [509], UNESCO. Director-General, 2009-2017 (Bokova, I.G.). writer of foreword and Ryder, Guy [writer of foreword], ***The United Nations world water development report, 2017: Wastewater: the untapped resource***. United Nations Educational, Scientific and Cultural Organization, 2017. https://unesdoc.unesco.org/ark:/48223/pf0000247153.

[5] Z. Ahsan, U. Kalsoom, H. N. Bhatti, K. Aftab, N. Khalid, and M. Bilal, "**Enzyme-assisted bioremediation approach for synthetic dyes and polycyclic aromatic hydrocarbons degradation**," *Journal of Basic Microbiology*, vol. 61, no. 11, pp. 960–981, 2021. https://doi.org/10.1002/jobm.202100218.

[6] "**Summary Progress Update 2021: SDG 6 — water and sanitation for all**," 2021. https://www.unwater.org/publications/summary-progress-update-2021-sdg-6-water-and-sanitation-all.

[7] M. Petrovic, S. Gonzalez, and D. Barcelo, "**Analysis and removal of emerging contaminants in wastewater and drinking water**," *TrAC Trends in Analytical Chemistry*, vol. 22, pp. 685–696, Nov. 2003. https://doi.org/10.1016/S0165-9936(03)01105-1.

[8] V. Geissen, H. Mol, E. Klumpp, G. Umlauf, M. Nadal, M. van der Ploeg, S. E. A. T. M. van de Zee, and C. J. Ritsema, "**Emerging pollutants in the environment: A challenge for water resource management**," *International Soil and Water Conservation Research*, vol. 3, pp. 57–65, Mar. 2015. https://doi.org/10.1016/j.iswcr.2015.03.002.

[9] K. A. Al-Maqdi, N. Elmerhi, K. Athamneh, M. Bilal, A. Alzamly, S. S. Ashraf, and I. Shah, "**Challenges and Recent Advances in Enzyme-Mediated Wastewater Remediation—A Review**," *Nanomaterials*, vol. 11, p. 3124, Nov. 2021. Number: 11 Publisher: Multidisciplinary Digital Publishing Institute, https://doi.org/10.3390/nano11113124.

[10] A. Shah and M. Shah, "**Characterisation and bioremediation of wastewater: A review exploring bioremediation as a sustainable technique for pharmaceutical wastewater**," *Groundwater for Sustainable Development*, vol. 11, p. 100383, Oct. 2020. https://doi.org/10.1016/j.gsd.2020.100383.

[11] W. Zhou, W. Zhang, and Y. Cai, "**Laccase immobilization for water purification: A comprehensive review**," *Chemical Engineering Journal*, vol. 403, p. 126272, Jan. 2021. https://doi.org/10.1016/j.cej.2020.126272.

[12] U. Nations, "**Water – at the center of the climate crisis**." Publisher: United Nations, https://shorturl.at/kAEU9.

[13] "**A Peek into the History of Wastewater Treatment - Organica Biotech**," June 2020. Section: Wastewater Treatment, https://organicabiotech.com/a-peek-into-the-history-of-wastewater-treatment.

[14] G. Crini and E. Lichtfouse, "**Advantages and disadvantages of techniques used for wastewater treatment**," *Environmental Chemistry Letters*, vol. 17, pp. 145–155, Mar. 2019. https://doi.org/10.1007/s10311-018-0785-9.

[15] G. Crini and E. Lichtfouse, "**Wastewater Treatment: An Overview**," in *Green Adsorbents for Pollutant Removal: Fundamentals and Design* (G. Crini and E. Lichtfouse, eds.), Environmental Chemistry for a Sustainable World, pp. 1–21, Cham: Springer International Publishing, 2018. https://doi.org/10.1007/978-3-319-92111-2_1.

[16] J. Zdarta, T. Jesionowski, M. Pinelo, A. S. Meyer, H. M. N. Iqbal, M. Bilal, L. N. Nguyen, and L. D. Nghiem, "**Free and immobilized biocatalysts for removing micropollutants from water and wastewater: Recent progress and challenges**," *Bioresource Technology*, vol. 344, p. 126201, Jan. 2022. https://doi.org/10.1016/j.biortech.2021.126201.

[17] S. Bhandari, D. K. Poudel, R. Marahatha, S. Dawadi, K. Khadayat, S. Phuyal, S. Shrestha, S. Gaire, K. Basnet, U. Khadka, and N. Parajuli, "**Microbial Enzymes Used in Bioremediation**," *Journal of Chemistry*, vol. 2021, p. e8849512, Feb. 2021. Publisher: Hindawi, https://doi.org/10.1155/2021/8849512.

[18] T. Brugnari, D. M. Braga, C. S. A. dos Santos, B. H. C. Torres, T. A. Modkovski, C. W. I. Haminiuk, and G. M. Maciel, "**Laccases as green and versatile biocatalysts: from lab to enzyme market—an overview**," *Bioresources and Bioprocessing*, vol. 8, p. 131, Dec. 2021. https://doi.org/10.1186/s40643-021-00484-1.

[19] S. Ba, A. Arsenault, T. Hassani, J. P. Jones, and H. Cabana, "**Laccase immobilization and insolubilization: from fundamentals to applications for the elimination of emerging contaminants in wastewater treatment**," *Critical Reviews in Biotechnology*, vol. 33, pp. 404–418, Dec. 2013. Publisher: Taylor & Francis , https://doi.org/10.3109/07388551.2012.725390.

[20] H. Cabana, ***Elimination des perturbateurs endocriniens nonylphénol, bisphénol A et triclosan par l'action oxydative de la laccase de coriolopsis polyzona***. PhD thesis, UCL - Université Catholique de Louvain, 2008. https://dial.uclouvain.be/pr/boreal/fr/object/boreal%3A6865.

[21] L. Arregui, M. Ayala, X. Gómez-Gil, G. Gutiérrez-Soto, C. E. Hernández-Luna, M. Herrera de los Santos, L. Levin, A. Rojo-Domínguez, D. Romero-Martínez, M. C. N. Saparrat, M. A. Trujillo-Roldán, and N. A. Valdez-Cruz, "**Laccases: structure, function, and potential application in water bioremediation**," *Microbial Cell Factories*, vol. 18, p. 200, Nov. 2019. https://doi.org/10.1186/s12934-019-1248-0.

[22] D. M. Mate and M. Alcalde, "**Laccase: a multi-purpose biocatalyst at the forefront of biotechnology**," *Microbial Biotechnology*, vol. 10, pp. 1457–1467, Oct. 2016. https://doi.org/10.1111/1751-7915.12422.

[23] H. D. Kyomuhimbo and H. G. Brink, "**Applications and immobilization strategies of the copper-centred laccase enzyme; a review**," *Heliyon*,

vol. 9, p. e13156, Feb. 2023. https://doi.org/10.1016/j.heliyon.2023.e13156.

[24] M. Rodríguez, G. Aleman, J. Rodriguez-Delgado, G. Dieck-Assad, S. O. Martinez-Chapa, D. Barceló, and R. Parra, "**Laccase-based biosensors for detection of phenolic compounds**," *TrAC Trends in Analytical Chemistry*, vol. 74, pp. 21–45, Dec. 2015. https://doi.org/10.1016/j.trac.2015.05.008.

[25] K. Piontek, M. Antorini, and T. Choinowski, "**Crystal Structure of a Laccase from the FungusTrametes versicolor at 1.90-Å Resolution Containing a Full Complement of Coppers**," *Journal of Biological Chemistry*, vol. 277, pp. 37663–37669, Oct. 2002. https://doi.org/10.1074/jbc.M204571200.

[26] Y. Adamian, L. Lonappan, K. Alokpa, S. N. Agathos, and H. Cabana, "**Recent Developments in the Immobilization of Laccase on Carbonaceous Supports for Environmental Applications - A Critical Review**," *Frontiers in Bioengineering and Biotechnology*, vol. 9, 2021. https://doi.org/10.3389/fbioe.2021.778239.

[27] D. Brady and J. Jordaan, "**Advances in enzyme immobilisation**," *Biotechnology Letters*, vol. 31, pp. 1639–1650, Nov. 2009. https://doi.org/10.1007/s10529-009-0076-4.

[28] M. E. Hassan, Q. Yang, Z. Xiao, L. Liu, N. Wang, X. Cui, and L. Yang, "**Impact of immobilization technology in industrial and pharmaceutical applications**," *3 Biotech*, vol. 9, p. 440, Dec. 2019. https://www.ncbi.nlm.nih.gov/pmc/articles/PMC6841786/.

[29] A. vander Straeten, ***Protein-polyelectrolyte complexes for the surface immobilization of bioactive proteins***. PhD thesis, UCL - Université Catholique de Louvain, 2019. https://dial.uclouvain.be/pr/boreal/object/boreal:218057.

[30] G. Decher, J. Hong, and J. Schmitt, "Buildup of ultrathin multilayer films by a self-assembly process: III. Consecutively alternating adsorption of anionic and cationic polyelectrolytes on charged surfaces," *Thin Solid Films*, vol. 210-211, pp. 831–835, Apr. 1992. https://doi.org/10.1016/0040-6090(92)90417-A.

[31] S. Zhang, M. Xing, and B. Li, "**Biomimetic Layer-by-Layer Self-Assembly of Nanofilms, Nanocoatings, and 3D Scaffolds for Tissue Engineering**,"

International Journal of Molecular Sciences, vol. 19, p. 1641, June 2018. Number: 6 Publisher: Multidisciplinary Digital Publishing Institute, https://doi.org/10.3390/ijms19061641.

[32] J. Zhang, X. Huang, L. Zhang, Y. Si, S. Guo, H. Su, and J. Liu, "**Layer-by-layer assembly for immobilizing enzymes in enzymatic biofuel cells**," *Sustainable Energy & Fuels*, vol. 4, pp. 68–79, Dec. 2019. Publisher: The Royal Society of Chemistry, https://doi.org/10.1039/C9SE00643E.

[33] J. Borges and J. F. Mano, "**Molecular Interactions Driving the Layer-by-Layer Assembly of Multilayers**," *Chemical Reviews*, vol. 114, pp. 8883–8942, Sept. 2014. Publisher: American Chemical Society, https://doi.org/10.1021/cr400531v.

[34] S. Lee, B. Yeom, Y. Kim, and J. Cho, "**Layer-by-layer assembly for ultrathin energy-harvesting films: Piezoelectric and triboelectric nanocomposite films**," *Nano Energy*, vol. 56, pp. 1–15, Feb. 2019. https://doi.org/10.1016/j.nanoen.2018.11.024.

[35] A. M. Díez-Pascual and A. Rahdar, "**LbL Nano-Assemblies: A Versatile Tool for Biomedical and Healthcare Applications**," *Nanomaterials*, vol. 12, p. 949, Jan. 2022. Number: 6 Publisher: Multidisciplinary Digital Publishing Institute,https://doi.org/10.3390/nano12060949.

[36] R. Sarma, M. S. Islam, A.-F. Miller, and D. Bhattacharyya, "**Layer-by-Layer-Assembled Laccase Enzyme on Stimuli-Responsive Membranes for Chloro-Organics Degradation**," *ACS Applied Materials & Interfaces*, vol. 9, pp. 14858–14867, May 2017. Publisher: American Chemical Society, https://doi.org/10.1021/acsami.7b01999.

[37] A. vander Straeten, D. Lefèvre, S. Demoustier-Champagne, and C. Dupont-Gillain, "**Protein-based polyelectrolyte multilayers**," *Advances in Colloid and Interface Science*, vol. 280, p. 102161, June 2020. https://doi.org/10.1016/j.cis.2020.102161.

[38] J. J. Richardson, M. Björnmalm, and F. Caruso, "**Technology-driven layer-by-layer assembly of nanofilms**," *Science*, vol. 348, p. aaa2491, Apr. 2015. https://www.science.org/doi/10.1126/science.aaa2491.

[39] C. Holm, J. F. Joanny, K. Kremer, R. R. Netz, P. Reineker, C. Seidel, T. A. Vilgis, and R. G. Winkler, "Polyelectrolyte Theory," in ***Polyelectrolytes with Defined Molecular Architecture II*** (M. Schmidt, ed.), Advances in Polymer Science, pp. 67–111, Berlin, Heidelberg: Springer, 2004. https://doi.org/10.1007/b11349.

[40] B. Dickhaus and R. Priefer, "**Determination of polyelectrolyte pKa values using surface-to-air tension measurements**," *Colloids and Surfaces A: Physicochemical and Engineering Aspects*, vol. 488, pp. 15–19, Jan. 2016. https://doi.org/10.1016/j.colsurfa.2015.10.015.

[41] J. J. Virgen-Ortiz, J. C. S. d. Santos, A. Berenguer-Murcia, O. Barbosa, R. C. Rodrigues, and R. Fernandez-Lafuente, "**Polyethylenimine: a very useful ionic polymer in the design of immobilized enzyme biocatalysts**," *Journal of Materials Chemistry B*, vol. 5, pp. 7461–7490, Sept. 2017. Publisher: The Royal Society of Chemistry, https://doi.org/10.1039/C7TB01639E.

[42] "**QCM**-D | Measurements | Biolin Scientific." https://www.biolinscientific.com/measurements/qcm-d.

[43] I. Reviakine, D. Johannsmann, and R. P. Richter, "**Hearing What You Cannot See and Visualizing What You Hear: Interpreting Quartz Crystal Microbalance Data from Solvated Interfaces**," *Analytical Chemistry*, vol. 83, pp. 8838–8848, Dec. 2011. Publisher: American Chemical Society,https://doi.org/10.1021/ac201778h.

[44] S. Gao, A. Holkar, and S. Srivastava, "**Protein–Polyelectrolyte Complexes and Micellar Assemblies**," *Polymers*, vol. 11, p. 1097, June 2019. https://doi.org/10.3390/polym11071097.

[45] N. Woitovich Valetti, M. E. Brassesco, and G. A. Picó, "**Polyelectrolytes–protein complexes: a viable platform in the downstream processes of industrial enzymes at scaling up level**," *Journal of Chemical Technology & Biotechnology*, vol. 91, no. 12, pp. 2921–2928, 2016. https://doi.org/10.1002/jctb.5050.

[46] C. L. Cooper, P. L. Dubin, A. B. Kayitmazer, and S. Turksen, "**Polyelectrolyte–protein complexes**," *Current Opinion in Colloid & Interface Science*, vol. 10, pp. 52–78, Aug. 2005. https://doi.org/10.1016/j.cocis.2005.05.007.

[47] J. M. Horn, R. A. Kapelner, and A. C. Obermeyer, "**Macro- and Microphase Separated Protein-Polyelectrolyte Complexes: Design Parameters and Current Progress**," *Polymers*, vol. 11, p. 578, mar 2019. https://doi.org/10.3390/polym11040578.

[48] X. Wang, K. Zheng, Y. Si, X. Guo, and Y. Xu, "**Protein–Polyelectrolyte Interaction: Thermodynamic Analysis Based on the Titration Method**," *Polymers*, vol. 11, p. 82, Jan. 2019. https://doi.org/10.3390/polym11010082.

[49] T. Kurinomaru and K. Shiraki, "**Aggregative protein–polyelectrolyte complex for high-concentration formulation of protein drugs**," *International Journal of Biological Macromolecules*, vol. 100, pp. 11–17, July 2017. http://dx.doi.org/10.1016/j.ijbiomac.2016.06.016.

[50] A. vander Straeten, A. Bratek-Skicki, A. M. Jonas, C.-A. Fustin, and C. Dupont-Gillain, "**Integrating Proteins in Layer-by-Layer Assemblies Independently of their Electrical Charge**," *ACS Nano*, vol. 12, pp. 8372–8381, Aug. 2018. Publisher: American Chemical Society, https://doi.org/10.1021/acsnano.8b03710.

[51] R. Chollakup, W. Smitthipong, C. D. Eisenbach, and M. Tirrell, "**Phase Behavior and Coacervation of Aqueous Poly(acrylic acid)−Poly(allylamine) Solutions**," *Macromolecules*, vol. 43, pp. 2518–2528, Mar. 2010. Publisher: American Chemical Society, https://doi.org/10.1021/ma902144k.

[52] B. G. Kitchener, J. Wainwright, and A. J. Parsons, "**A review of the principles of turbidity measurement**," *Progress in Physical Geography: Earth and Environment*, vol. 41, pp. 620–642, Oct. 2017. https://doi.org/10.1177/0309133331772.

[53] H.-M. Buchhammer, M. Mende, and M. Oelmann, "**Preparation of monodisperse polyelectrolyte complex nanoparticles in dilute aqueous solution**," in *Aqueous Polymer Dispersions* (K. Tauer, ed.), pp. 98–102, Berlin, Heidelberg: Springer Berlin Heidelberg, June 2004. https://doi.org/10.1007/978-3-540-36474-0_20.

[54] A. B. Kayitmazer, D. Seeman, B. B. Minsky, P. L. Dubin, and Y. Xu, "**Protein–polyelectrolyte interactions**," *Soft Matter*, vol. 9, pp. 2553–2583, Feb. 2013. Publisher: The Royal Society of Chemistry,DOIhttps://doi.org/10.1039/C2SM27002A.

[55] H.-M. Buchhammer, M. Mende, and M. Oelmann, "**Preparation of monodisperse polyelectrolyte complex nanoparticles in dilute aqueous solution**," in *Aqueous Polymer Dispersions* (K. Tauer, ed.), pp. 98–102, Berlin, Heidelberg: Springer Berlin Heidelberg, June 2004. https://doi.org/10.1007/978-3-540-36474-0_20.

[56] "**The principles of dynamic light scattering :: Anton Paar Wiki**." https://wiki.anton-paar.com/en/the-principles-of-dynamic-light-scattering/.

[57] "**Understanding Dynamic Light Scattering**." https://www.wyatt.com/library/theory/dynamic-light-scattering-theory.html.

[58] S. Bhattacharjee, "**DLS and zeta potential – What they are and what they are not?**," *Journal of Controlled Release*, vol. 235, pp. 337–351, Aug. 2016. https://doi.org/10.1016/j.jconrel.2016.06.017.

[59] "**SDTech Nano**." http://www.nano.sd-tech.com/files/fr/pdf/publication/2017/Zeta.pdf.

[60] W.-F. Tan, W. Norde, and L. K. Koopal, "**Humic substance charge determination by titration with a flexible cationic polyelectrolyte**," *Geochimica et Cosmochimica Acta*, vol. 75, pp. 5749–5761, Oct. 2011. https://doi.org/10.1016/j.gca.2011.07.015.

[61] M. Bilal, S. Noreen, M. Asgher, and S. Parveen, "**Development and characterization of cross-linked laccase aggregates (Lac-CLEAs) from Trametes versicolor IBL-04 as ecofriendly biocatalyst for degradation of dye-based environmental pollutants**," *Environmental Technology & Innovation*, vol. 21, p. 101364, Feb. 2021. https://doi.org/10.1016/j.eti.2021.101364.

[62] A. Li, Y. Zhu, L. Xu, W. Zhu, and X. Tian, "**Comparative study on the determination of assay for laccase of Trametes sp**," *African Journal of Biochemistry Research*, vol. 2, pp. 181–183, Sept. 2008. https://www.researchgate.net/publication/228345841_Comparative_study_on_the_determination_of_assay_for_laccase_of_Trametes_sp.

[63] iGEM Team Stuttgart 2020, "**Team:Stuttgart - 2020.igem.org - Laccase wiki Methods**." https://2020.igem.org/Team:Stuttgart/Laccasewiki-Methods.

[64] ENERGENESIS BIOMEDICAL CO., LTD., "**Visual Protein | Product**," 2020. https://www.visualprotein.com/zh_tw/product/8/37/48.

[65] "**Bicinchoninic Acid Assay - an overview | ScienceDirect Topics**." https://www.sciencedirect.com/topics/biochemistry-genetics-and-molecular-biology/bicinchoninic-acid-assay.

[66] C.-H. Shen, "**Quantification and Analysis of Proteins**," in *Diagnostic Molecular Biology*, pp. 187–214, Elsevier, 2019. https://doi.org/10.1016/B978-0-12-802823-0.00008-0.

[67] E. Jurrus, D. Engel, K. Star, K. Monson, J. Brandi, L. E. Felberg, D. H. Brookes, L. Wilson, J. Chen, K. Liles, M. Chun, P. Li, D. W. Gohara, T. Dolinsky, R. Konecny, D. R. Koes, J. E. Nielsen, T. Head-Gordon, W. Geng, R. Krasny, G. Wei, M. J. Holst, J. A. McCammon, and N. A. Baker, "**Improvements to the APBS biomolecular solvation software suite**," *Protein Science*, vol. 27, pp. 112–128, Jan. 2018. https://server.poissonboltzmann.org/.

[68] T. P. Operator, "What Exactly Is pH?," Nov. 2013. Publisher: Treatment Plant Operator, https://www.tpomag.com/editorial/2013/12/what_exactly_is_ph.

[69] d. M. Juliette, ***Development of an enzyme immobilization system combining LbL and Avidin-biotin interaction***. PhD thesis, UCL - Université Catholique de Louvain, 2023. https://dial.uclouvain.be.

[70] L. M. M. Officer, SEPMAG Chief Scientific, "**BCA protein assay**." https://www.sepmag.eu/blog/bca-protein-assay.

[71] C. Vranckx, L. Lambricht, V. Préat, O. Cornu, C. Dupont-Gillain, and A. Vander Straeten, "**Layer-by-Layer Nanoarchitectonics Using Protein-Polyelectrolyte Complexes toward a Generalizable Tool for Protein Surface Immobilization**," *Langmuir: the ACS journal of surfaces and colloids*, vol. 38, pp. 5579–5589, May 2022. https://doi.org/10.1021/acs.langmuir.2c00191.

[72] I. Migneault, C. Dartiguenave, M. J. Bertrand, and K. C. Waldron, "**Glutaraldehyde: behavior in aqueous solution, reaction with proteins, and application to enzyme crosslinking**," *BioTechniques*, vol. 37, pp. 790–802, Nov. 2004. Publisher: Future Science, https://doi.org/10.2144/04375RV01.

[73] M. Salem, Y. Mauguen, and T. Prangé, "**Revisiting glutaraldehyde crosslinking: the case of the Arg–Lys intermolecular doublet**," *Acta Crystallographica Section F: Structural Biology and Crystallization Communications*, vol. 66, pp. 225–228, Feb. 2010. https://www.ncbi.nlm.nih.gov/pmc/articles/PMC2833024/.

UNIVERSITÉ CATHOLIQUE DE LOUVAIN
École polytechnique de Louvain
Rue Archimède, 1 bte L6.11.01, 1348 Louvain-la-Neuve, Belgique | **www.uclouvain.be/epl**